REPORT TITLE/ TITTEL

Source Rock/Hydrocarbon Staining Correlation in Well 6610/7-1.

CLIENT/ OPPDRAGSGIVER

Statoil

RESPONSIBLE SCIENTIST/ PROSJEKTANSVARLIG

L. Schou

AUTHORS/ FORFATTERE

L. Schou, J. Akernes and E. Hustad

DATE/ DATO	REPORT NO./ RAPPORT NR.	NO. OF PAGES/ ANT. SIDER	NO. OF ENCLOSURES/ ANT. BILAG
22.12.83	05.0201/1/83	99	-

IKU

INSTITUTT FOR KONTINENTALSOKKELUNDERSØKELSER

CONTINENTAL SHELF INSTITUTE, NORWAY

Håkon Magnussons gt. 1B – N-7000 Trondheim – Norway – Telephone (07) 92 06 11 – Telex 55434

Institutt for kontinentalsokkelundersøkelser
CONTINENTAL SHELF INSTITUTE, NORWAY
Håkon Magnussons gt. 1 B • Postboks 1883 • 7001 Trondheim, Norway • Tlf. (07) 92 06 11
Telex 55434 IKU N • Telegram «NORSHELF» • Telefax (07) 92 09 24 (Aut.)

Confidential

REPORT TITLE/ TITTEL

Source Rock/Hydrocarbon Staining Correlation in Well 6610/7-1.

CLIENT/ OPPDRAGSGIVER

Statoil

RESPONSIBLE SCIENTIST/ PROSJEKTANSVARLIG

L. Schou

AUTHORS/ FORFATTERE

L. Schou, J. Akernes and E. Hustad

DATE/ DATO	REPORT NO./ RAPPORT NR.	NO. OF PAGES/ ANT. SIDER	NO. OF ENCLOSURES/ ANT. BILAG
22.12.83	05.0201/1/83	99	-

SUMMARY/ SAMMENDRAG

Ten source rock samples were analysed together with three sandstone cores in an attempt to correlate hydrocarbon staining of the sandstones with the source rocks from the same well. GC-MS and $\delta^{13}C$ isotope data were applied in addition to GC and bulk geochemical methods. The most likely main source of the hydrocarbons is a more mature stage of the Upper Jurassic claystones in this well.

The Upper Jurassic claystones in 6610/7-1 are of too low maturity to have sourced the hydrocarbons.

KEY WORDS/ STIKKORD

Correlation
Trænabanken
GC-MS
δ^{13} isotopes

CONTENTS

CONTENTS continued

1. INTRODUCTION

Ten source rock samples (seven cuttings and three SWC's) were analysed together with three sandstone cores in an attempt to correlation hydrocarbons in the sandstones with the source rocks. The analysed samples cover the Jurassic section of the well. The samples are listed in Table 1.

Evaluation of the possible source rocks in the well has been performed previously (Betts et al., 1983). Some of the GC data from this previous report is presented here together with additional GC results and GC-MS and $\delta^{13}C$ isotope data. For the bulk geochemistry parameters we refer to the source rock report, only summaries of some data are reported here.

In this report a correlation of the hydrocarbons found in the three sandstone cores will be performed before source rock/hydrocarbons correlation is attempted.

1.1 Molecular ratios

Geochemical fossils or biological marker components are characteristic of the type of organic matter present at the time the sediments were deposited. The biological isomers of these components undergo changes due to increased maturity in particular, but also to a certain degree caused by migration and weathering processes.

1.1.1 Source characteristics parameters

In the m/e 191 mass chromatograms, representing terpanes, the hopanes and moretanes are the major components in most extracts and oils. Of the hopanes the C_{27} and C_{29}-C_{35} homologs are ubiquitous, while the C_{28} bisnorhopane is believed to be typical of certain types of source rocks. The amounts of tricyclic terpanes relative to the hopanes are also believed to a certain extent to be characteristic of the source rock. This is also the case for the component, probably gammacerane, sometimes seen to coelute with the 22S isomer of the C_{31} 17α(H)-hopanes (H). In the sterane mass chromatograms, m/e 217 and m/e 218, the molecular weight distribution of the C_{27}-C_{29} regular steranes is believed to be representative of the original input of organic matter. The highest molecular weight compounds, the C_{29} steranes, represent organic matter of terre-

strial origin, while the lower molecular weight analogs originate from more marine type environments.

1.1.2 Maturity parameters

The biological isomers of the hopanes, the 17β(H), 21β(H)-hopanes, undergo structural changes during the maturation process. The isomerisation reactions are thought to produced via the 17β(H), 21α(H)-hopanes (moretanes) to the most stable 17α(H), 21β(H)-hopanes. At equilibrium 100% of the 17α(H)-hopanes are seen. The ratio αβ/αβ+βα is used to describe this reaction. In the extended hopanes ($\geq C_{31}$), the thermally stable S configurations at C-22 become increasingly more abundant as compared to the biological preferred R configurations at increased maturity level. The equilibrium ratio is approximately 60% of the 22S configuration. Another ratio that is known to change with maturity is the Tm/Ts (Seifert et al., 1978) of the C_{27} hopanes. The maturable 18α(H)-trisnorneohopane (Tm) is reduced in intensity relative to the more stable 17α(H)-trisnorhopane (Ts), causing the Tm/Ts to decrease at increased maturity. This ratio is also believed to be source dependant, and this should be born in mind when applying the ratio for maturity comparison. The amount of tricyclic terpanes is also to a certain extent seen to be maturity dependant.

Two isomerisation reactions taking place in the steranes are most commonly applied for maturity assignments from the m/z 217 mass chromatograms. The biologically preferred 14α(H), 17α(H)-isomers of the regular steranes is transformed to the thermally stable 14α(H), 17β(H)-steranes, the %ββ approaching 75% at equilibrium. An equilibrium concentration of 50% is seen of the stable S configuration at C-20 as opposed to the 100% of the biological 20R epimer (Mackenzie et al., 1980). The abundance of rearranged steranes increases with increasing maturity.

One of the reactions taking place at an early stage of diagenesis is the aromatisation of steranes, leading to the formation of mono- and triaromatic analogs. This process is measured as the abundance of triaromatic relative to mono-aromatic compounds (% tri/tri + mono) in the m/z 231 and 253 mass chromatograms, respectively. In addition the degree of side chain cracking, as $\%C_{20}/C_{26,\ 27}$ and $\%C_{21}/C_{28,29}$ respectively, is applied. These cracking processes are also taking place during early diagenesis, and are used for maturity assignment together with

the previously mentioned ratios.

1.1.3 Migration and weathering

The effect on the geochemical fossils of migration and weathering, is less apparent than the maturity induced changes. Migration is believed to cause an increase in the relative amounts of rearranged and 14β(H), 17β(H) regular steranes (Seifert and Moldowan, 1978, 1981). Severe biological alteration leads to the formation of desmethyl-hopanes (Seifert and Moldowan, 1979).

2. EXPERIMENTAL

2.1 Extractable Organic Matter

Approximately 50gm of powdered rock was extracted by flowblending for 3 minutes using dichloromethane (DCM) as solvent. The DCM used was of organic geochemical grade and blank analyses showed the occurrence of negligible amounts of contaminating hydrocarbons.

Activated copper fillings were used to remove any free sulphur from the samples.

After extraction the solvent was removed on a Buchi Rotavapor and the amount of extractable organic matter (EOM) was determined.

2.2 Chromatographic Separation

The extractable organic matter (EOM) was separated into saturated fraction, aromatic fraction and non hydrocarbon fraction using a MPLC system with hexane as eluant (Radke et al., Anal. Chem., 1980). The various fractions were evaporated on a Buchi Rotavapor and transferred to glass vials and dried in stream of nitrogen.

2.3 Gas Chromatographic Analysis

The saturated hydrocarbon fractions were each diluted with n-hexane and analysed on a HP 5730A gas chromatograph, fitted with a 25m OV-101 fused silica capillary column. Hydrogen (0.7ml/min) was used as carrier gas. The total aromatic fractions were after dilution with n-hexane, analysed on a Carlo Erba Fractovap Series 2150 GC fitted with a 20mm SE-54 fused silica column.

Injections on both systems were performed in the split mode (1:20). The temperature program applied was 80^{o}C (2 min) to 260^{o}C at 4^{o}C/min.

The data processing for all the GC analyses was performed on a VG Multichrom System.

2.4 Gas chromatography - mass spectrometry (GC-MS)

GC-MS analyses were performed on a VG Micromass 70-70H GC-MS-DS system. The Varian Series 3700 GC was fitted with a fused silica OV-1 capillary column (30m x 0.3mm i.d.). Helium (0.7kg/cm^2) was used as carrier gas and the injections were performed in splitless mode (1.5µl, split ratio 1:15). The GC oven was programmed from 70^{o}C to 280^{o}C at 4^{o}C/min. after an initial isothermal period of 2 minutes.

The saturated hydrocarbons were analysed in multiple ion mode (MID) at a scan cycle time of approximately 2 secs. Full data collection was applied for the aromatic hydrocarbons at a scan time of 1 sec/decade. The mass spectrometer operated at 70eV electron energy and an ion source temperature of 200^{o}C. Data acquisition was done by a GC data system.

Peak identification was performed applying knowledge of elution patterns in certain mass chromatograms. Calculation of peak ratios was done from peak height in the appropriate mass chromatograms.

2.5 δ^{13}C isotope analysis

The δ^{13}C isotope analyses were performed by mass spectrometry at the Institute for Energy Technology (IFE) in Oslo. Their value for the NBS standard is reported to -29.8.

3. RESULTS AND DISCUSSION

The results will be discussed in three separate parts. First a summary of the source rock potential of the well is presented. Then a correlation of the hydrocarbons in the three sandstone cores is performed before the attempt to correlate these hydrocarbons with the source rocks.

In addition to the cuttings and core samples analysed and reported in the source rock report on well 6610/7-1 (Betts et al., 1983) three sidewall cores were analysed for this correlation study.

3.1 Summary of source rock potential in well 6610/7-1

Table 2 lists various bulk parameters for the source rock samples from the Jurassic section of the well. The Upper Jurassic part of the well seems to contain the most promising source rocks with regard to hydrogen rich kerogen types. Sample A-5841 was re-extracted to get enough material for $\delta^{13}C$ isotope analyses, and thus two sets of some of the data are given. The agreement between TOC-values in the two sets of data is not good, probably because of difficulties encountered in picking the same lithology for the extractions. The data from the second extraction are applied in the further discussion, since these chromatographic fractions were analysed further.

The hydrogen and oxygen indices suggest that the fine claystones/shales in the Upper Jurassic part contain type II and mixed type II/III kerogen. The petroleum potentials (PP) are high in all the samples, while the production indices (PI) are low and imply indigenous and very little migrated hydrocarbons. An increase in the amount of hydrocarbons is seen with increasing depth and the SAT/ARO ratios are relatively low. The maturity of the Upper Jurassic section is low, with vitrinite reflectance values of less than 0.5% in most cases (Table 3).

The Middle and Lower parts of the Jurassic section have poorer kerogen types than the zone above. Very high TOC-values are seen in the lowest part, probably due to coal. As above the production indices are relatively low and migrated hydrocarbons are not expected to create problems in the correlation. The high SAT/ARO ratio of sample A-6394 is probably not representative but due to the low weights of the chromatographic fractions. Vitrinite reflectance and T_{max} values indicate

that the Middle and Lower Jurassic claystones are moderate mature to mature.

Thus the most promising source rocks based on kerogen types, the Upper Jurassic claystones, are too immature for hydrocarbon generation in this well. However, more mature stages of these claystones may very well be the source of the hydrocarbons in the sandstone cores. The Middle and Lower Jurassic claystones are most likely not at least the main source of the hydrocarbons, based on the hydrogen poor kerogen types generally encountered.

3.2 Correlation of hydrocarbons in sandstone cores

3.2.1 Extraction and chromatographic separation

Extraction data presented in Tables 4a-d show that the cores contain good to rich amounts of extractable hydrocarbons relative to weight of rock extracted and rich values compared to total organic carbon (% TOC) in the cores. The relative distribution of saturated to aromatic hydrocarbons, the SAT/ARO ratio, increases slightly towards the deeper cores. This is also the case for the relative abundance of hydrocarbons, a trend that fits well in with the richness of the samples. The shallowest core was seen to contain lowest amount of extractable hydrocarbons, it showed the lowest value for the SAT/ARO ratio and for the relative amount of hydrocarbons to non-hydrocarbons.

3.2.2 GC analysis of C_{15}+ saturated hydrocarbons

The saturated hydrocarbon GC's (Figure 1) show front end biased n-alkane profiles, with maximum intensities at nC_{17}. The shallowest sample shows a weak shoulder in the region around nC_{25}. This indicates that the front end biased n-alkane profile is typical of the main part of the migrated hydrocarbons, since this is most pronounced in the samples with highest abundance of hydrocarbons. The relative amounts of isoprenoids are similar in all three cores (Table 5).

3.2.3 GC analysis of aromatic hydrocarbons

A similar trend is seen in the GC's of aromatic hydrocarbons (Figure 2). The two deepest cores contain high amounts of the lower molecular

weight alkyl naphthalenes relative to the phenanthrenes. The general distribution of the individual components is very similar in these two samples. In the shallowest core less of the low molecular weight compounds was seen, and the general distribution was slightly different to what was seen for the deeper cores. This is most probably due to the overall lower total abundance of hydrocarbons in this shallowest core.

3.2.4 GC-MS analysis of saturated terpanes and steranes

Mass chromatograms representing terpanes (m/z 191) and steranes (m/z 217 and 218) are presented in Figure 3. The terpane chromatograms show the ubiquitous 17α(H),21β(H)-hopanes to be the dominating components in all three samples, indicating mature hydrocarbons to be present. Some minor variations are seen in the molecular ratios presented in Table 6. The bisnorhopane (Z) is found in high relative abundance in the two deepest samples, while it is very low in the shallowest core. The unidentified component X is more abundant in the shallow core than in the other two. Apart from these differences the distribution of terpanes seems to be similar. Only minor variations are seen also in the sterane mass chromatograms, the shallowest sample showing ratios slightly different to the other two.

3.2.5 GC-MS analysis of aromatic hydrocarbons

In the aromatic mass chromatograms shown in Figure 4, no variation is seen for the monoaromatic compounds (m/z 92 and 106), the naphthalenes (m/z 142, 156 and 170) or the phenanthrenes (m/z 178, 192 and 206). The mono- and tri-aromatic sterane traces, m/z 253 and 231, respectively, show different distributions for the shallowest samples compared to the other two. This could be due to the generally lower abundance of hydrocarbons in the shallowest core.

3.2.6 $\delta^{13}C$ isotope analysis

The $\delta^{13}C$ isotope data presented in Table 7 show the same trend as discussed above. The values for the two deepest cores are very similar for both saturated and aromatic hydrocarbons, while the shallowest sample is seen to be slightly heavier, especially in the aromatic fraction.

3.2.7 Summary on sandstone cores

Based on the previously discussed data, it may be concluded that the three cores contain hydrocarbons generated from the same or similar sources. The differences seen between the shallowest core (A-6419 at 2661.6m) and the two deeper ones (A-6420 at 2668.1m and A-6421 at 2706.0m) are thought to be due to the lower richness of the shallow sample. This make the core more liable to contamination by hydrocarbons from the claystones close to the core, and thus a mixed input to this sample cannot be excluded.

3.3 Correlation of source rocks and migrated hydrocarbons in sandstone cores

3.3.1 GC analysis of C_{15}^+ saturated hydrocarbons

Chromatograms are presented in Figure 1. The n-alkane distribution is fairly similar for most of the samples. Bimodal profiles with maxima at nC_{15} and nC_{27} are seen. The isoprenoids are very abundant relative to n-alkanes ($Pr/n\text{-}C_{17}$) and a CPI greater than 1.0 is encountered, especially in the Upper Jurassic part of the well. The deeper samples show lower values for the $Pr/n\text{-}C_{17}$ in agreement with the slightly higher maturity in this deeper section. For the deepest SWC the bimodality is less pronounced, with a profile more similar to those seen for the core samples. This could indicate that the Lower Jurassic claystone at 3148m, which is of oil window maturity (Ro = 0.66%), is a possible source for the hydrocarbons. There is, however, also the possibility that the hydrocarbons in this SWC have migrated from another source.

3.3.2 GC analysis of C_{15}^+ aromatic hydrocarbons

The GC chromatograms of the aromatic hydrocarbon fractions are relatively complex especially in the least mature part of the well. This is probably mainly due to the immature stage of the samples. Towards the base of the Jurassic section the mature pattern of alkylated naphthalenes and phenanthrenes is becoming more predominant. With the exception of sample A-6399, all the claystone fractions seem to contain higher abundance of phenanthrenes relative to naphthalenes than the

sandstone cores. A tentatively calculation of the methylphehanthrene ratio from these relatively poorly resolved chromatograms (Table 8) indicates that all claystone samples contain less of the first eluting isomers than the second. A nearly even distribution is seen for the shallowest sandstone core, while the other cores contain more of the second eluting isomers. This suggests that the main part of the hydrocarbons encountered in the cores originate from another source rock than the claystones analysed from this well. A mixed input from the less mature hydrocarbons in this well may explain the difference in the shallowest core.

3.3.3 GC-MS analysis of saturated terpanes and steranes

Mass chromatograms representing terpanes (m/z 191) and steranes (m/z 217 and 218) are presented in Figure 3, and calculated molecular ratios are given in Table 6. The main difference in the terpane chromatograms is the relative abundance of the bisnorhopane (Z). This peak is the main one in the Upper Jurassic samples, while it can hardly be detected in the deepest sample. The maturity was seen to be relatively low for all the samples, none of the isomerisation reactions having reached equilibrium. By comparison with the core mass chromatograms the most likely source for the hydrocarbons in the cores is a more mature stage of the Upper Jurassic claystones.

From the sterane traces (m/z 217) the four or five shallowest samples seem to be fairly similar, all showing relatively low amounts of 14β(H),17β(H)-steranes. The two deeper samples were seen to contain less of the lower molecular weight C_{27} and C_{28} steranes. This is probably due to the amount of coal in these samples and can be seen more clearly from the m/z 218 chromatograms and the triangular plots shown in Figure 5. Apart from the maturity differences the core samples are most similar to the Upper Jurassic samples.

3.3.4 GC-MS analysis of aromatic hydrocarbons

Mass chromatograms are presented in Figure 4. Total ion chromatograms are not shown, since they look very similar to the normal GC traces.

Even with the high complexity seen in the traces representing monoaromatic components (m/z 92 and 106) a trend can be seen. Generally the

shallowest claystones exhibit patterns most similar to the cores. The naphthalene homologs (m/z 142, 156 and 170) do not reveal big differences between the samples, and the main difference seen in the phenanthrene chromatograms (m/z 178 + 192 + 206) is the distribution of the methyl-phenanthrenes (m/z 192). As seen from the GC's the abundance of the first eluting isomers is more pronounced in the deepest cores than in the other samples. This could be solely a maturity related variation.

From the aromatic sterane chromatograms (m/z 231 and 253) the Upper Jurassic samples are seen to be similar to the two deepest cores. The shallowest core with lowest amount of extractable hydrocarbons shows patterns intermediate between the other cores and the Lower Jurassic samples.

3.3.5 $\delta^{13}C$ isotope analyses

The data in Table 7 show that none of the source rock extracts have $\delta^{13}C$ isotope ratios in good agreement with the data for the core extracts. The shallowest claystones seem to give values closest to the cores, both for the saturated and the aromatic hydrocarbon fractions.

4. CONCLUSIONS

The analyses suggest that the migrated hydrocarbons in the sandstone cores originate from the same or similar source rocks, with the possible contribution from a second source to at least the shallowest core. Comparison with the source rock analyses indicate that a more mature stage of the Upper Jurassic claystones is the most likely main source of the hydrocarbons. The mixed input in the shallowest core is probably due to contamination by hydrocarbons from the claystones close to this sandstone. The Upper Jurassic claystones in this well are of too low maturity to have sourced the main part of the hydrocarbons encountered in the sandstones.

5. REFERENCES

BETTS, S., MILLS, N., RENDALL, H., VINGE, T. and HAUGEN, G., 1983. IKU report 05.0138.

MACKENZIE, A.S., PATIENCE, R.L., MAXWELL, J.R., VANDENBROUCKE, M. and DURAND, B., 1980. Geochim. Cosmochim. Acta, 44, pp.1709-1721.

RADKE, M., WILLSCH, H. and WELTE, D.H., 1980. Anal. Chem., 52, pp.406-411.

SEIFERT, W.K. and MOLDOWAN, J.M., 1978. Geochim. Cosmochim. Acta, 42, pp.77-95.

SEIFERT, W.K. and MOLDOWAN, J.M., 1979. Geochim. Cosmochim. Acta, 43, pp.111-126.

SEIFERT, W.K. and MOLDOWAN, J.M., 1981. Geochim. Cosmochim. Acta, 45, pp.783-794.

Table 1: List of samples analysed.

IKU Code	Sample type	Lithology	Zone	Depth (m)
A-6424	SWC		C	2283
A-5841	Cuttings	clst/sh	"	2285-2300
A-6426	SWC		"	2303
A-5850	Cuttings	clst/sh	"	2420-2435
A-5861	Cuttings	clst	"	2585-2600
A-6419	Core	sst	"	2661.60-2661.64
A-6420	Core	sst	"	2668.05-2668.12
A-5869	Cuttings	clst	D	2705-2720
A-6421	Core	sst	"	2706.00-2706.05
A-5874	Cuttings	clst	"	2780-2795
A-6394	Cuttings	clst	E	2960-2975
A-6399	Cuttings	clst/sh	F	3035-3050
A-6429	SWC		F	3148

Table 2. Summary of source rock parameters.

Lithology	IKU code	Depth(m)	HI	OI	Pet. Pot.	Prod. Ind.	%HC	SAT/ARO	mgs HC/ g TOC
Upper Jurassic									
Claystone SWC	A-6424 9.8 %TOC type II/III	2283	387	27	26.64	0.10	4	0.4	4.6
Clst./shale	A-5841 18.8 %TOC type II/III	2300	376	12	46.65	0.09	(28) 15	(3.5) 0.7	(31.5) 5.8
Claystone SWC	A-6426 9.3 %TOC type II/III	2303	330	11	31.03	0.03	14	0.5	6.0
Clst./Shale	A-5850 2.2 %TOC type II/III	2435	273	13	18.45	0.04	69	0.8	24.4
Claystone	A-5861 1.5 %TOC type III	2600	168	10	6.26	0.04	52	0.9	19.7
Middle/Lower Jurassic									
Claystone	A-5869 1.3 %TOC type III	2720	76	29	0.96	0.17	49	0.9	27.9
Claystone	A-5874 2.5 %TOC	2795	-	-	-	-	17	0.3	22.4
Claystone	A-6394 1.8 %TOC type III	2975	125	19	1.54	0.08	33	2.5	36.4
Clst./Shale	A-6399 28.6 %TOC type III	3050	100	17	0.98	0.09	(19) 24	(0.7) 0.5	(18.0) 9.0
Claystone SWC	A-6429 32.2 %TOC type II/III	3148	198	3	76.32	0.03	11	0.9	2.2

Table 3. Vitrinite reflectance values for Jurassic source rocks.

IKU code	Lithology	Depth (m)	Ro	
A-6424	clst (SWC)	2283	0.56 (16)	
A-5841	clst/sh	2300	0.47 (12)	
A-6426	clst (SWC)	2303	0.42 (15)	
A-5850	clst	2435	0.51 (17)	0.78 (1)
A-5861	clst	2600	0.46 (6)	0.60 (2)
A-5869	clst	2720	0.51 (8)	
A-5874		2795	N.D.P.	
A-6394		2975	-	
A-6399	clst/sh	3050	0.68 (20)	0.92 (1)
A-6429	clst (SWC)	3148	0.66 (19)	

T A B L E : 4a.

CONCENTRATION OF EOM AND CHROMATOGRAPHIC FRACTIONS

IKU-No	DEPTH (m)	Rock Extr. (g)	EOM (mg)	Sat. (mg)	Aro. (mg)	HC (mg)	Non HC (mg)	TOC (%)
A 6424	2283	9.3	99.6	1.1	3.1	4.2	95.4	9.81
A 5841 *	2300	10.1	73.9	4.6	6.4	11.0	62.9	18.75
A 5841	2300	2.7	17.5	3.8	1.1	4.9	12.6	5.77
A 6426	2303	10.0	39.7	1.9	3.7	5.6	34.1	9.28
A 5850	2435	3.4	2.6	0.8	1.0	1.8	0.8	2.17
A 5861	2600	9.1	5.0	1.2	1.4	2.6	2.4	1.45
A 5869	2720	20.3	15.0	3.5	3.8	7.3	7.7	1.29
A 5874	2795	10.9	36.6	1.4	4.8	6.2	30.4	2.54
A 6394	2975	4.4	8.6	2.0	0.8	2.8	5.8	1.75
A 6399 *	3050	3.4	46.6	3.5	5.3	8.8	37.8	28.64
A 6399	3050	1.4	25.7	1.9	4.2	6.1	19.6	23.19
A 6429	3148	9.1	59.8	3.0	3.4	6.4	53.4	32.22
A 6419	2661.60	20.1	15.0	3.5	2.9	6.4	8.6	0.24
A 6420	2668.05	20.2	54.2	18.9	13.4	32.3	21.9	0.33
A 6421	2706.00	18.7	34.4	11.5	8.0	19.5	14.9	0.05

DATE : 21 - 12 - 83.

* Parallels applied for $\delta^{13}C$ analyses.

T A B L E : 4b.

WEIGHT OF EOM AND CHROMATOGRAPHIC FRACTIONS

(Weight ppm OF rock)

IKU-No	DEPTH (m)	EOM	Sat.	Aro.	HC	Non HC
A 6424	2283	10710	118	333	452	10258
A 5841	2300	7317	455	634	1089	6228
A 5841	2300	6481	1407	407	1815	4667
A 6426	2303	3970	190	370	560	3410
A 5850	2435	765	235	294	529	235
A 5861	2600	549	132	154	286	264
A 5869	2720	739	172	187	360	379
A 5874	2795	3358	128	440	569	2789
A 6394	2975	1955	455	182	636	1318
A 6399	3050	13706	1029	1559	2588	11118
A 6399	3050	18357	1357	3000	4357	14000
A 6429	3148	6571	330	374	703	5868
A 6419	2661.60	747	174	144	319	428
A 6420	2668.05	2688	938	665	1602	1086
A 6421	2706.00	1843	616	428	1044	798

DATE : 21 - 12 - 83.

T A B L E : 4c.

CONCENTRATION OF EOM AND CHROMATOGRAPHIC FRACTIONS

(mg/g TOC)

IKU-No	DEPTH (m)	EOM	Sat.	Aro.	HC	Non HC
A 6424	2283	109.2	1.2	3.4	4.6	104.6
A 5841	2300	39.0	2.4	3.4	5.8	33.2
A 5841	2300	112.3	24.4	7.1	31.5	80.9
A 6426	2303	42.8	2.0	4.0	6.0	36.7
A 5850	2435	35.2	10.8	13.6	24.4	10.8
A 5861	2600	37.9	9.1	10.6	19.7	18.2
A 5869	2720	57.3	13.4	14.5	27.9	29.4
A 5874	2795	132.2	5.1	17.3	22.4	109.8
A 6394	2975	111.7	26.0	10.4	36.4	75.3
A 6399	3050	47.9	3.6	5.4	9.0	38.8
A 6399	3050	79.2	5.9	12.9	18.8	60.4
A 6429	3148	20.4	1.0	1.2	2.2	18.2
A 6419	2661.60	311.1	72.6	60.1	132.7	178.4
A 6420	2668.05	814.7	284.1	201.4	485.5	329.2
A 6421	2706.00	3685.1	1231.9	857.0	2088.9	1596.1

DATE : 21 - 12 - 83.

T A B L E : 4d.

COMPOSITION IN % OF MATERIAL EXTRACTED FROM THE ROCK

IKU-No	DEPTH (m)	Sat / EOM	Aro / EOM	HC / EOM	SAT / Aro	Non HC / EOM	HC / Non HC
A 6424	2283	1.1	3.1	4.2	35.5	95.8	4.4
A 5841	2300	6.2	8.7	14.9	71.9	85.1	17.5
A 5841	2300	21.7	6.3	28.0	345.5	72.0	38.9
A 6426	2303	4.8	9.3	14.1	51.4	85.9	16.4
A 5850	2435	30.8	38.5	69.2	80.0	30.8	225.0
A 5861	2600	24.0	28.0	52.0	85.7	48.0	108.3
A 5869	2720	23.3	25.3	48.7	92.1	51.3	94.8
A 5874	2795	3.8	13.1	16.9	29.2	83.1	20.4
A 6394	2975	23.3	9.3	32.6	250.0	67.4	48.3
A 6399	3050	7.5	11.4	18.9	66.0	81.1	23.3
A 6399	3050	7.4	16.3	23.7	45.2	76.3	31.1
A 6429	3148	5.0	5.7	10.7	88.2	89.3	12.0
A 6419	2661.60	23.3	19.3	42.7	120.7	57.3	74.4
A 6420	2668.05	34.9	24.7	59.6	141.0	40.4	147.5
A 6421	2706.00	33.4	23.3	56.7	143.7	43.3	130.9

DATE : 21 - 12 - 83.

T A B L E 5.

TABULATION OF DATA FROM THE GASCHROMATOGRAMS

IKU No.	DEPTH (m)	PRISTANE / n-C17	PRISTANE / PHYTANE	CPI
A 6424	2283	2.2	1.1	0.8
A 5841	2300	1.9	1.2	2.1
A 6426	2303	3.6	2.1	0.9
A 5850	2435	1.5	2.3	1.7
A 5861	2600	1.1	2.2	1.6
A 5869	2720	1.1	2.1	1.3
A 5874	2795	1.1	2.6	1.3
A 6394	2975	1.4	5.4	1.3
A 6399	3050	1.7	5.6	1.1
A 6429	3148	0.7	6.1	1.1
A 6419	2661.60	0.5	2.7	1.1
A 6420	2668.05	0.6	1.3	0.9
A 6421	2706	0.6	1.2	1.0

DATE : 21 - 12 - 83.

Table 6. Molecular parameters calculated from GC-MS mass chromatograms.

		m/z 191						m/z 217	
IKU code	Sample type	Q/E	Z/E	X/E	αβ/αβ+βα[1]	%22S[2]	rearr./reg[3]	%20S[4]	%ββ[5]
A-5841	cuttings	0.06	2.54	0.08	0.82	58.3	1.1	54.0	44.6
A-5850	"	0.04	1.09	0.05	0.72	52.5	1.0	50.8	47.8
A-5861	"	0.04	1.09	0.08	0.66	44.6	1.0	37.2	47.7
A-5869	"	0.06	1.19	0.09	0.74	46.9	0.8	46.2	48.0
A-5874	"	0.05	0.67	0.07	0.72	49.2	0.6	42.5	49.0
A-6394	"	0.02	0.16	0.08	0.77	54.3	0.4	45.9	62.7
A-6399	"	0.01	-	0.10	0.77	59.8	0.2	46.9	57.8
A-6419	sst. core	0.10	0.10	0.22	0.86	62.1	0.9	45.5	70.9
A-6420	"	0.08	0.55	0.05	0.90	60.9	1.1	51.7	70.3
A-6421	"	0.07	0.56	0.06	0.90	57.8	1.1	53.8	75.7

1) E/E+F in m/z 191 (Figure 3)
2) J_1/J_1+J_2 in m/z 191 (Figure 3)
3) a+b/h+k in m/z 217 (Figure 3)
4) q/q+t in m/z 217 (Figure 3)
5) 2(r+s)/2(r+s)+q+t in m/z 217 (Figure 3)

Table 7. δ^{13} isotope data

IKU code	Sample type	SAT	ARO
A-6424	cuttings	- 30.6	- 30.2
A-5841	"	- 30.3	- 29.6
A-6426	"	- 28.3	- 26.8
A-6399	"	- 29.0	- 28.0
A-6429	"	- 28.5	- 26.6
A-6419	sst. Core	- 31.1	- 29.0
A-6420	"	- 31.3	- 30.6
A-6421	"	- 31.4	- 30.5

Table 8. Tentatively assigned methylphenanthrene ratios.

IKU code	Sample type	3+2/9+1 methylphenanthrenes
A-6424	SWC	-
A-5841	cuttings	0.8
A-6426	SWC	0.5
A-5850	cuttings	0.7
A-5861	"	0.8
A-5869	"	0.9
A-5874	"	0.8
A-6394	"	0.8
A-6399	"	0.9
A-6492	SWC	0.8
A-6419	sst. Core	1.0
A-6420	"	1.8
A-6421	"	1.4

FIGURE 1.

Gas chromatograms of saturated hydrocarbons

a - $n\text{-}C_{17}$
b, Pr - pristane
c, Ph - phytane

Printed at 16:02 on 26/Nov/83

RAW DATA PLOT-CHANNEL 3 Box 1 of 1

Analysis :050201A6424S Sample #: 1 Injection #: 1
Sample Name :A-6424,SAT,TB Maximum signal (%): 11.80

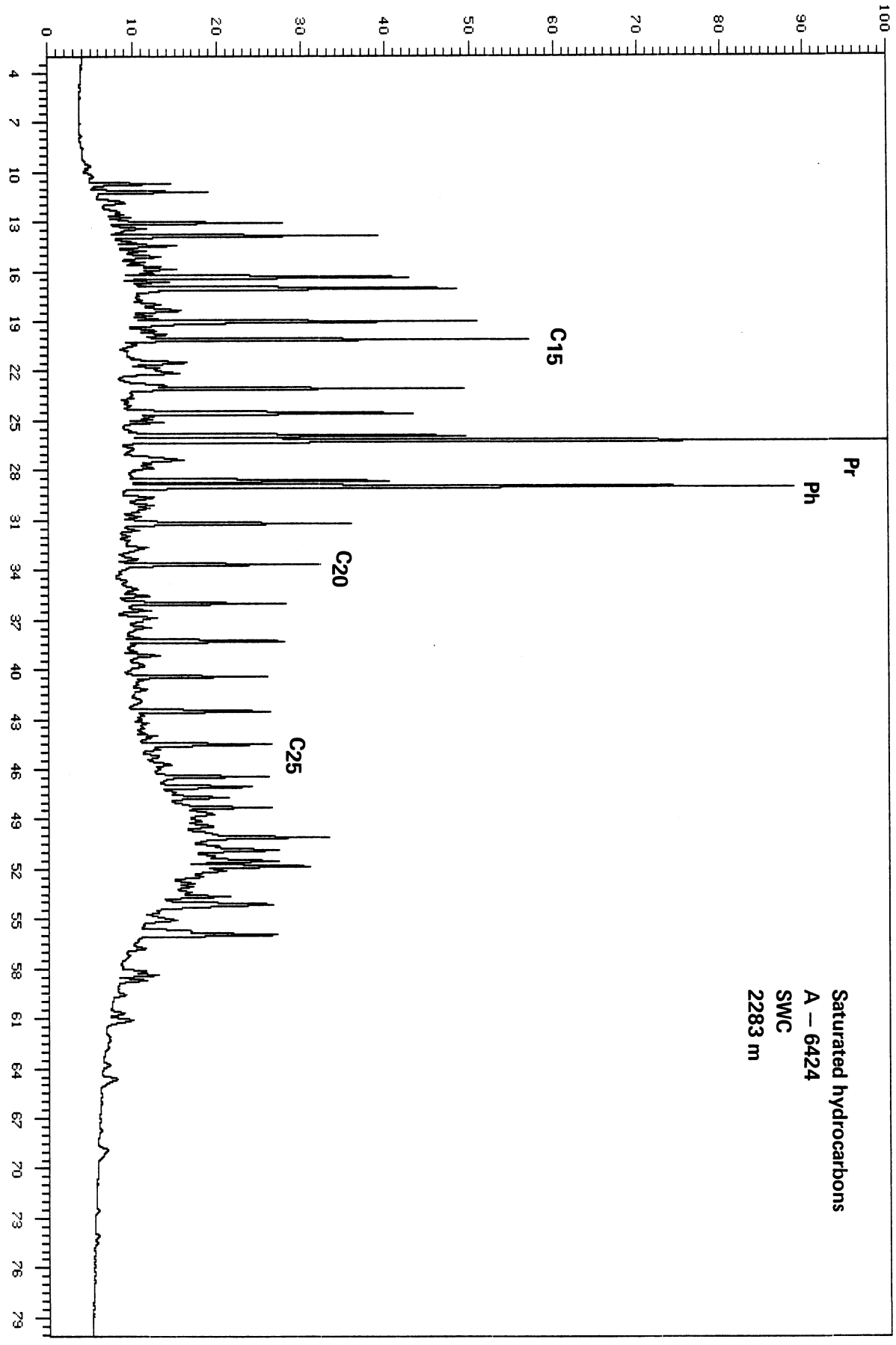

Printed at 10:05 on 26/Nov/83

RAW DATA PLOT-CHANNEL 3 Box 1 of 1

Analysis :050201A5841S Sample #: 1 Injection #: 1
Sample Name :A-5841,SAT,TB Maximum signal (%): 5.15

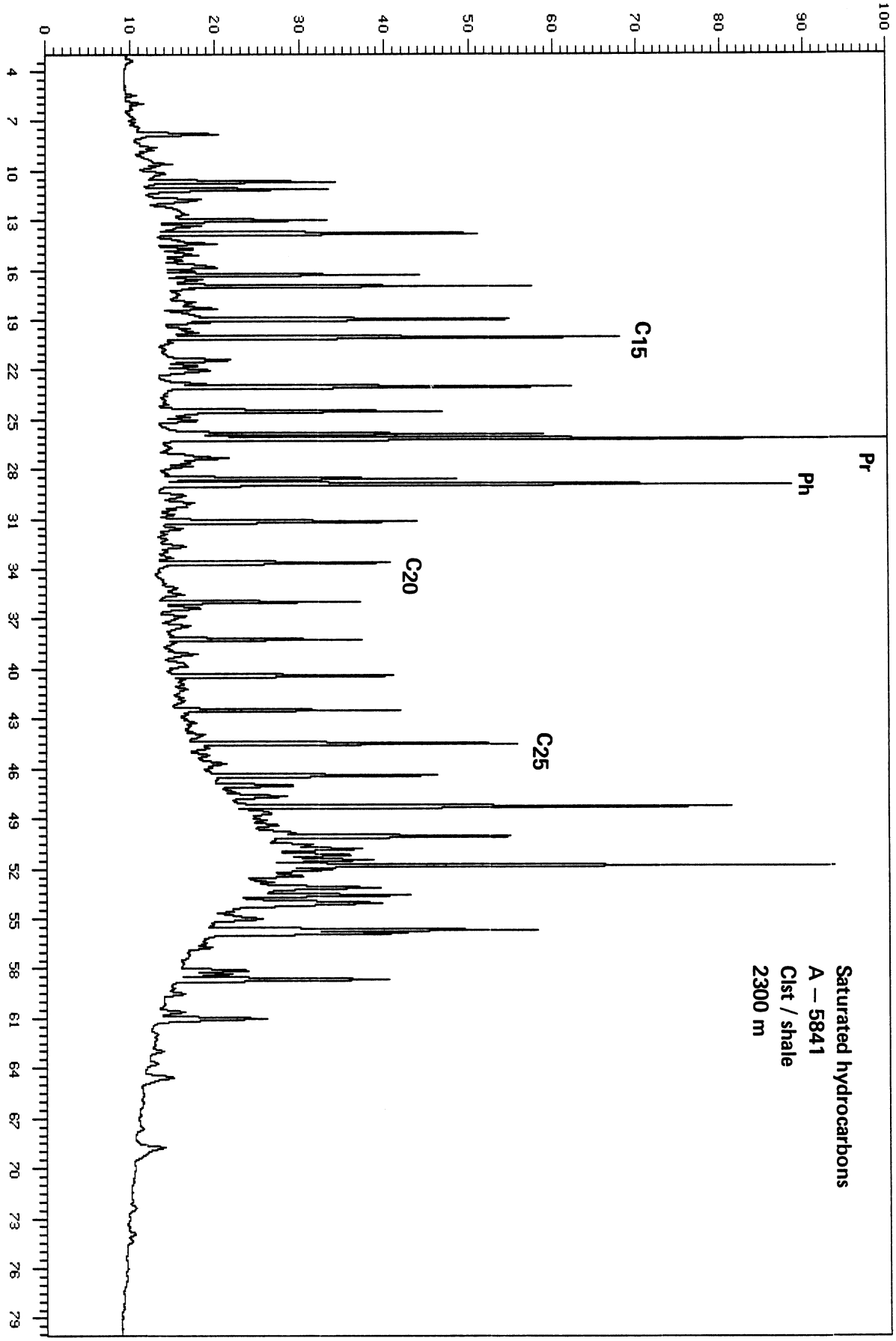

Printed at 12:58 on 26/Nov/83

RAW DATA PLOT-CHANNEL 3 Box 1 of 1

Analysis :050201A6426S Sample #: 1 Injection #: 1
Sample Name :A-6426,SAT,TB Maximum signal (%): 5.96

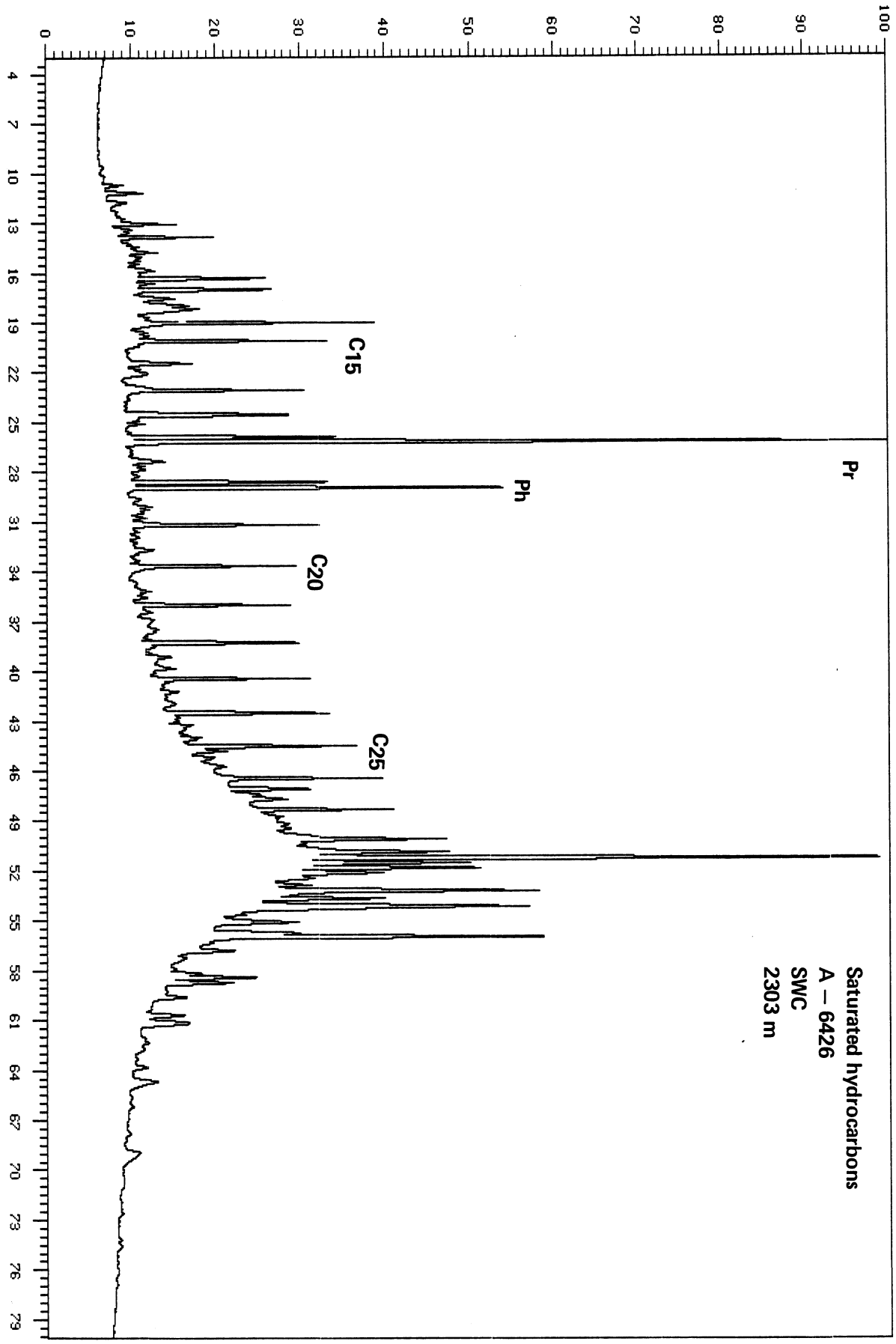

Printed at 23:21 on 25/Jul/83

RAW DATA PLOT-CHANNEL 5 Box 1 of 1

Analysis :50138A5850S1 Sample #: 1 Injection #: 1
Sample Name :A-5850,S,6610/7-1,TV Maximum signal (%): 6.63

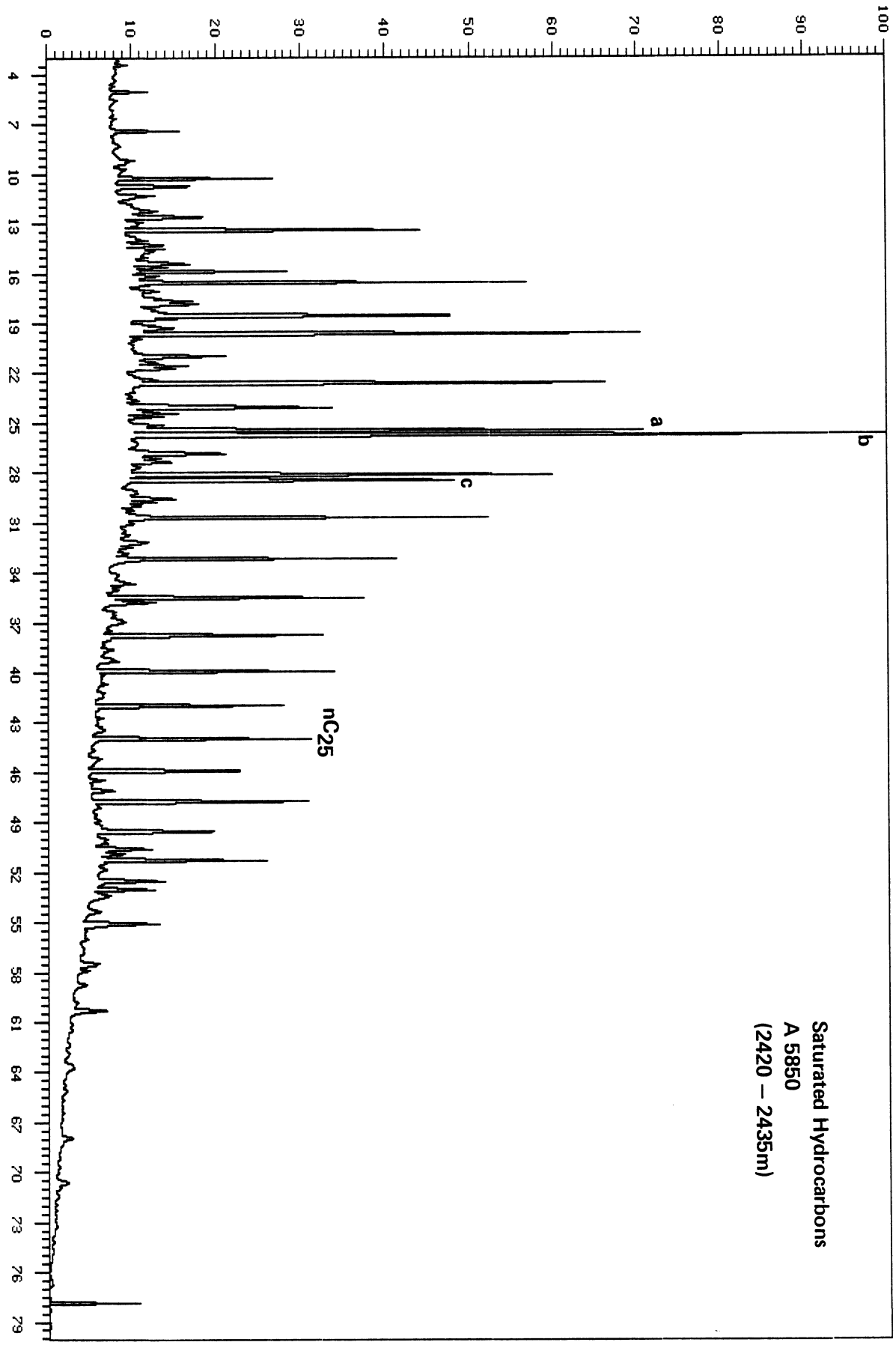

Printed at 14:51 on 28/Jul/83

RAW DATA PLOT-CHANNEL 5

Box 1 of 1

Analysis :50138A5861S1 Sample #: 1 Injection #: 1
Sample Name :A5861,c,6610/7-1,TV Maximum signal (%): 12.60

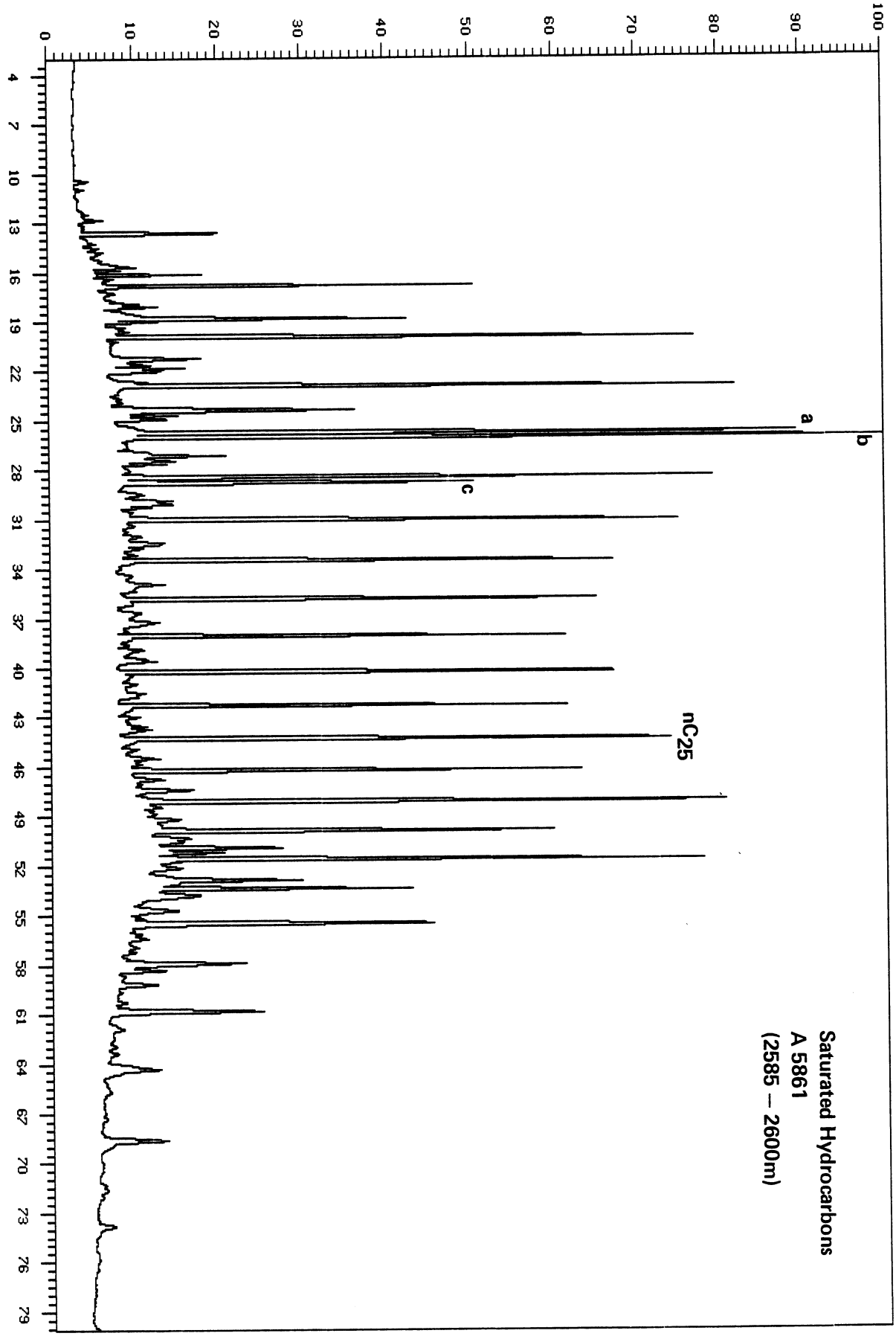

Printed at 17:17 on 29/Jul/83

RAW DATA PLOT-CHANNEL 5 Box 1 of 1

Analysis :50138A5869S1 Sample #: 1 Injection #: 1
Sample Name :A-5869,S,6610/7-1,TV Maximum signal (%): 21.21

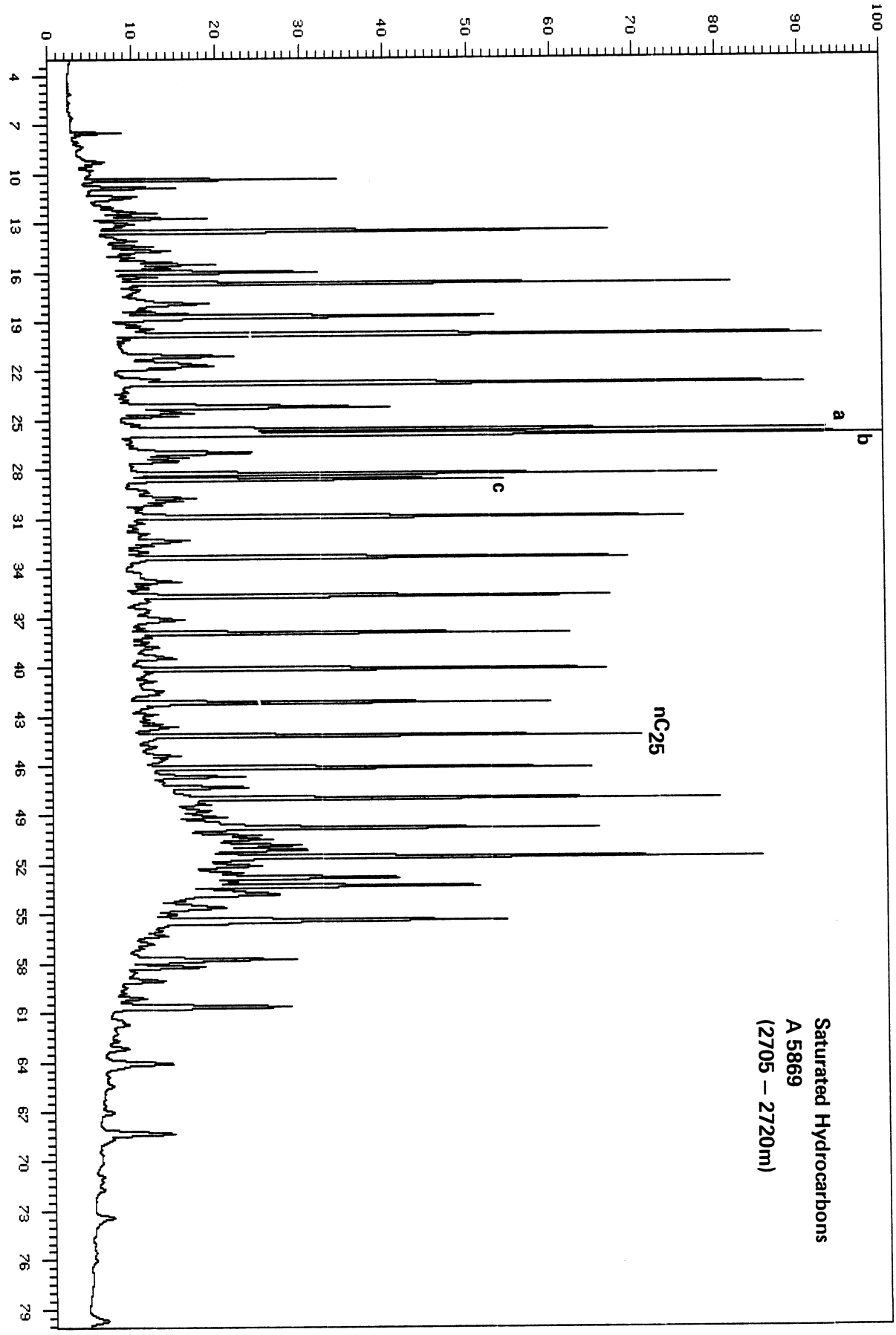

Printed at 09:57 on 28/Jul/83

RAW DATA PLOT-CHANNEL 5 Box 1 of 1

Analysis :50138A5874S1 Sample #: 1 Injection #: 1
Sample Name :A-5874,S,6610/7-1,TV Maximum signal (%): 25.27

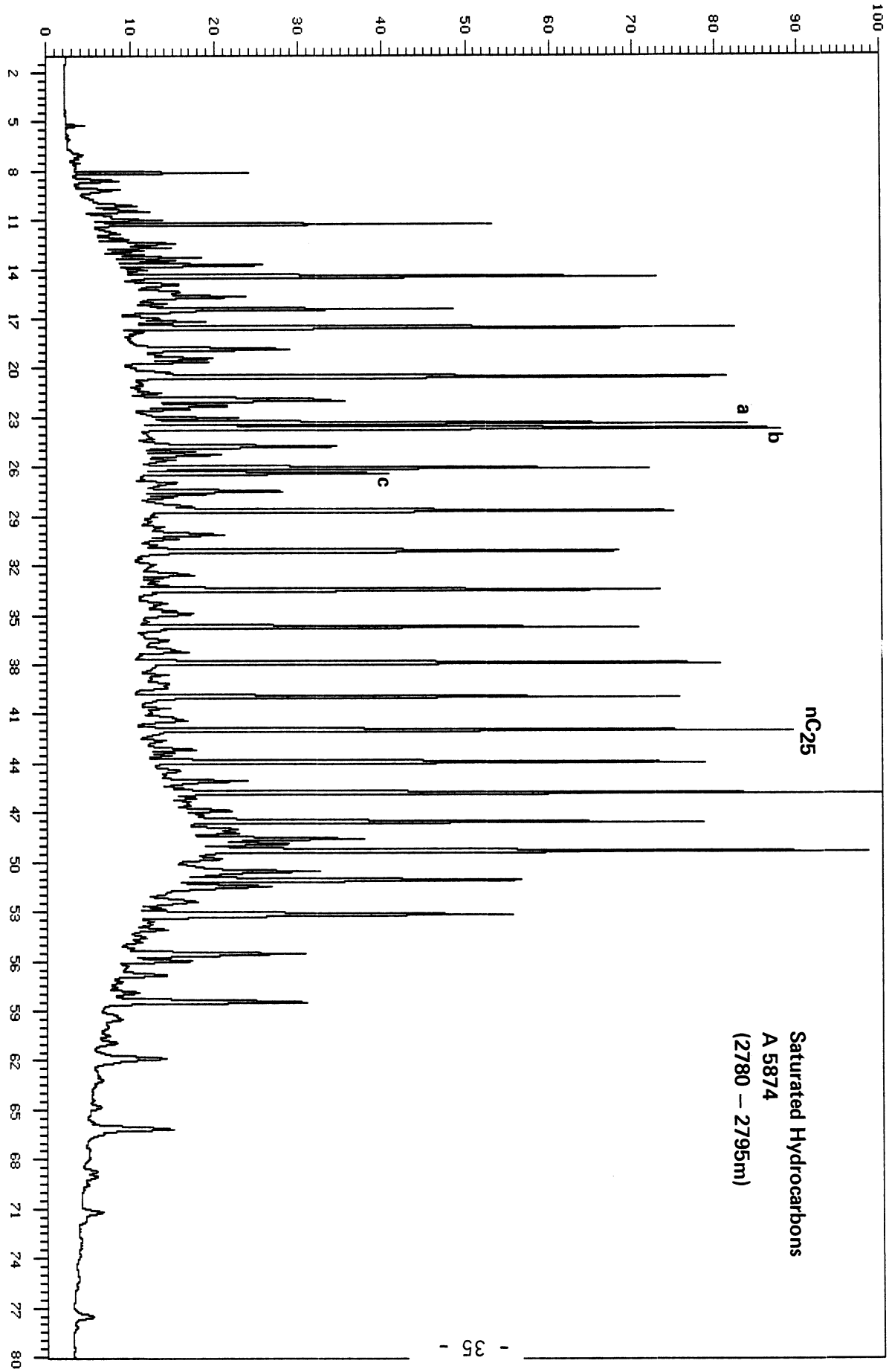

Printed at 00:59 on 26/Jul/83

RAW DATA PLOT-CHANNEL 5 Box 1 of 1

Analysis :50138A6394S1 Sample #: 1 Injection #: 1
Sample Name :A-6394,S,6610/7-1,TV Maximum signal (%): 9.52

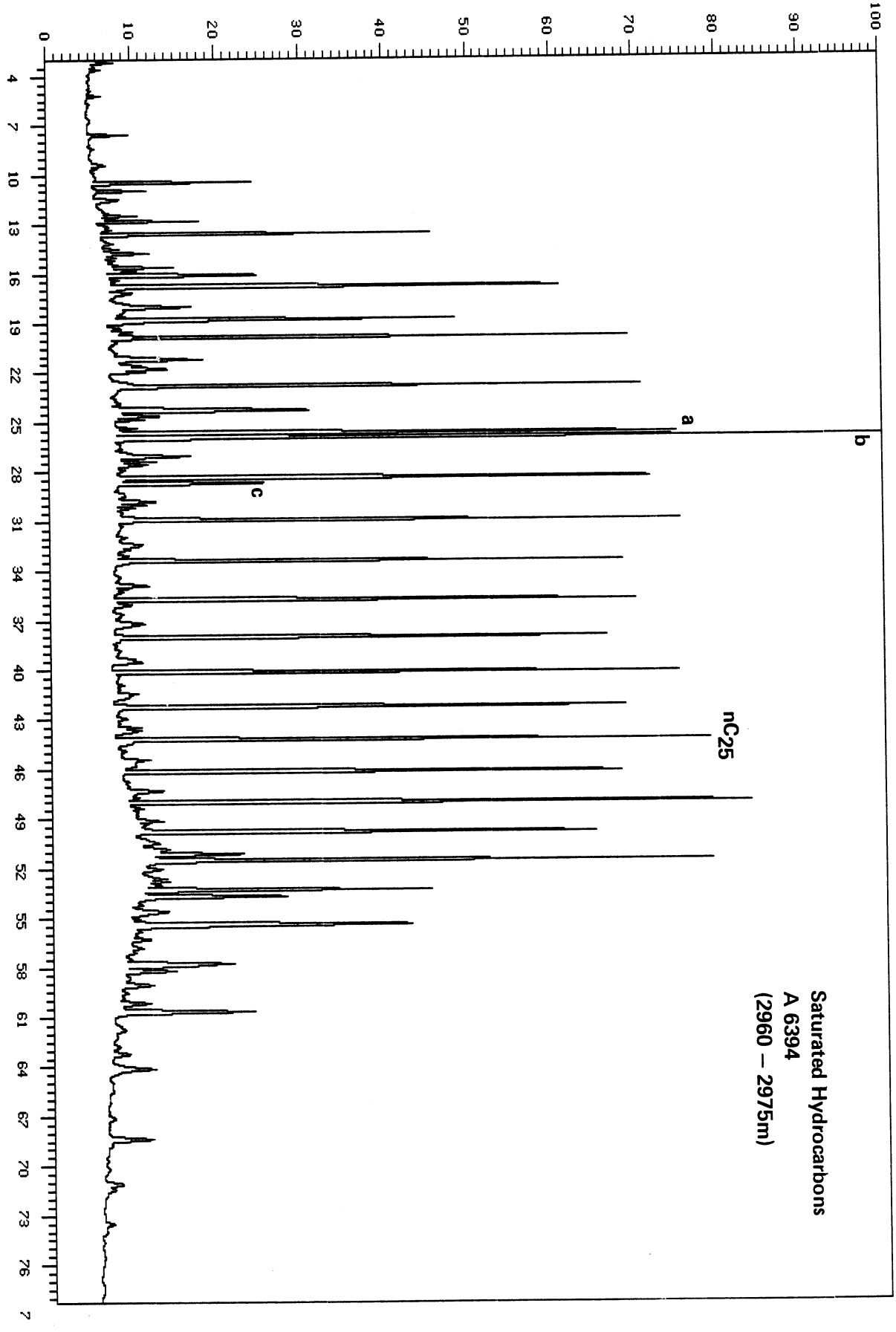

Printed at 17:19 on 29/Jul/83

RAW DATA PLOT-CHANNEL 5 Box 1 of 1

Analysis :50138A6399S1 Sample #: 1 Injection #: 1
Sample Name :A-6399,S,6610/7-1,TV Maximum signal (%): 21.03

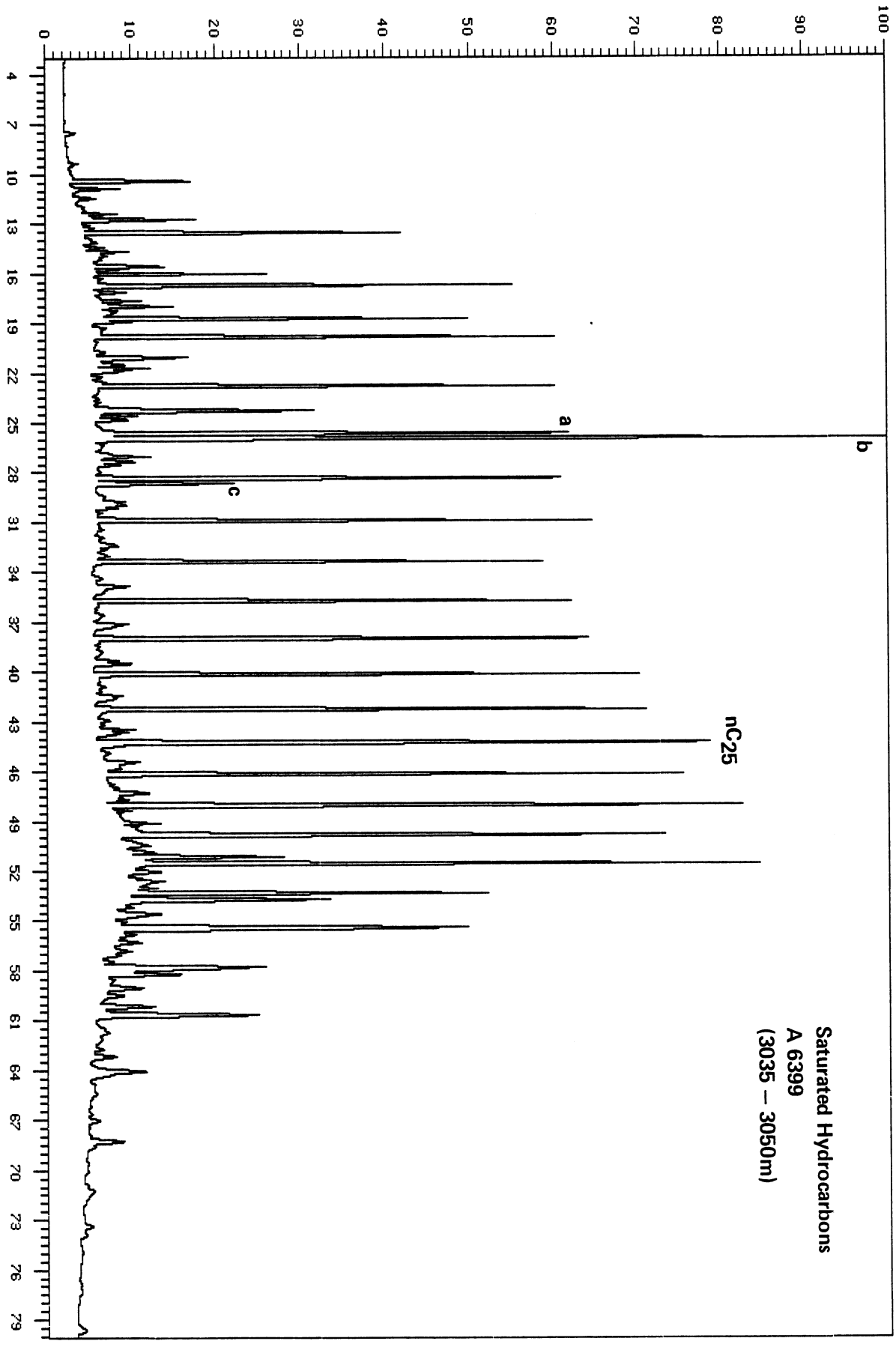

Printed at 19:09 on 26/Nov/83

RAW DATA PLOT-CHANNEL 3 Box 1 of 1

Analysis :050201A6429S Sample #: 1 Injection #: 1
Sample Name :A-6429,SAT,TB Maximum signal (%): 17.43

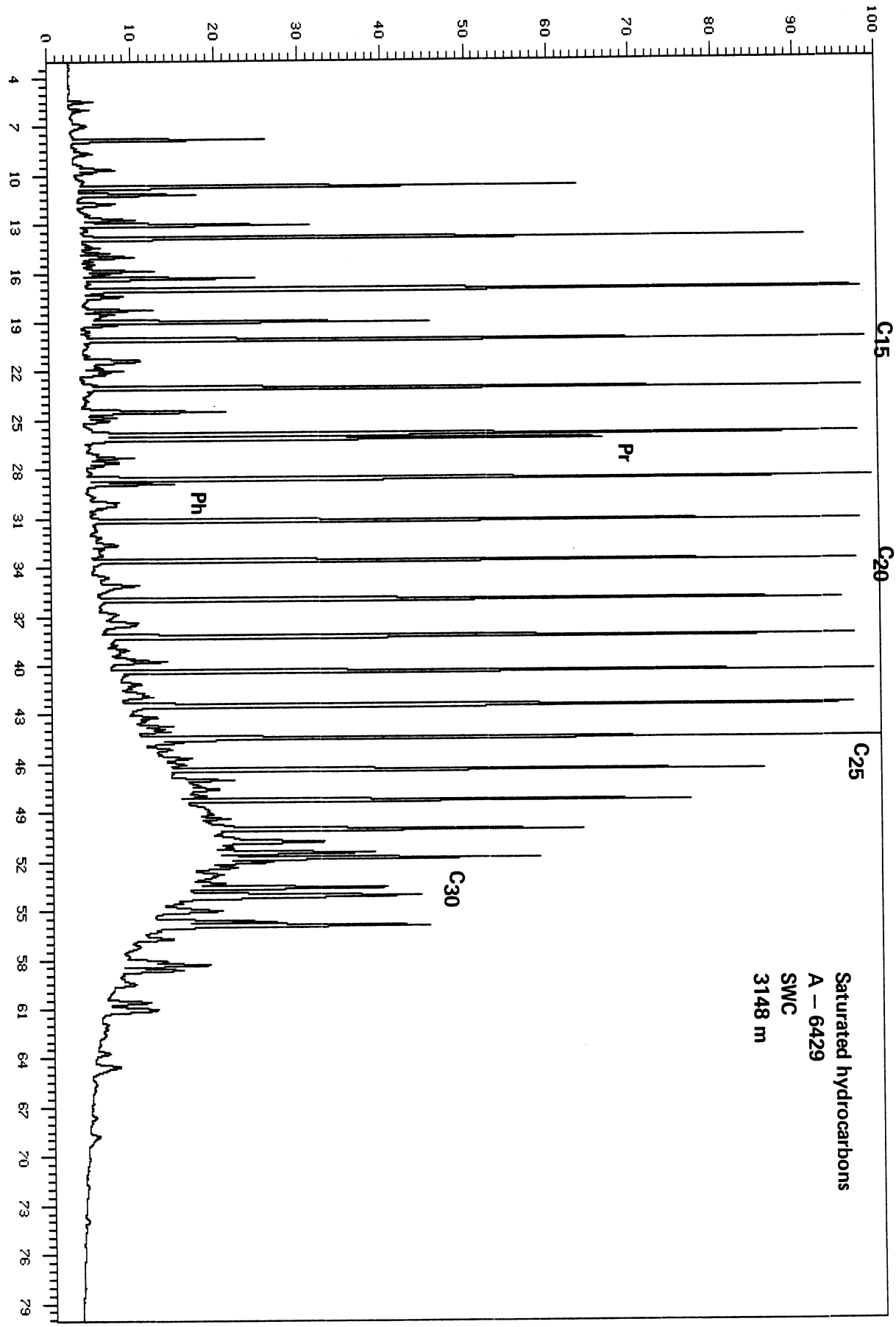

Printed at 16:13 on 30/Jul/83

RAW DATA PLOT-CHANNEL 5 Box 1 of 1

Analysis :50138A6419S1 Sample #: 1 Injection #: 1
Sample Name :A-6419,S,6610/7-1,TV Maximum signal (%): 21.86

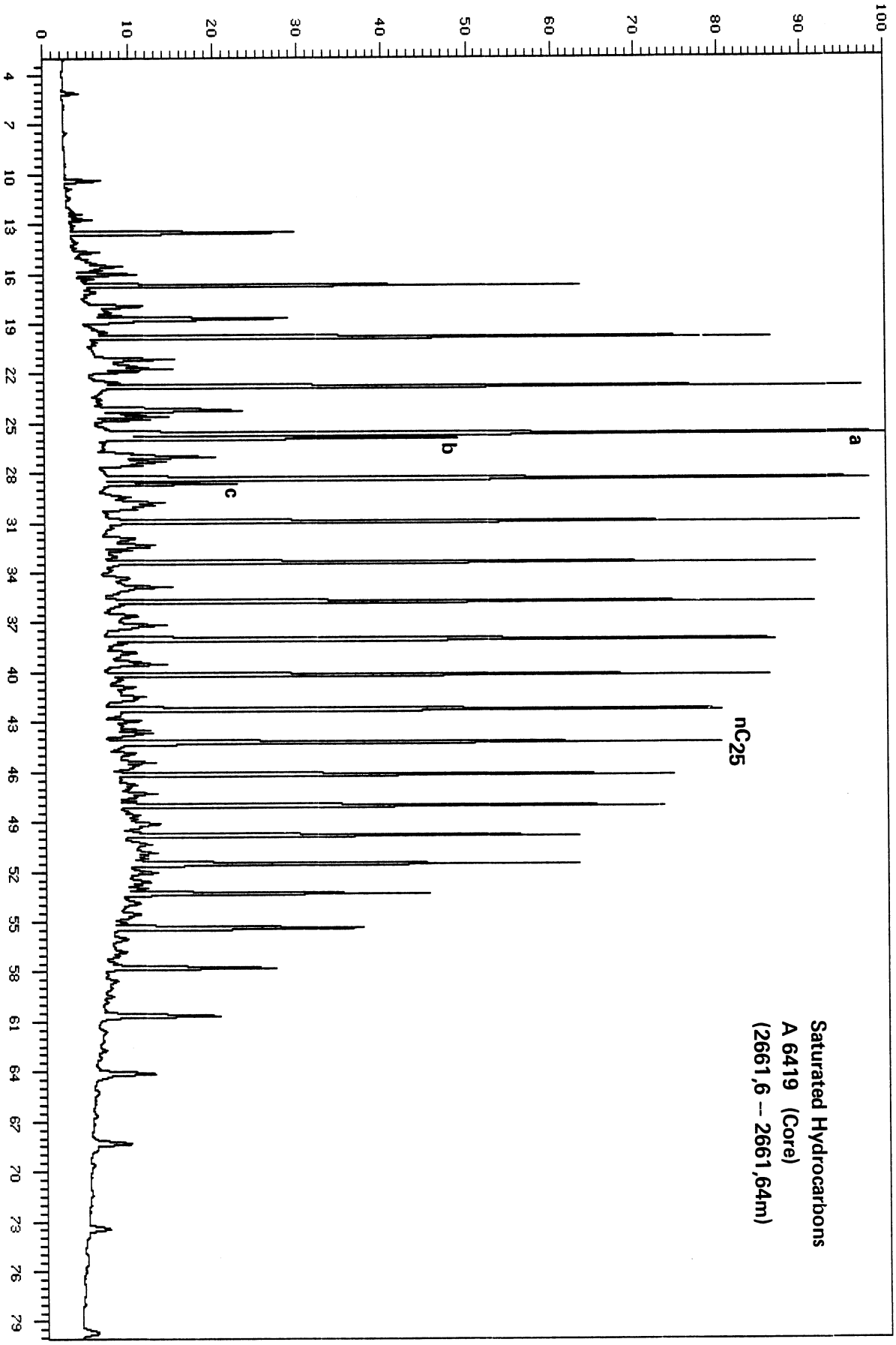

Printed at 16:20 on 30/Jul/83

RAW DATA PLOT-CHANNEL 5 Box 1 of 1

Analysis :50138A6420S1 Sample #: 1 Injection #: 1
Sample Name :A-6420,S,6610/7-1,TV Maximum signal (%): 11.29

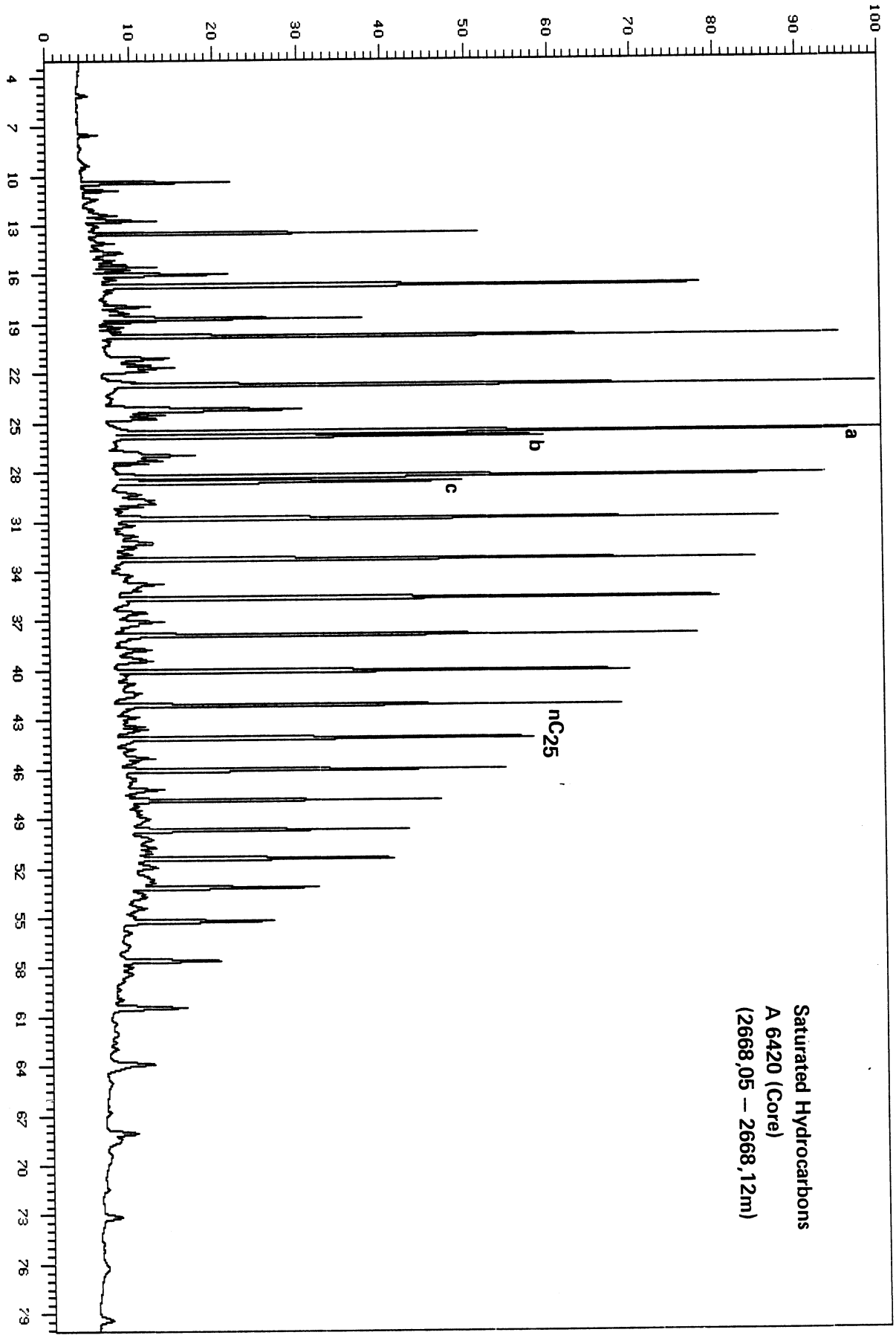

Printed at 16:56 on 30/Jul/83

PAW DATA PLOT-CHANNEL 5 Box 1 of 1

Analysis :50138A6421S1 Sample #: 1 Injection #: 1
Sample Name :A-6421,S,6610/7-1,TV Maximum signal (%): 19.22

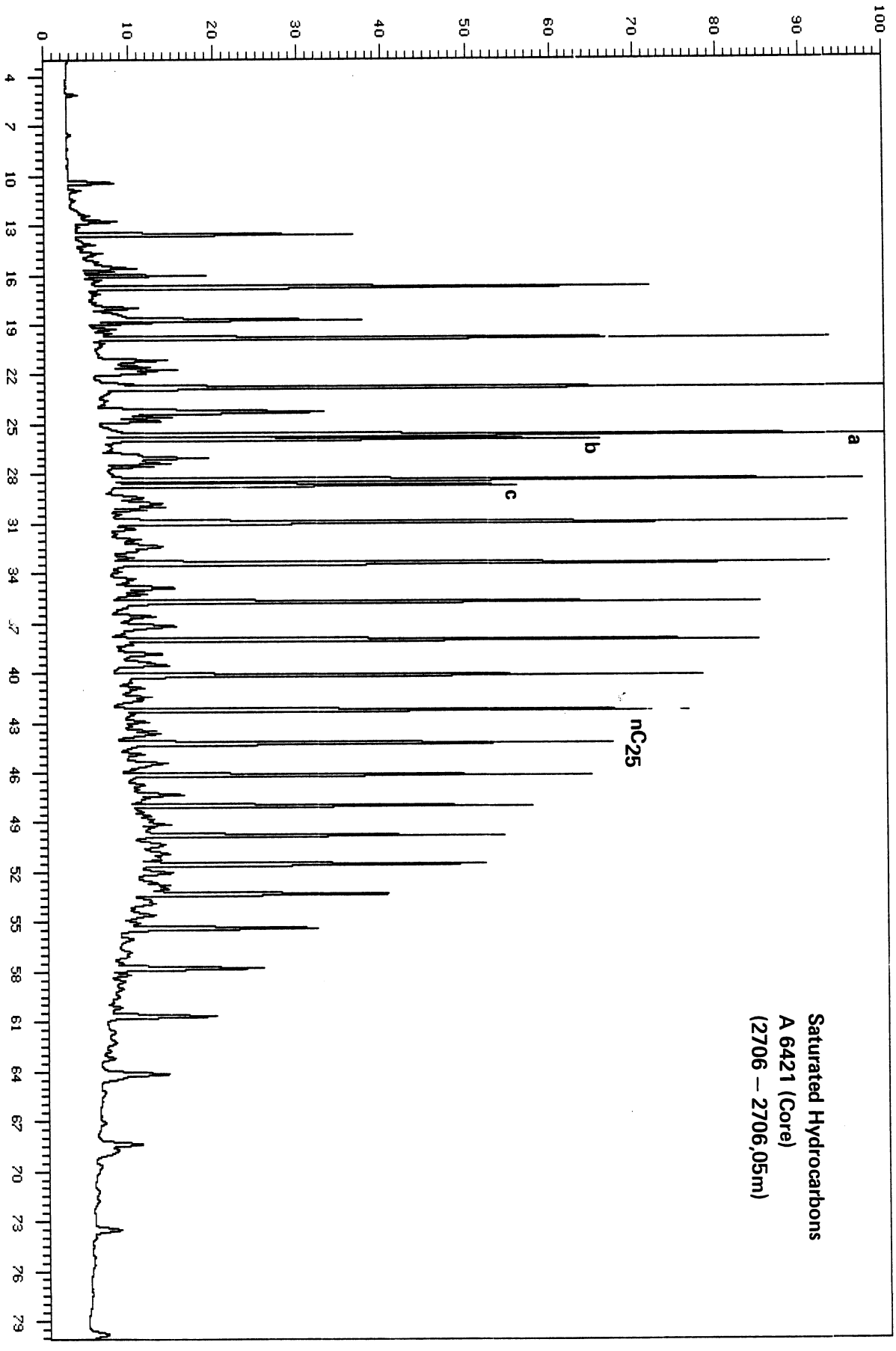

FIGURE 2.

Gas chromatograms of aromatic hydrocarbons

N - naphthalene
MN - C_1-naphthalenes
DMN - C_2-naphthalenes
TMN - C_3-naphthalenes
P - phenanthrene
MP - C_1-phenanthrene
DMP - C_2-phehanthrene
A - aromatic sterane region

Printed at 13:46 on 05/Dec/83

RAW DATA PLOT-CHANNEL 4 Box 1 of 1

Analysis :050201A6424A Sample #: 1 Injection #: 1
Sample Name :A-6424,ARO;JA Maximum signal (%): 8.01

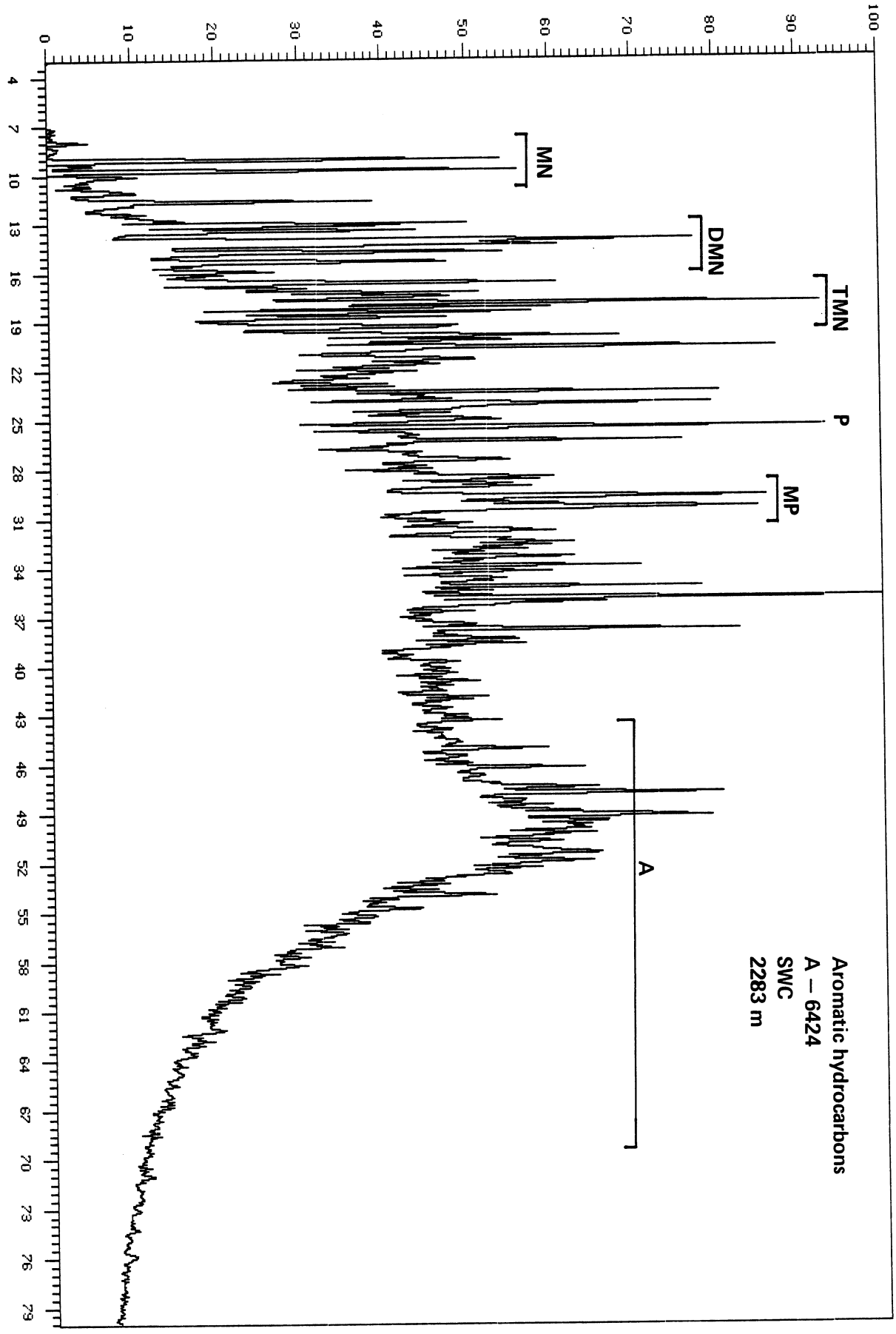

Printed at 08:49 on 20/Oct/83

RAW DATA PLOT-CHANNEL 4 Box 1 of 1

Analysis :50201A5841A1 Sample #: 1 Injection #: 1
Sample Name :A5841,ARO,EH Maximum signal (%): 37.42

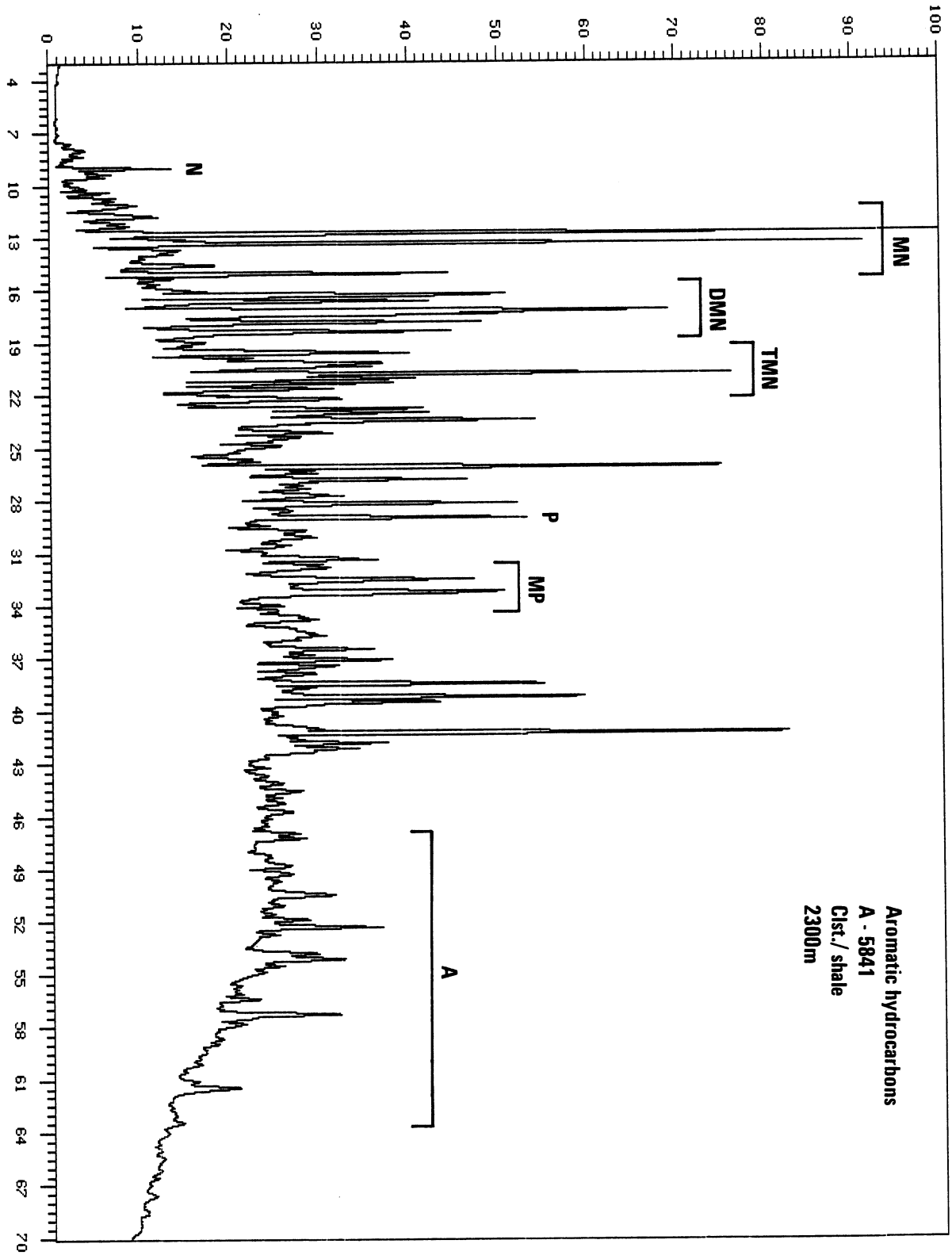

Printed at 13:49 on 05/Dec/83

RAW DATA PLOT-CHANNEL 4

Box 1 of 1

Analysis :080211A6426A Sample #: 1 Injection #: 1
Sample Name :A-6426,ARO,JA Maximum signal (%): 17.42

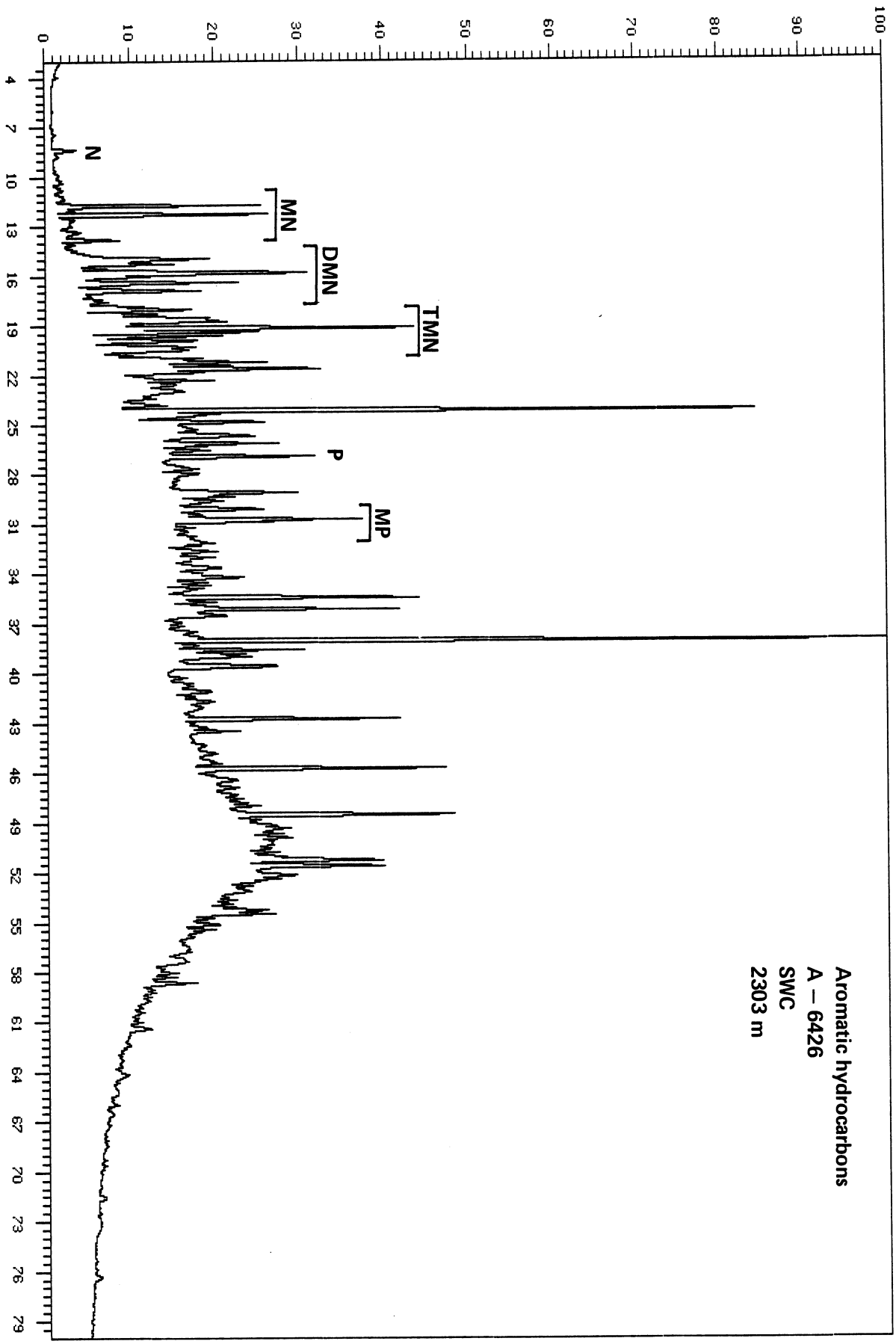

Printed at 12:46 on 20/Oct/83

RAW DATA PLOT-CHANNEL 4 Box 1 of 1

Analysis :50201A5850A1 Sample #: 1 Injection #: 1
Sample Name :A5850,ARO,EH Maximum signal (%): 10.14

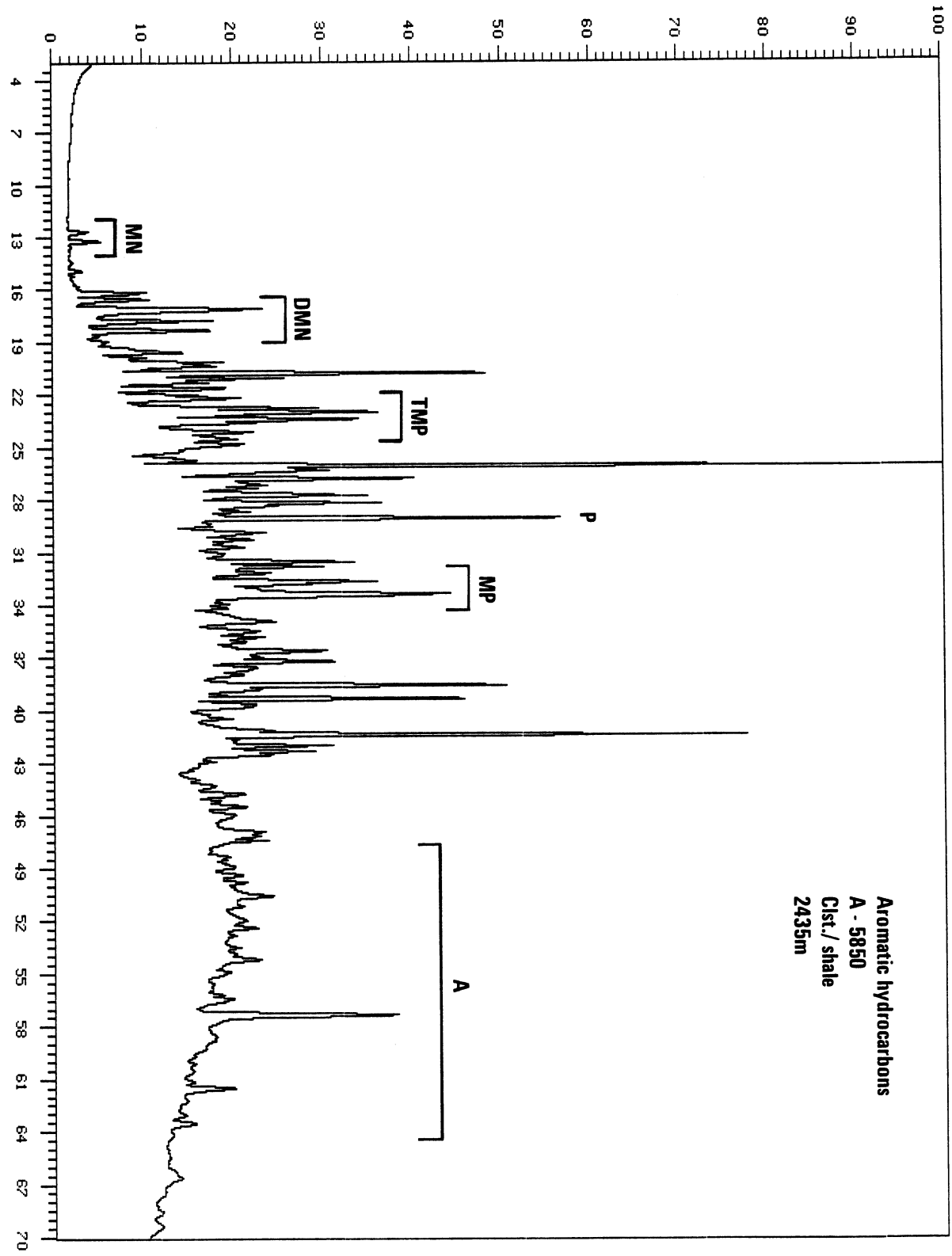

Printed at 14:54 on 20/Oct/83

RAW DATA PLOT-CHANNEL 4 Box 1 of 1

Analysis :50201A5861A1 Sample #: 1 Injection #: 1
Sample Name :A5861,ARO,EH Maximum signal (%): 9.48

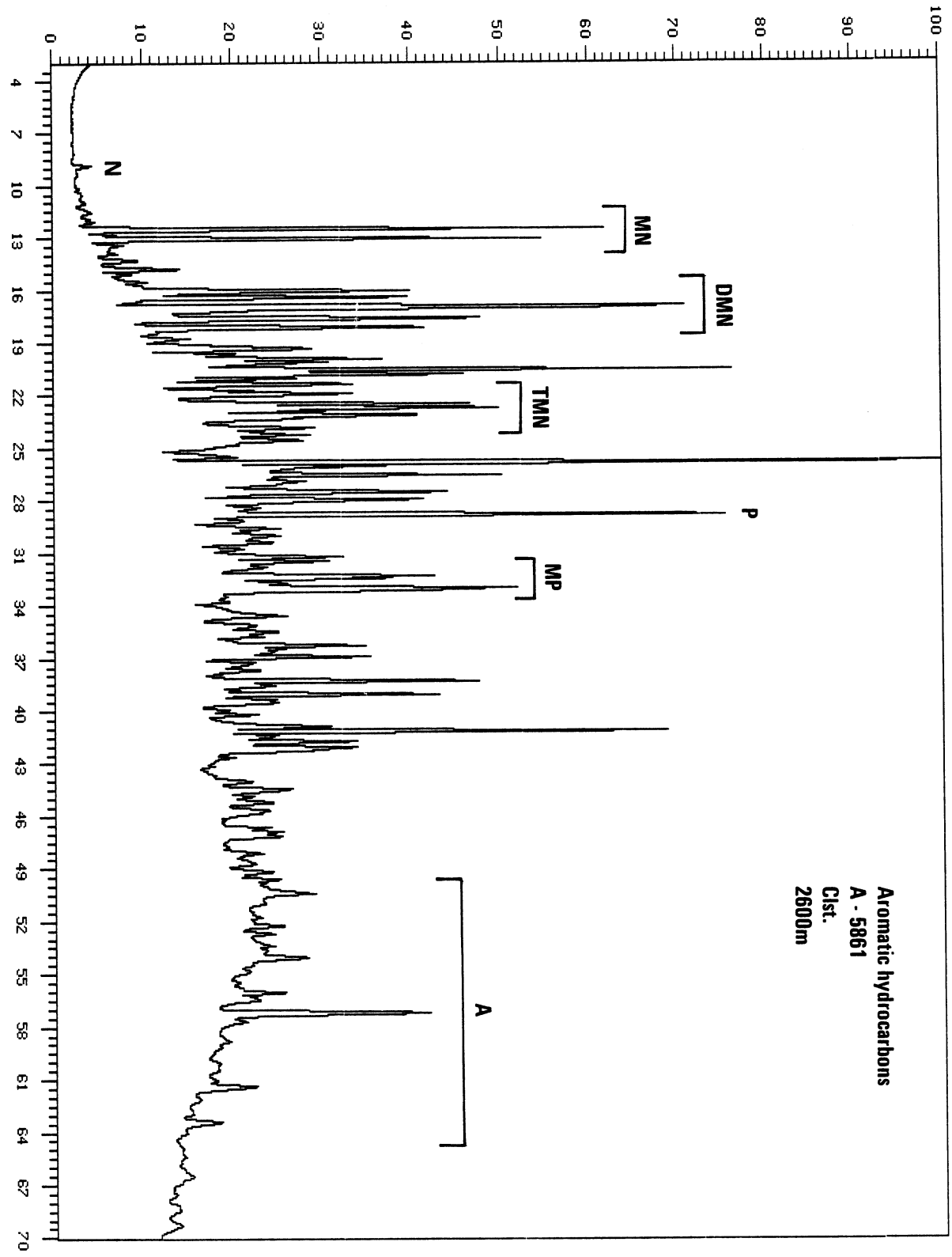

Printed at 16:22 on 20/Oct/83

RAW DATA PLOT-CHANNEL 4 Box 1 of 1

Analysis :50201A5869A1 Sample #: 1 Injection #: 1
Sample Name :A5869,ARO,EH Maximum signal (%): 18.16

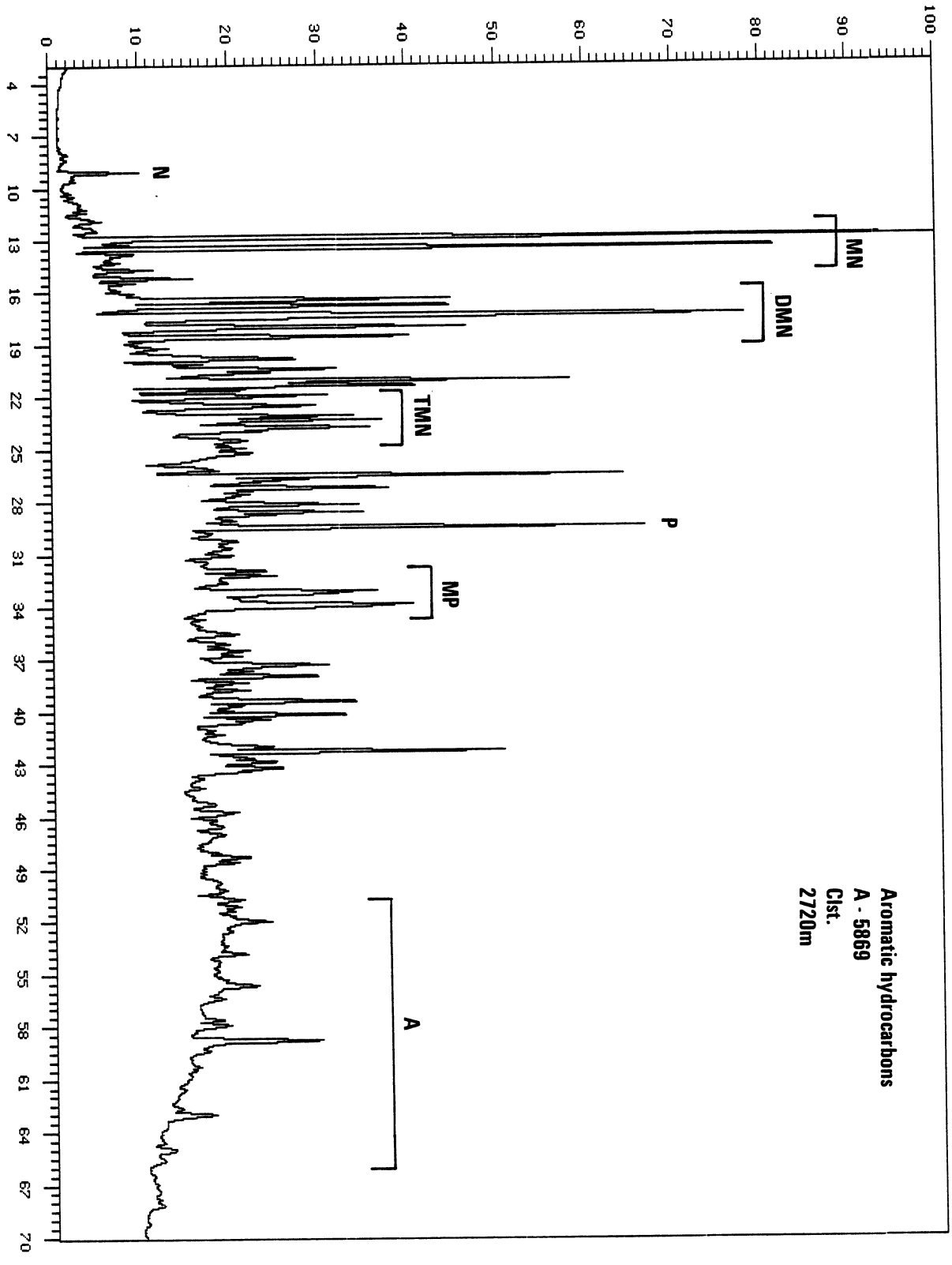

Printed at 08:27 on 21/Oct/83

RAW DATA PLOT-CHANNEL 4 Box 1 of 1

Analysis :50201A5874A1 Sample #: 1 Injection #: 1
Sample Name :A5874,ARO,EH Maximum signal (%): 15.95

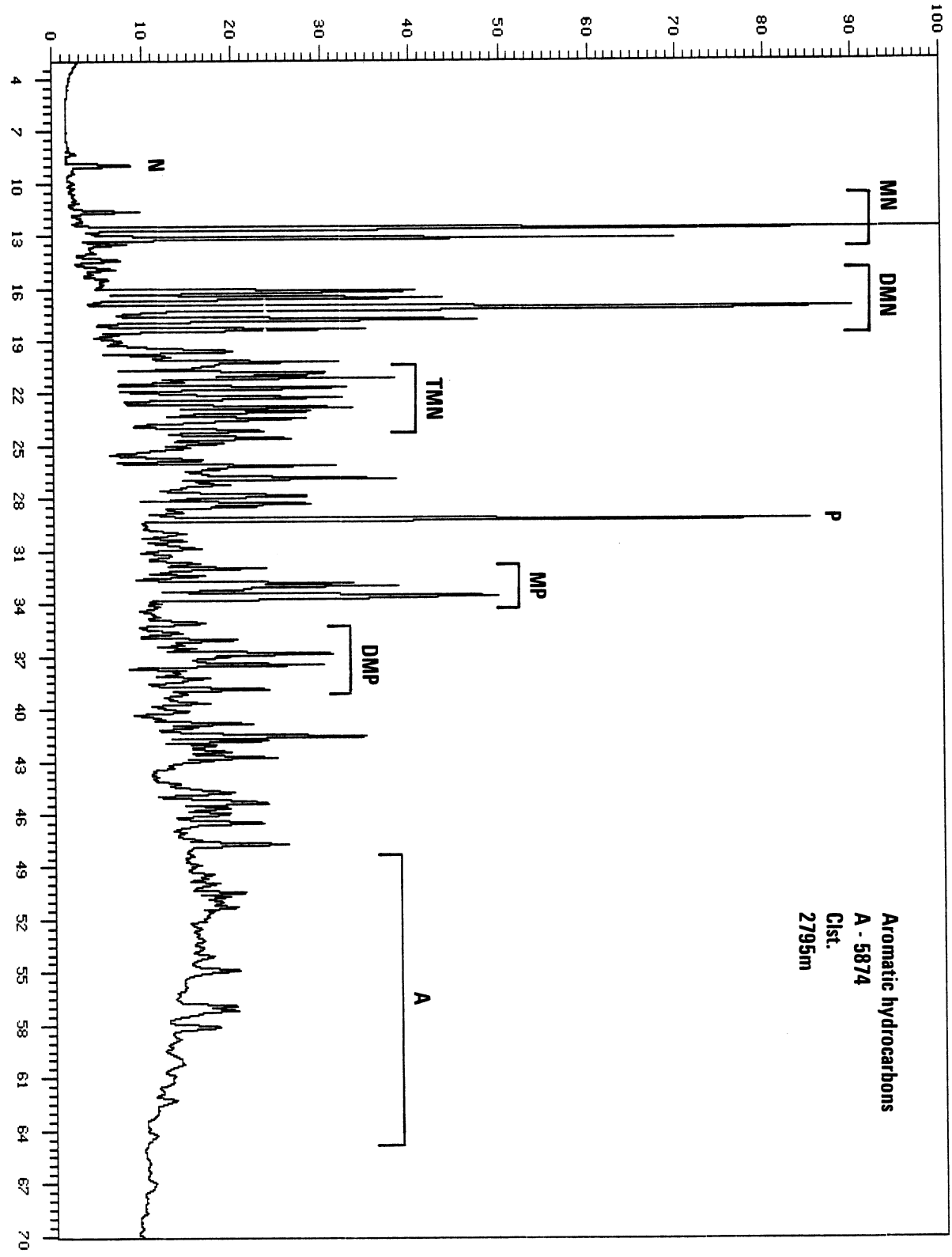

Printed at 10:36 on 21/Oct/83

RAW DATA PLOT-CHANNEL 4 Box 1 of 1

Analysis :50201A6394A1 Sample #: 1 Injection #: 1
Sample Name :A6394,ARO,EH Maximum signal (%): 20.10

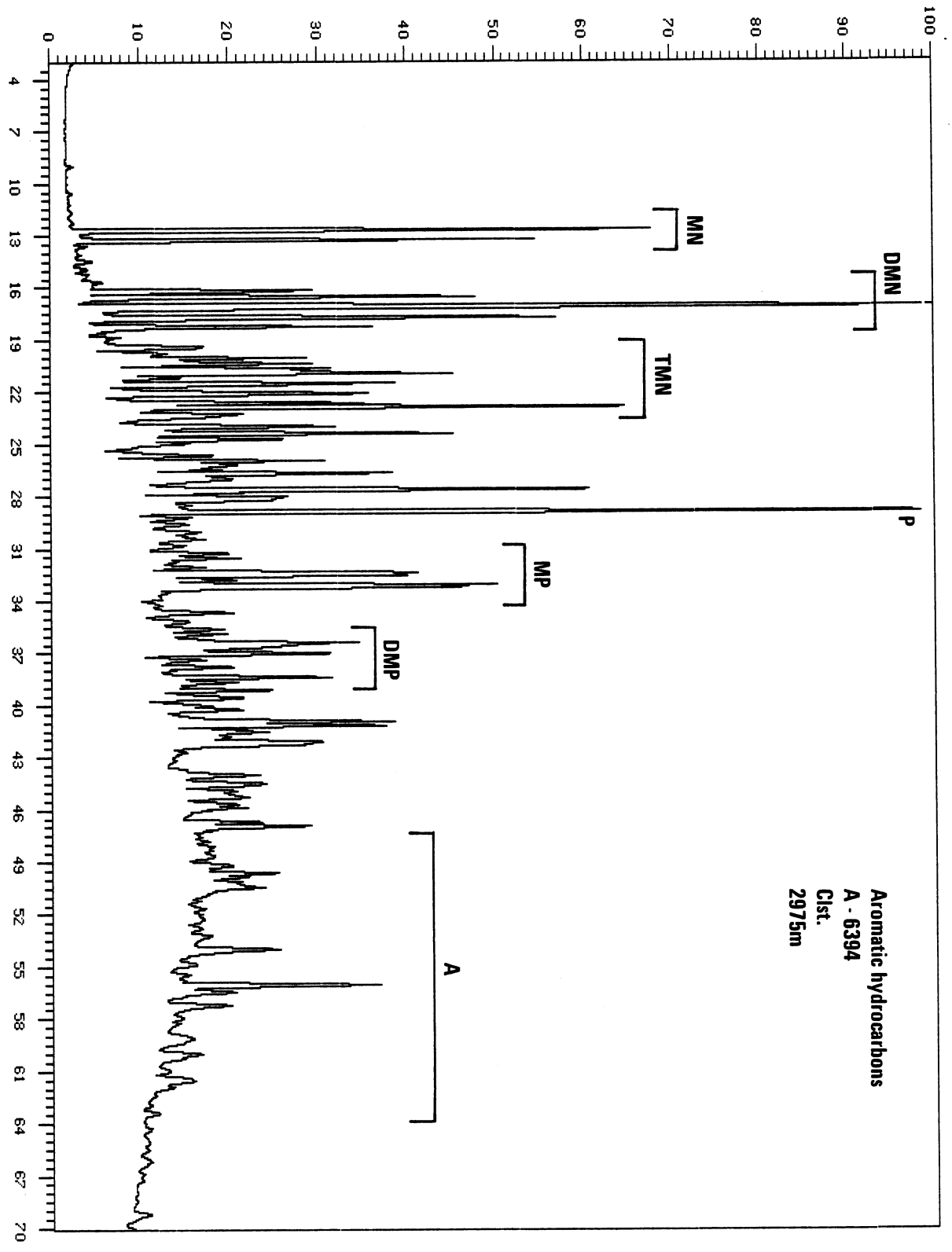

Printed at 15:10 on 21/Oct/83

RAW DATA PLOT-CHANNEL 4 Box 1 of 1

Analysis :50201A6399A1 Sample #: 1 Injection #: 1
Sample Name :A6399,ARO,EH Maximum signal (%): 42.70

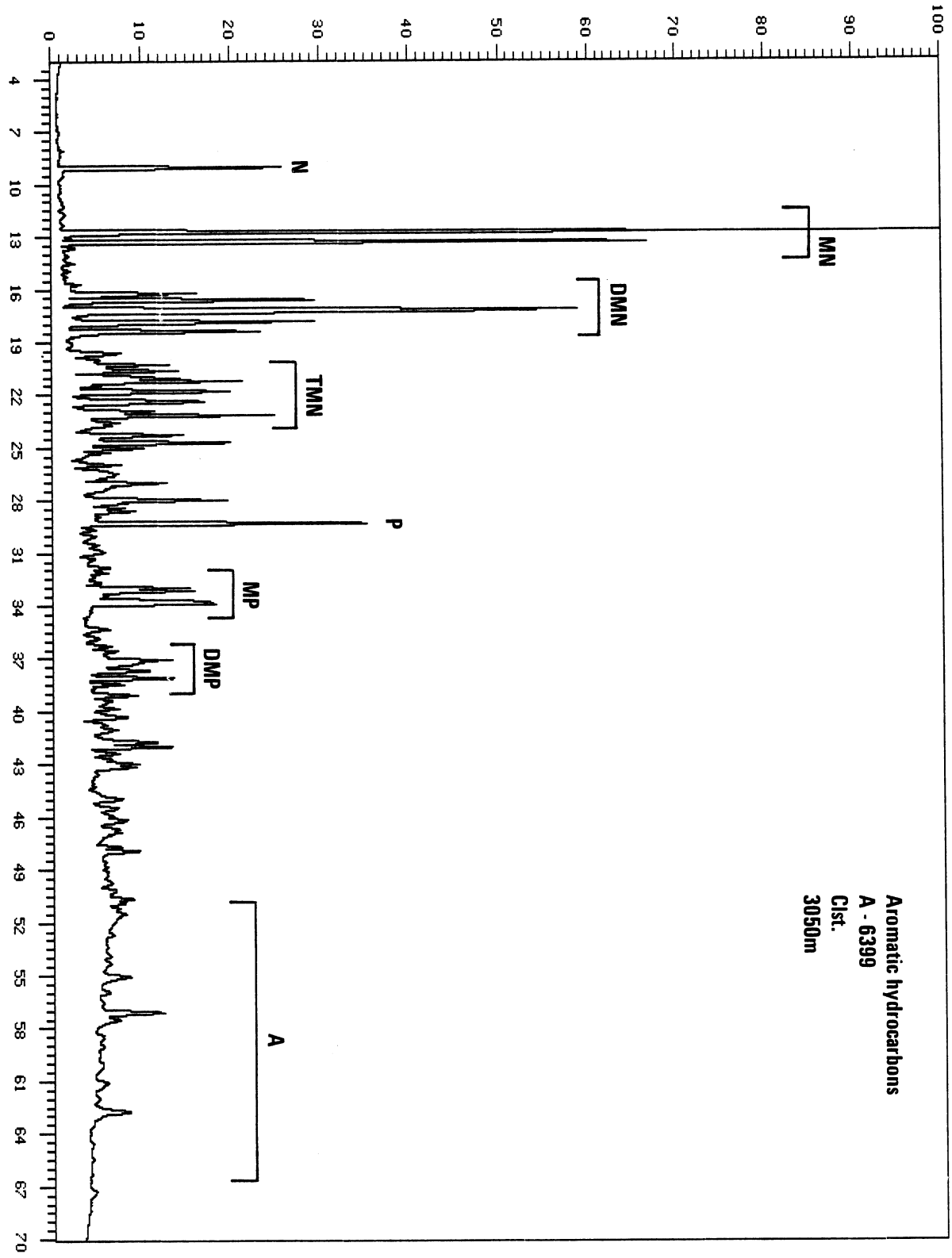

Printed at 13:54 on 05/Dec/83

RAW DATA PLOT-CHANNEL 4 Box 1 of 1

Analysis :05020iA6429A Sample #: 1 Injection #: 1
Sample Name :A-6429,ARO.JA Maximum signal (%): 16.47

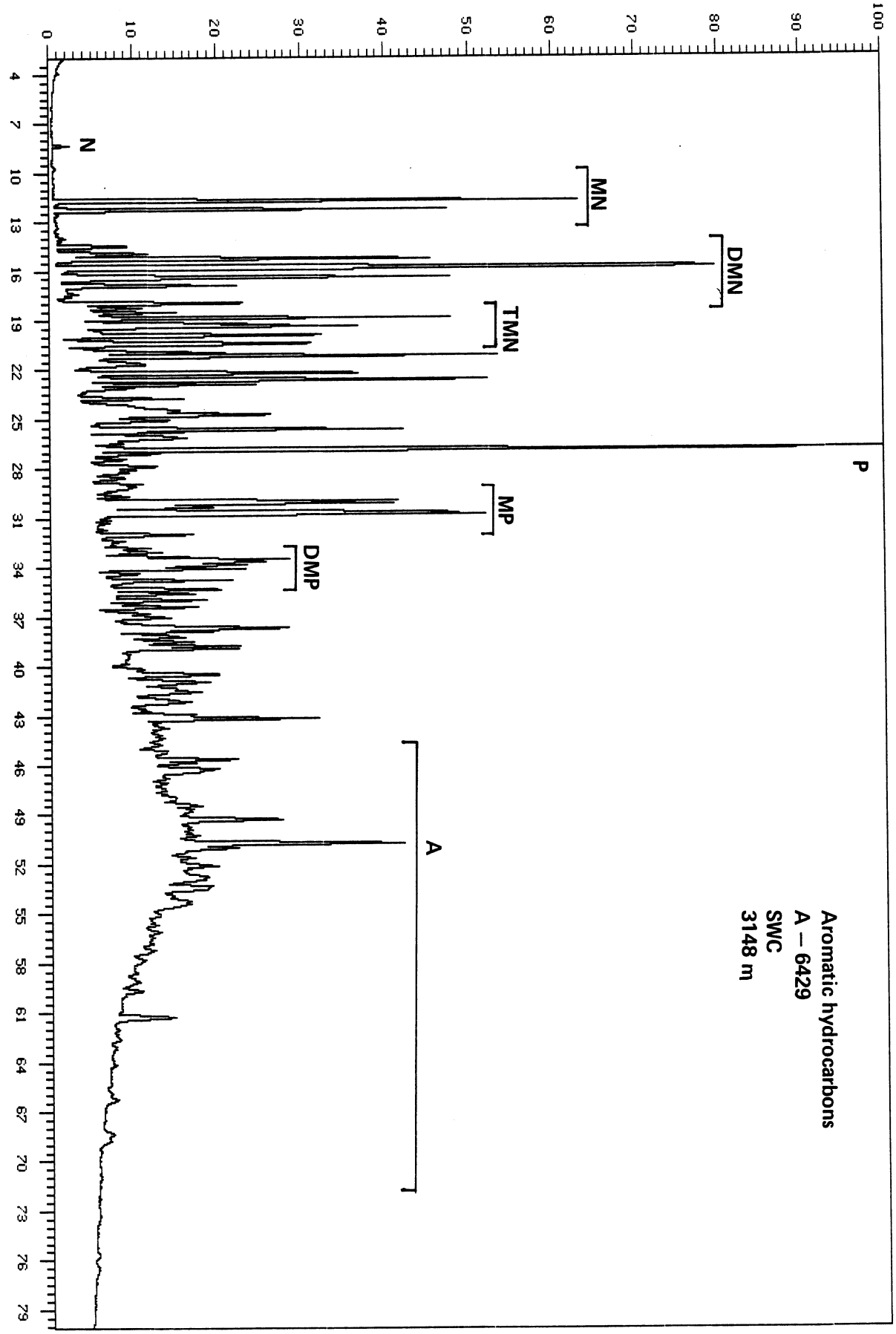

Printed at 16:29 on 21/Oct/83

RAW DATA PLOT-CHANNEL 4 Box 1 of 1

Analysis :50201A6419A1 Sample #: 1 Injection #: 1
Sample Name :A6419,ARO,EH Maximum signal (%): 11.10

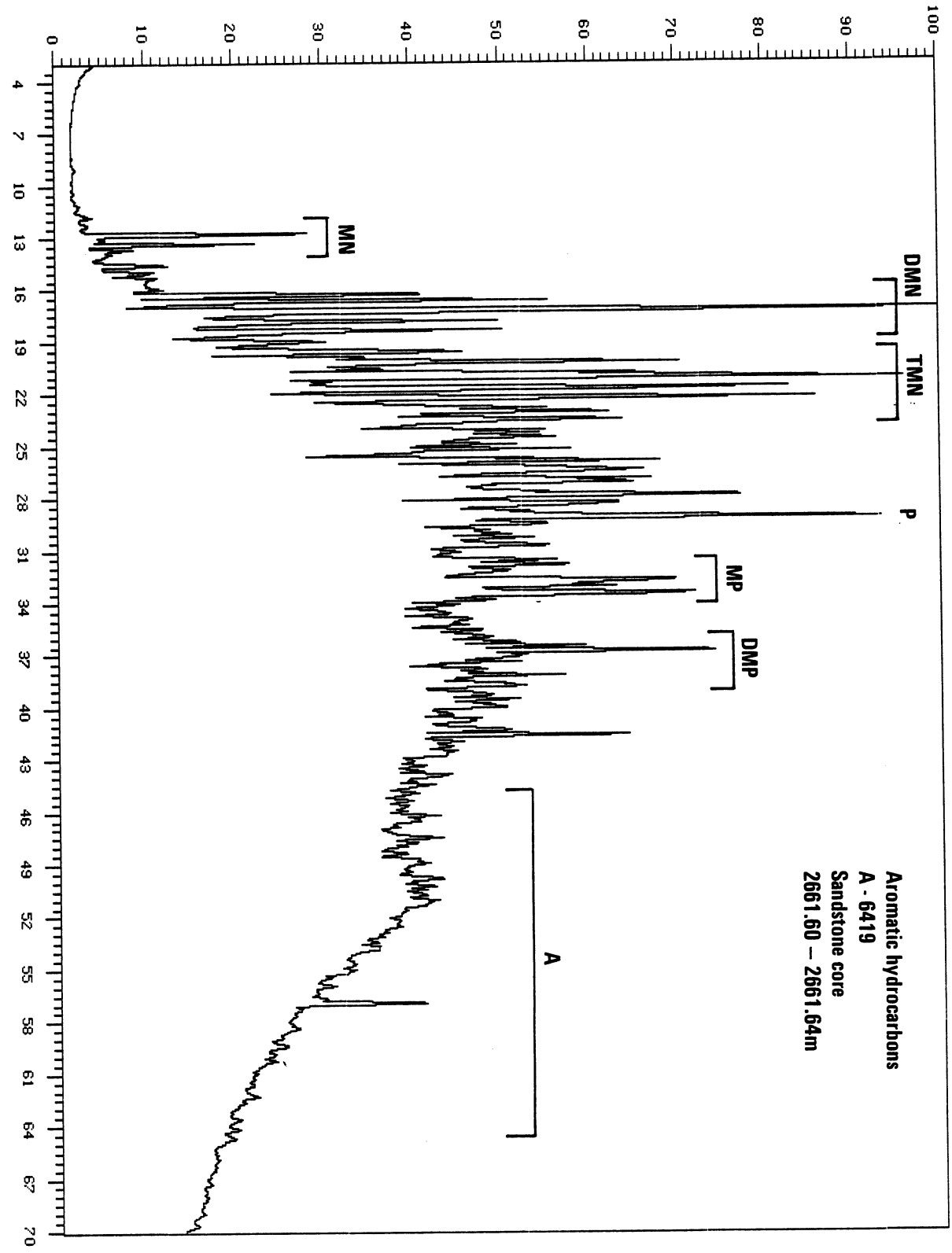

Printed at 09:25 on 24/Oct/83

RAW DATA PLOT-CHANNEL 4

Box 1 of 1

Analysis :50201A6420A1 Sample #: 1 Injection #: 1
Sample Name :A6420,ARO,EH

Maximum signal (%): 21.98

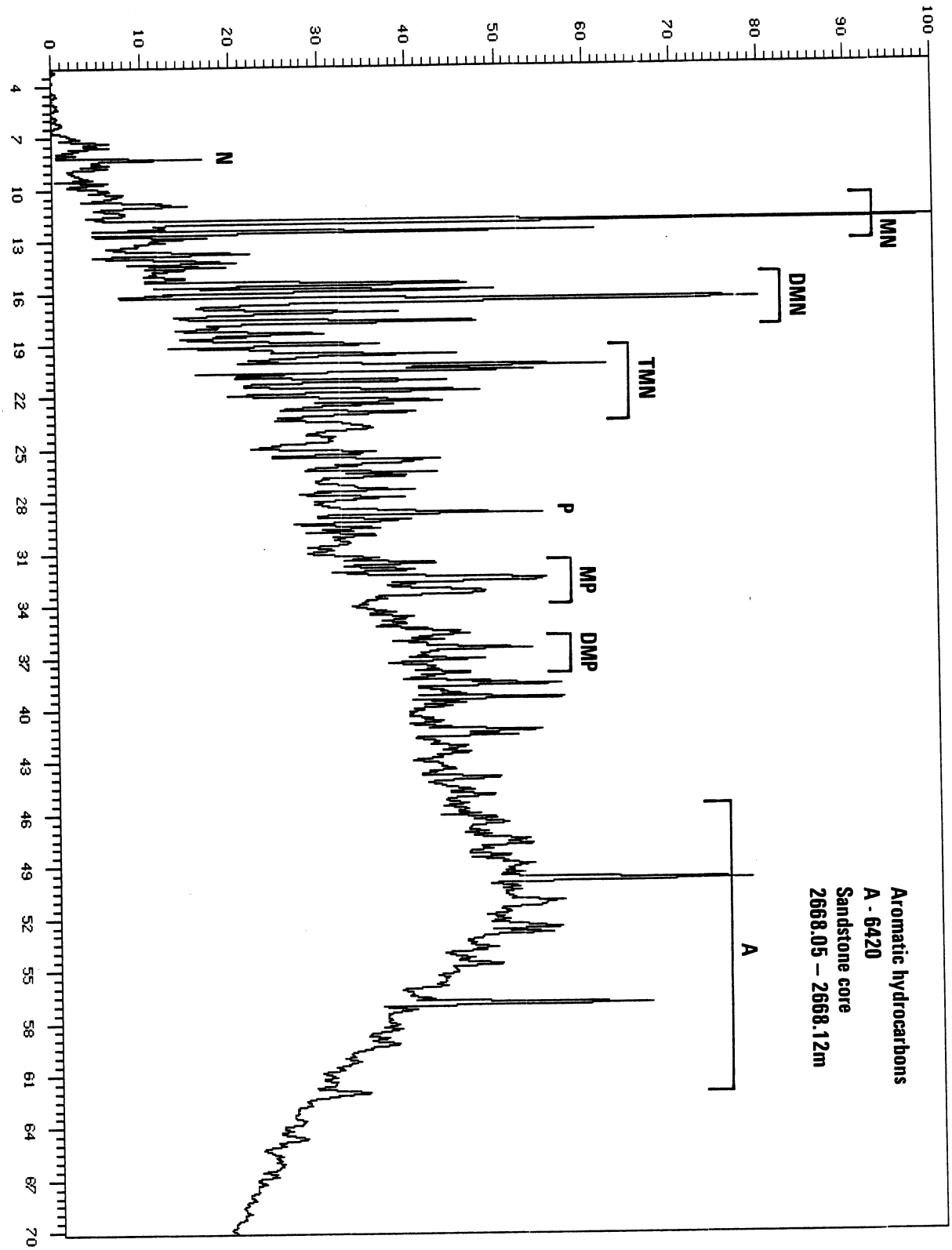

Printed at 14:24 on 24/Oct/83

RAW DATA PLOT-CHANNEL 4

Box 1 of 1

Analysis :50201A6421A1 Sample #: 1 Injection #: 1
Sample Name :A6421,ARO,EH

Maximum signal (%): 5.11

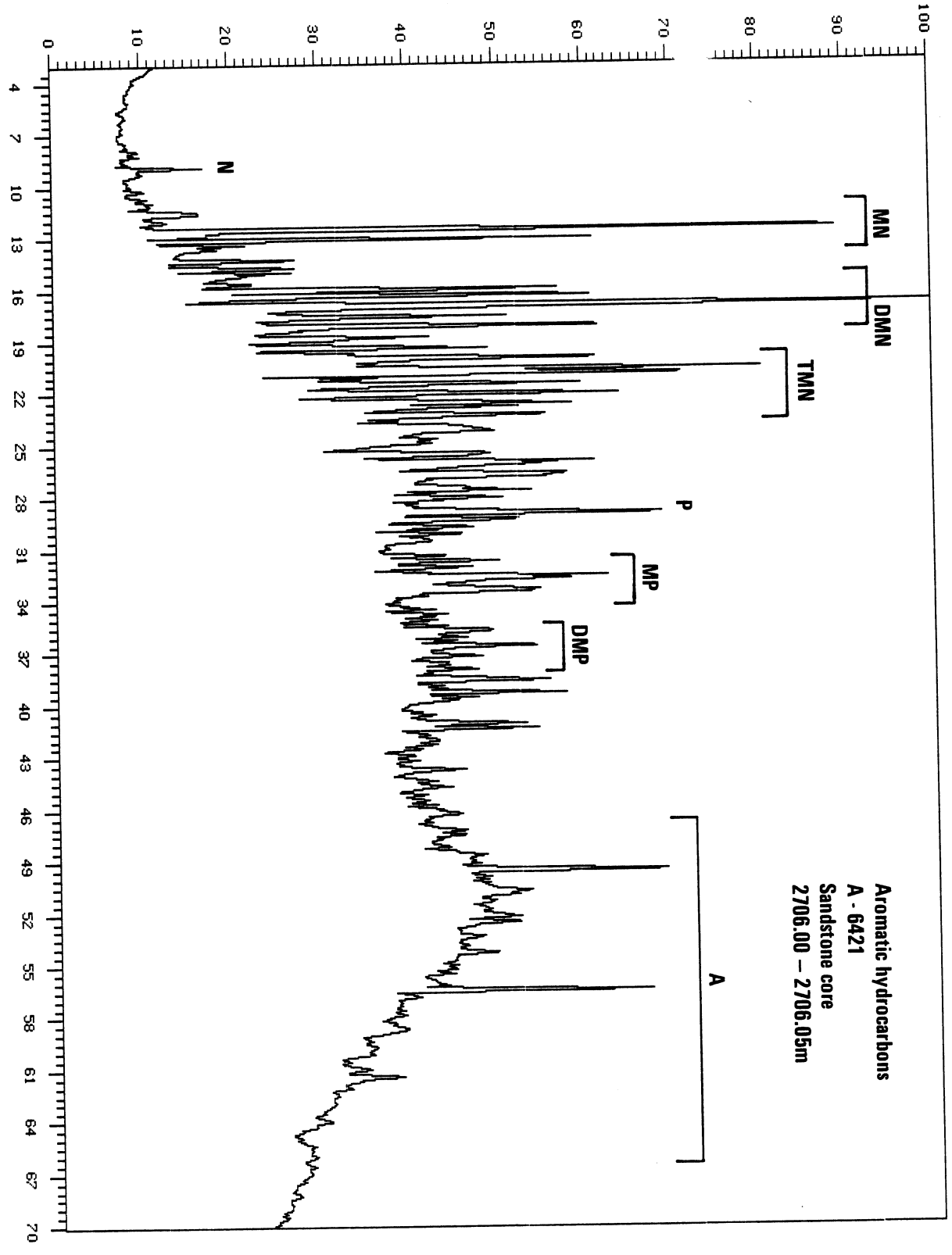

Figure 3a.

Mass chromatograms representing terpanes (m/z 191)

A	T_s, 18α(H)-trisnorneohopane	$C_{27}H_{46}$	(III)
B	T_m, 17α(H)-trisnorhopane	$C_{27}H_{46}$	(I,R=H)
C	17α(H)-norhopane	$C_{29}H_{50}$	(I,R=C_2H_5)
D	17β(H)-normoretane	$C_{29}H_{50}$	(II,R=C_2H_5)
E	17α(H)-hopane	$C_{30}H_{52}$	(I,R=C_3H_7)
F	17β(H)-moretane	$C_{30}H_{52}$	(II,R=C_3H_7)
G	17α(H)-homohopane (22S)	$C_{31}H_{54}$	(I,R=C_4H_9)
H	17α(H)-homohopane (22R)	$C_{31}H_{54}$	(I,R=C_4H_9)
	+ unknown triterpane (gammacerane?)		
I	17β(H)-homomoretane	$C_{31}H_{54}$	(II,R=C_4H_9)
J	17α(H)-bishomohopane (22S,22R)	$C_{32}H_{56}$	(I,R=C_5H_{11})
K	17α(H)-trishomohopane (22S,22R)	$C_{33}H_{58}$	(I,R=C_6H_{13})
L	17α(H)-tetrakishomohopane (22S,22R)	$C_{34}H_{60}$	(I,R,=C_7H_{15})
M	17α(H)-pentakishomohopane (22S,22R)	$C_{35}H_{62}$	(I,R=C_8H_{17})
Z	bisnorhopane	$C_{28}H_{48}$	
X	unknown triterpane	$C_{30}H_{52}$	
P	tricyclic terpane	$C_{23}H_{42}$	(IV,R=C_4H_9)
Q	tricyclic terpane	$C_{24}H_{44}$	(IV,R=C_5H_{11})
R	tricyclic terpane (17R,17S)	$C_{25}H_{46}$	(IV,R=C_6H_{13})
S	tetracyclic terpane	$C_{24}H_{42}$	(V)
T	tricyclic terpane (17R,17S)	$C_{26}H_{48}$	(IV,R=C_7H_{15})

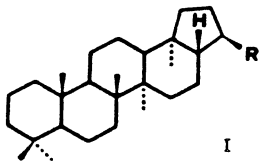

I

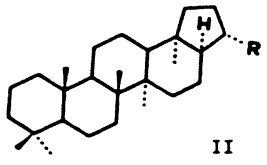

II

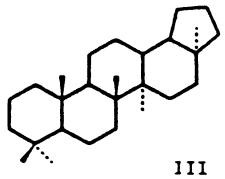

III

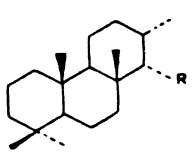

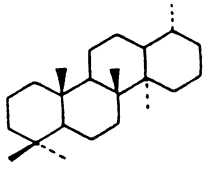

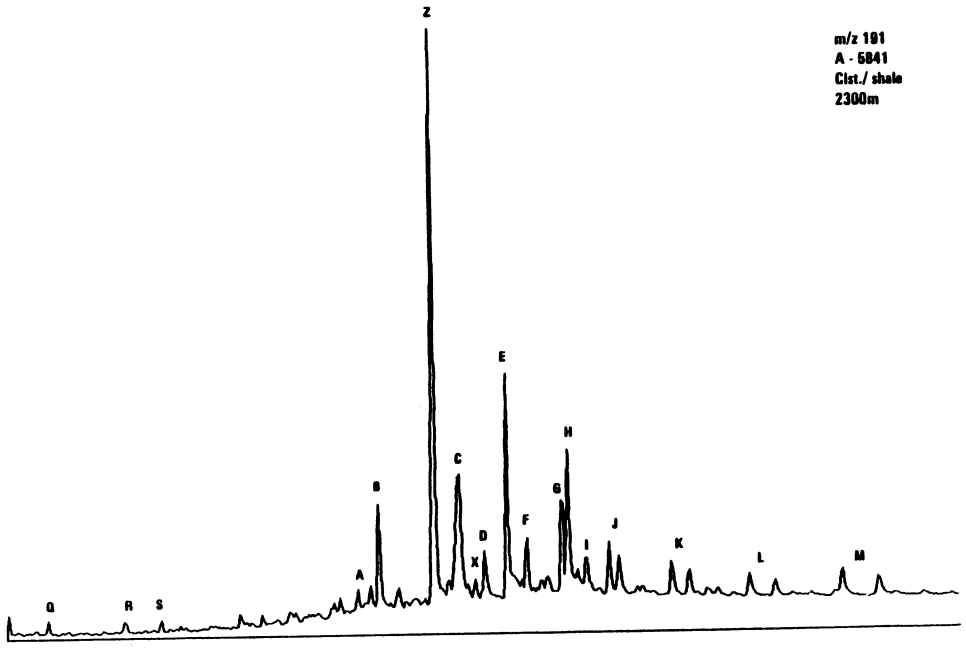
m/z 191
A - 5841
Clst./ shale
2300m
Q
R
S
A
B
Z
C
D
X
E
F
G
H
I
J
K
L
M

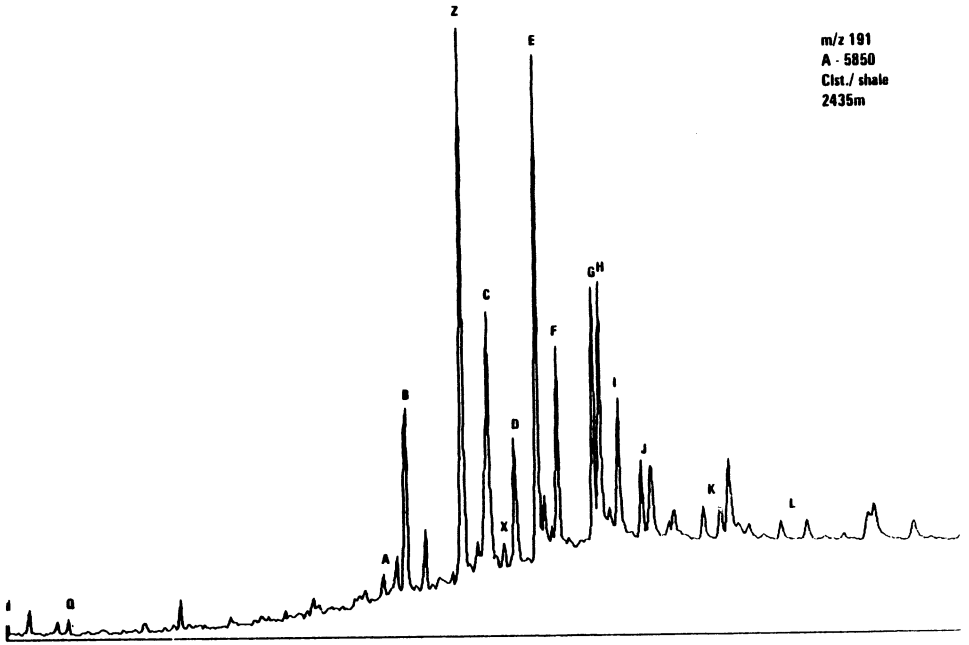
m/z 191
A - 5850
Clst./ shale
2435m
Q
A
B
Z
C
D
X
E
F
G
H
I
J
K
L

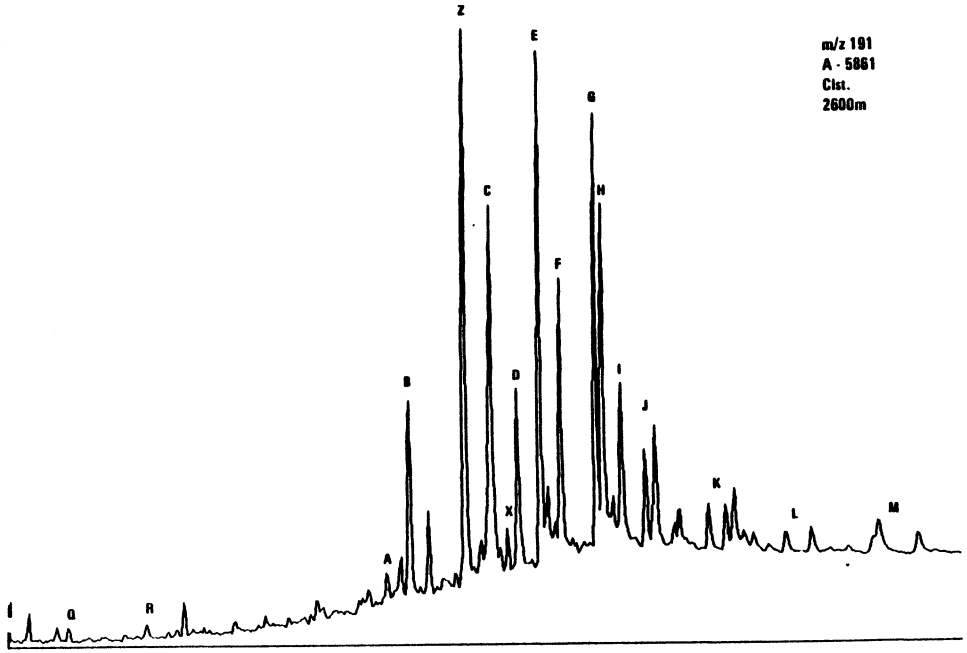
m/z 191
A - 5861
Clst.
2600m
Q
R
A
B
Z
C
D
X
E
F
G
H
I
J
K
L
M

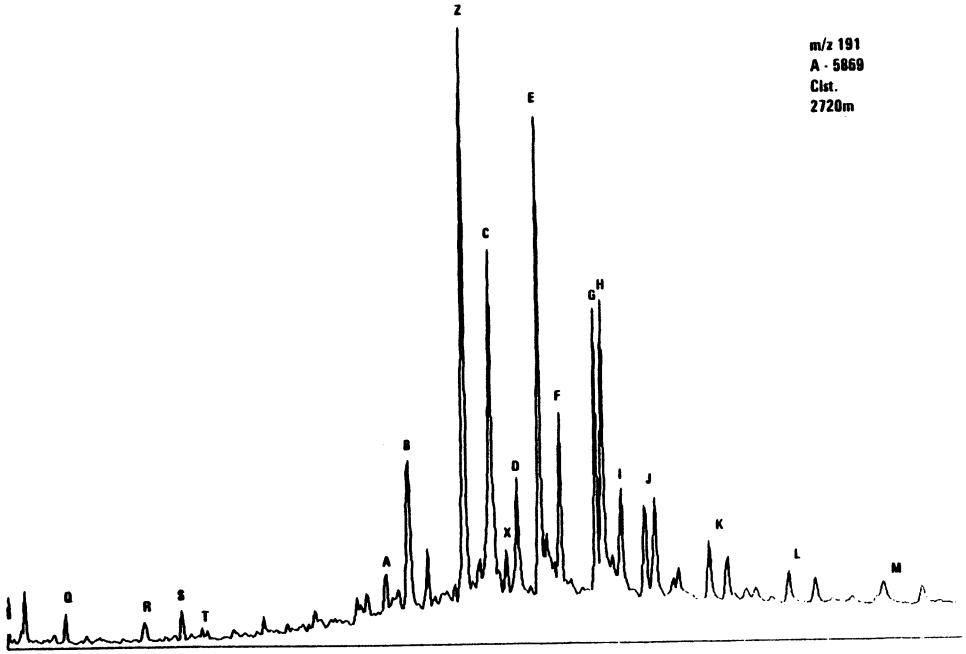
m/z 191
A - 5869
Clst.
2720m
Q
R
S
T
A
B
Z
C
D
X
E
F
G
H
I
J
K
L
M

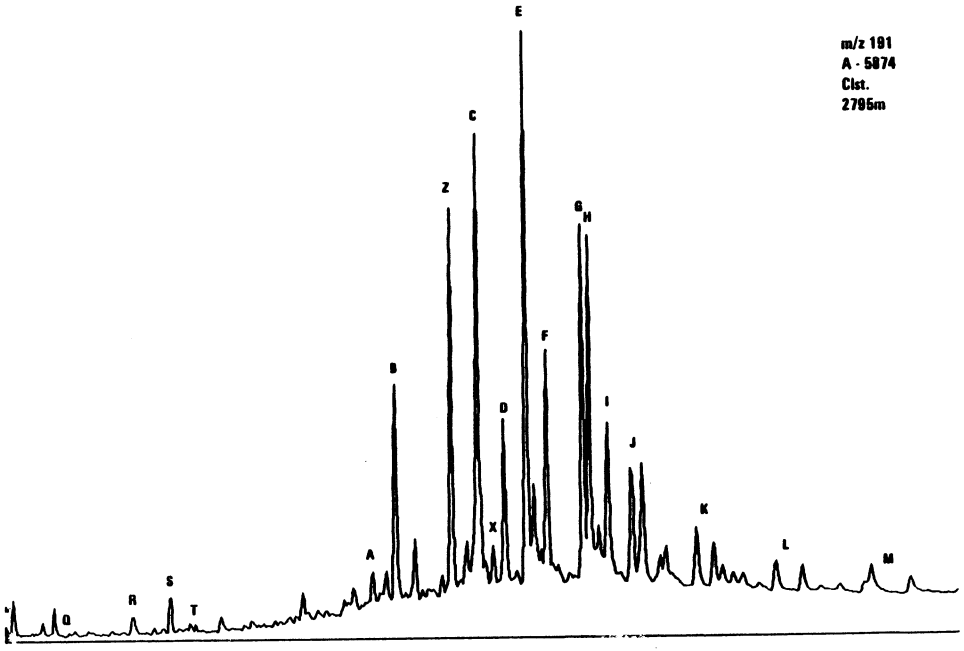
m/z 191
A - 5874
Clst.
2795m
Q
R
S
T
A
B
Z
C
X
D
E
F
G
H
I
J
K
L
M

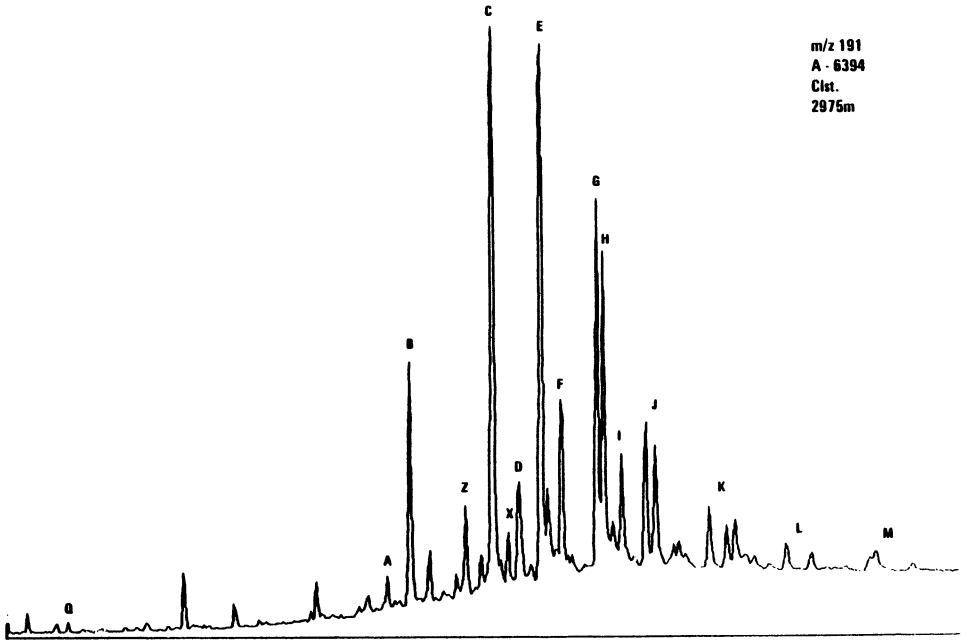
m/z 191
A - 6394
Clst.
2975m
Q
A
B
Z
C
X
D
E
F
G
H
I
J
K
L
M

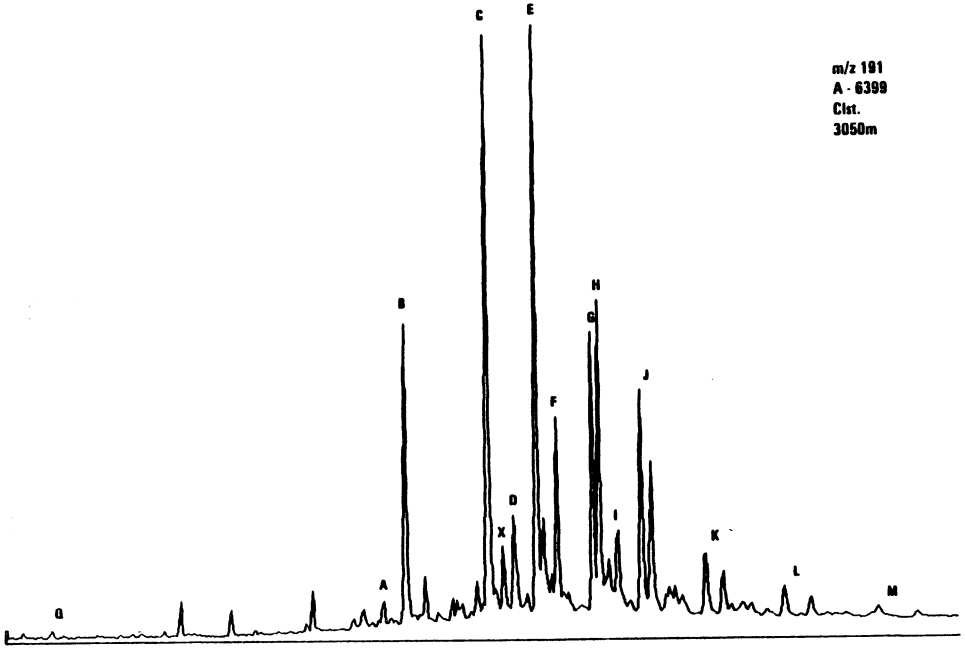
m/z 191
A - 6399
Clst.
3050m
Q
A
B
C
X
D
E
F
G
H
I
J
K
L
M

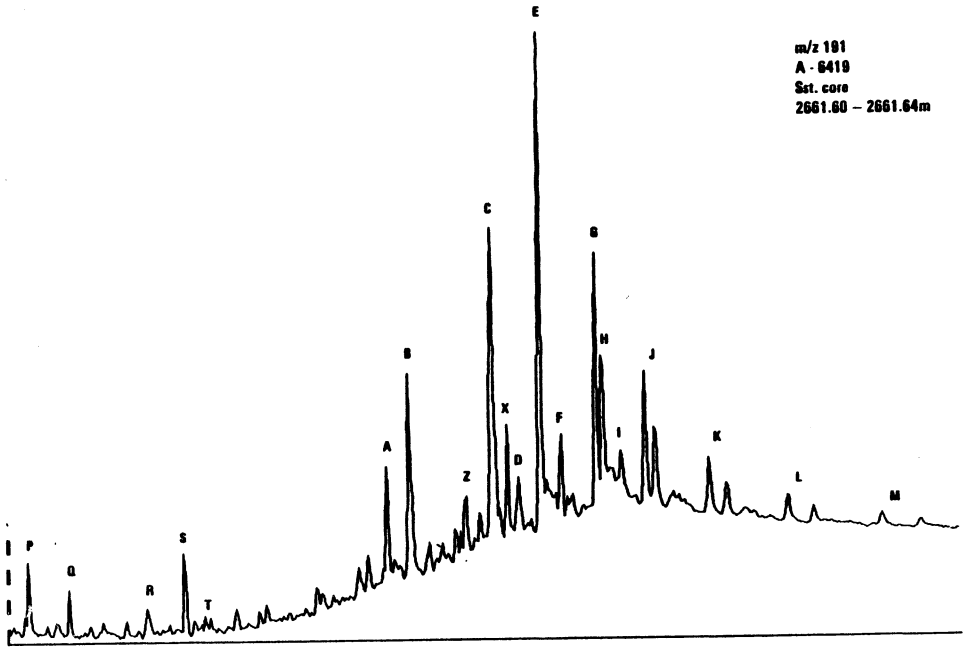
m/z 191
A - 6419
Sst. core
2661.60 – 2661.64m
P
Q
R
S
T
A
B
C
D
E
F
G
H
I
J
K
L
M
X
Z

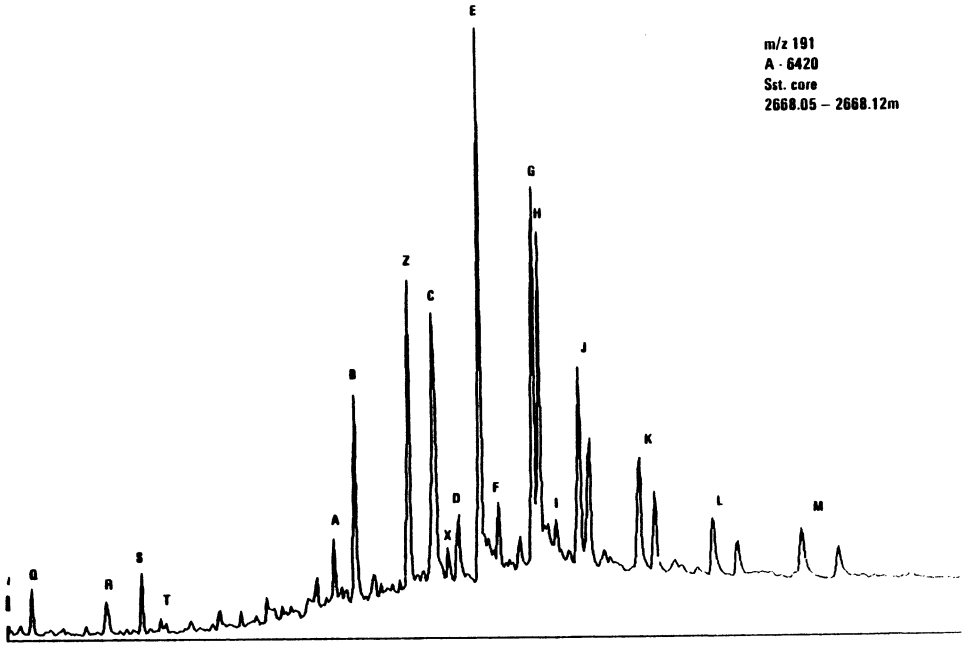
m/z 191
A - 6420
Sst. core
2668.05 – 2668.12m
Q
R
S
T
A
B
C
D
E
F
G
H
I
J
K
L
M
X
Z

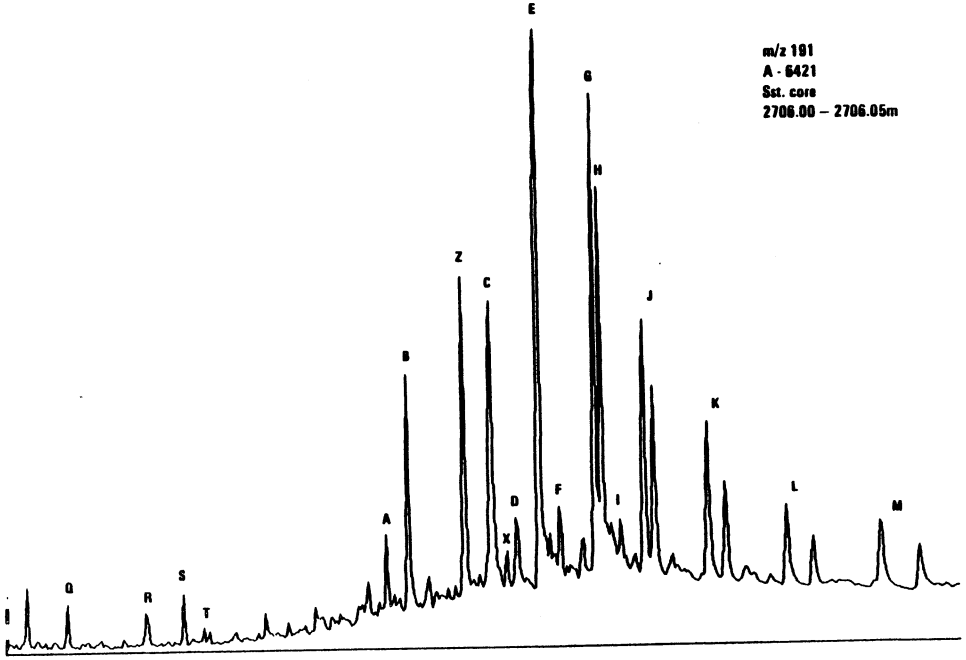
m/z 191
A - 6421
Sst. core
2706.00 – 2706.05m
Q
R
S
T
A
B
C
D
E
F
G
H
I
J
K
L
M
X
Z

Figure 3b.

Mass chromatograms representing steranes (m/z 217 and 218)

a	13β(H),17α(H)-diasterane (20S)	$C_{27}H_{48}$	(III,R=H)
b	13β(H),17α(H)-diasterane (20R)	$C_{27}H_{48}$	(III,R=H)
c	13α(H),17β(H)-diasterane (20S)	$C_{27}H_{48}$	(IV,R=H)
d	13α(H),17β(H)-diasterane (20R)	$C_{27}H_{48}$	(IV,R=H)
e	13β(H),17α(H)-diasterane (20S)	$C_{28}H_{50}$	(III,R=CH_3)
f	13β(H),17α(H)-diasterane (20R)	$C_{28}H_{50}$	(III,R=CH_3)
g	13α(H),17β(H)-diasterane (20S)	$C_{28}H_{50}$	(IV,R=CH_3)
	+ 14α(H),17α(H)-sterane (20S)	$C_{27}H_{48}$	(I,R=H)
h	13β(H),17α(H)-diasterane (20S)	$C_{29}H_{52}$	(III,R=C_2H_5)
	+ 14α(H),17α(H)-sterane (20R)	$C_{27}H_{48}$	(II,R=H)
i	14β(H),17β(H)-sterane (20S)	$C_{27}H_{48}$	(II,R=H)
	+ 13α(H),17β(H)-diasterane (20R)	$C_{28}H_{50}$	(IV,R=CH_3)
j	14α(H),17α(H)-sterane (20R)	$C_{27}H_{48}$	(I,R=H)
k	13β(H),17α(H)-diasterane (20R)	$C_{29}H_{52}$	(III,R=C_2H_5)
l	13α(H),17β(H)-diasterane (20S)	$C_{29}H_{52}$	(III,R=C_2H_5)
m	14α(H),17α(H)-sterane (20S)	$C_{28}H_{50}$	(I,R=CH_3)
n	13α(H),17β(H)-diasterane (20R)	$C_{29}H_{52}$	(III,R=C_2H_5)
	+ 14β (H),17β (H)-sterane (20R)	$C_{28}H_{50}$	(II,R=CH_3)
o	14β(H),17β(H)-sterane (20S)	$C_{28}H_{50}$	(II,R=CH_3)
p	14α(H),17α(H)-sterane (20R)	$C_{28}H_{50}$	(I,R=CH_3)
q	14α(H),17α(H)-sterane (20S)	$C_{29}H_{52}$	(I,R=C_2H_5)
r	14β(H),17β(H)-sterane (20R)	$C_{29}H_{52}$	(II,R=C_2H_5)
	+ unknown sterane		
s	14β(H),17β(H)-sterane (20S)	$C_{29}H_{52}$	(II,R=C_2H_5)
t	14α(H),17β(H)-sterane (20R)	$C_{29}H_{52}$	(I,R=C_2H_5)
u	5α(H)-sterane	$C_{21}H_{36}$	(V,R=C_2H_5)
v	5α(H)-sterane	$C_{22}H_{38}$	(IV,R=C_3H_7)

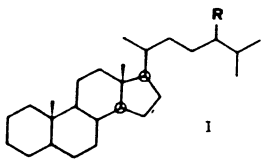

I

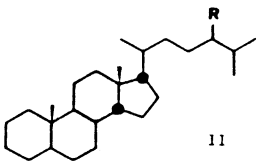

II

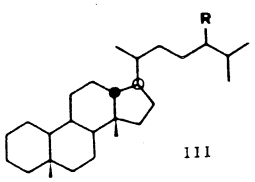

III

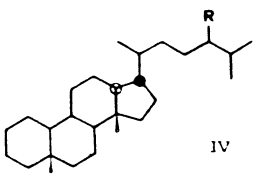

IV

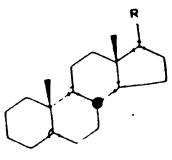

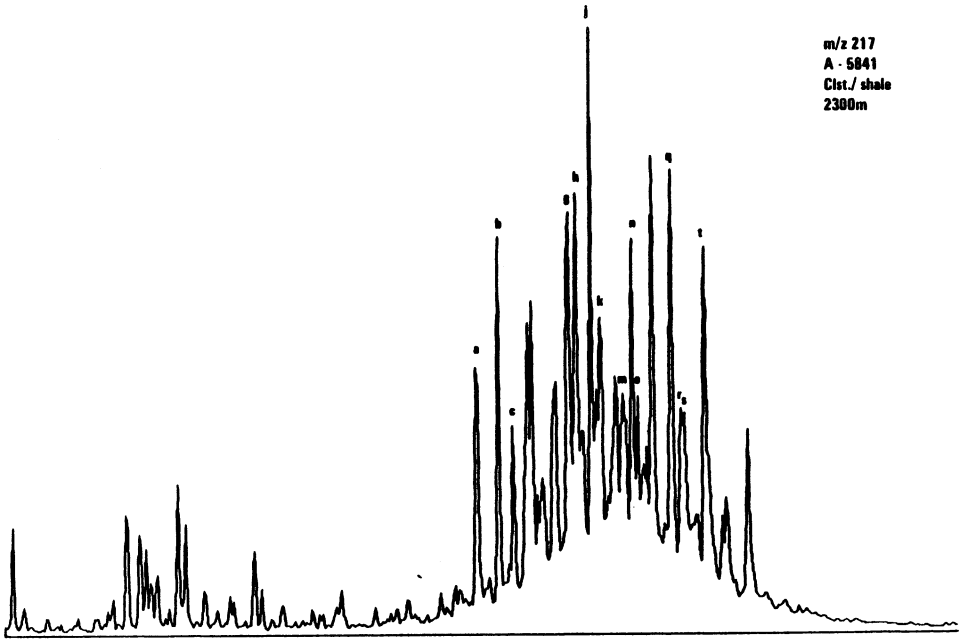
m/z 217
A - 5841
Clst./ shale
2300m

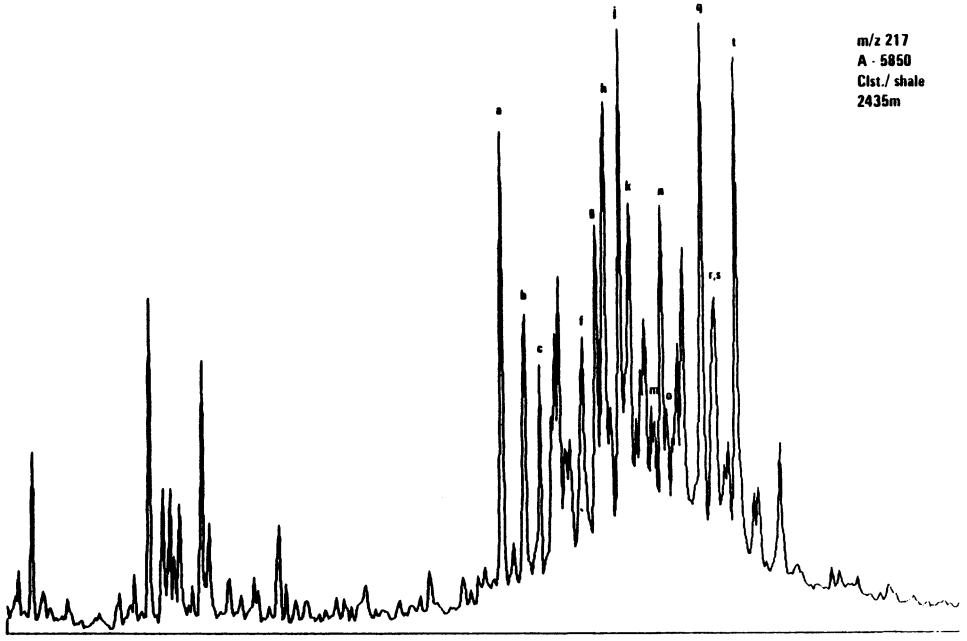
m/z 217
A - 5850
Clst./ shale
2435m

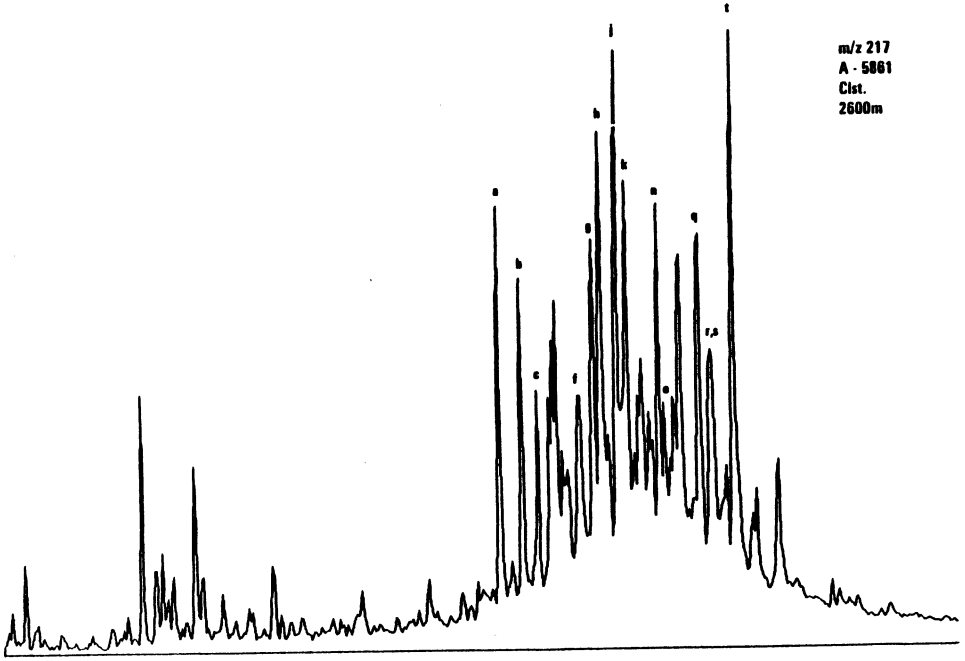
m/z 217
A - 5861
Clst.
2600m

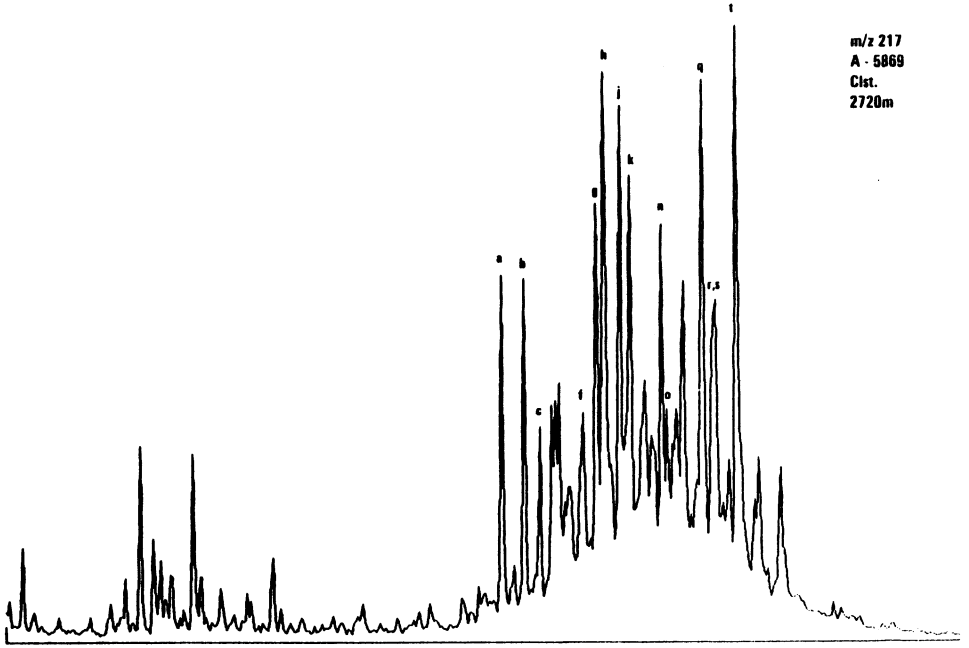
m/z 217
A - 5869
Clst.
2720m

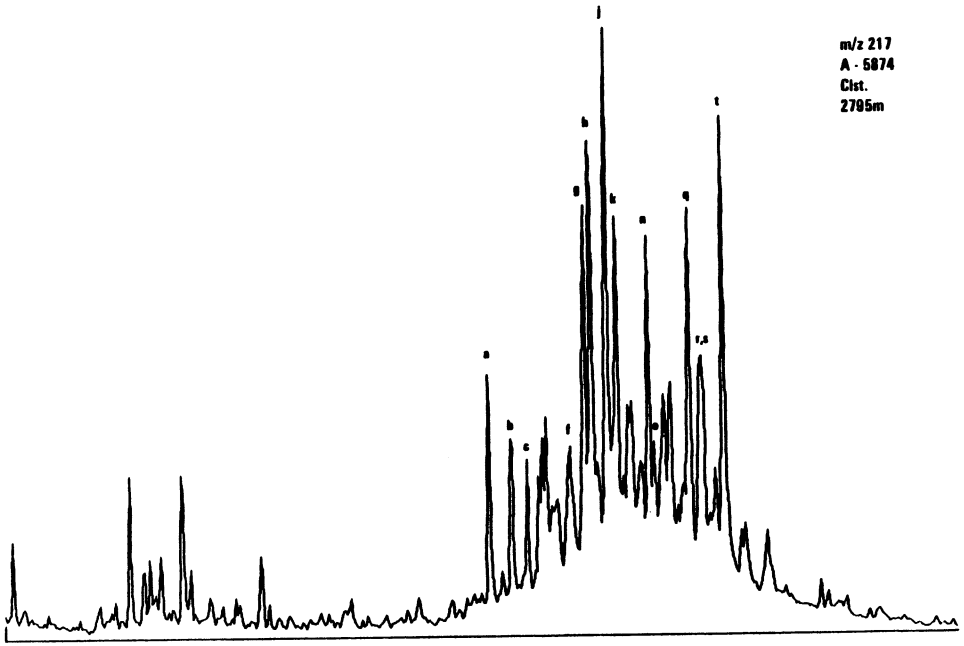
m/z 217
A - 6874
Clst.
2795m

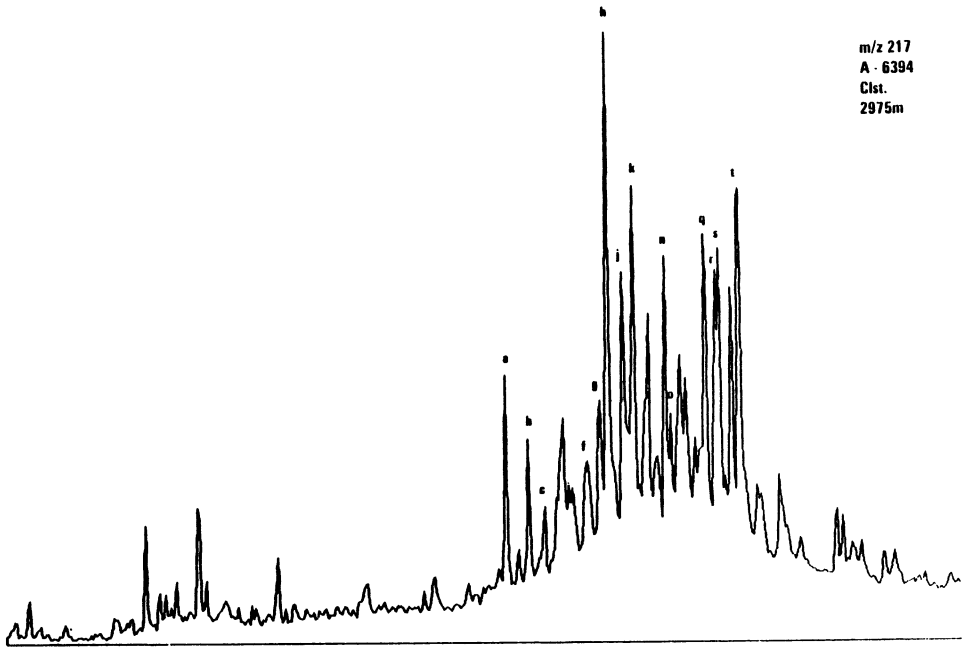
m/z 217
A - 6394
Clst.
2975m

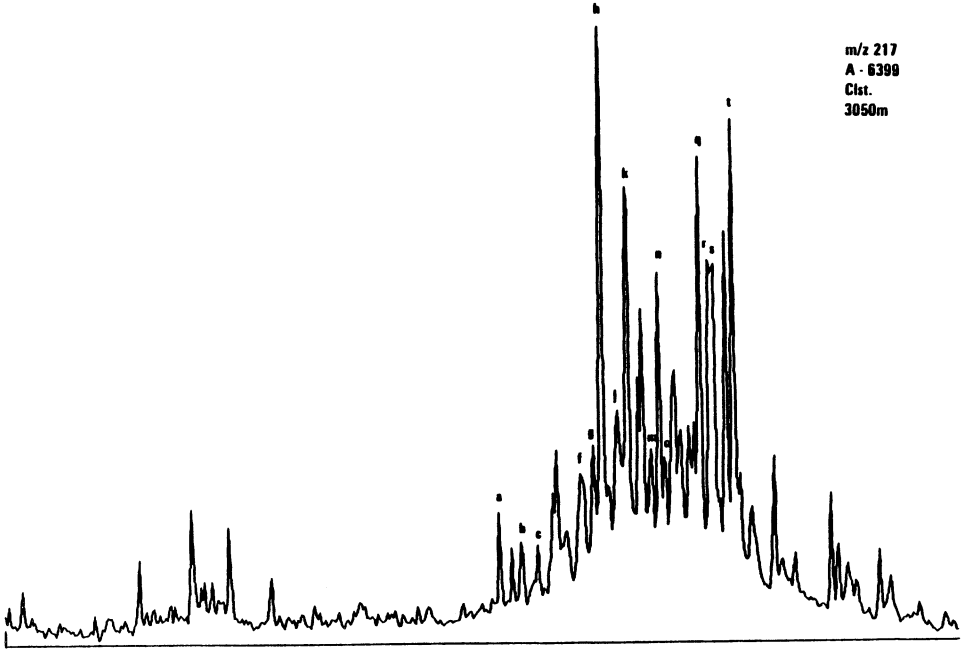
m/z 217
A - 6399
Clst.
3050m

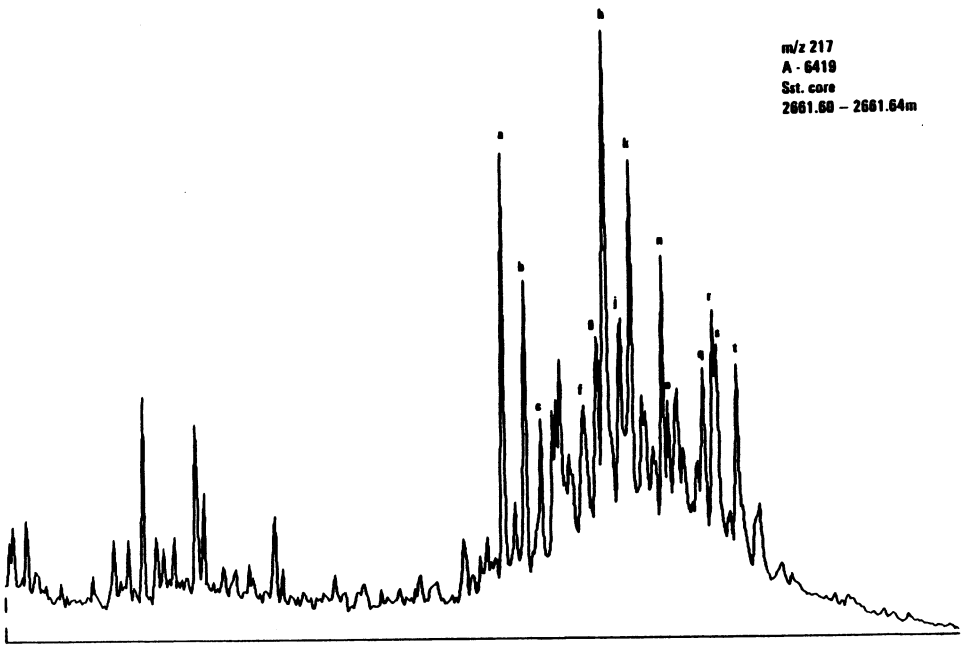
m/z 217
A - 6419
Sst. core
2661.60 – 2661.64m

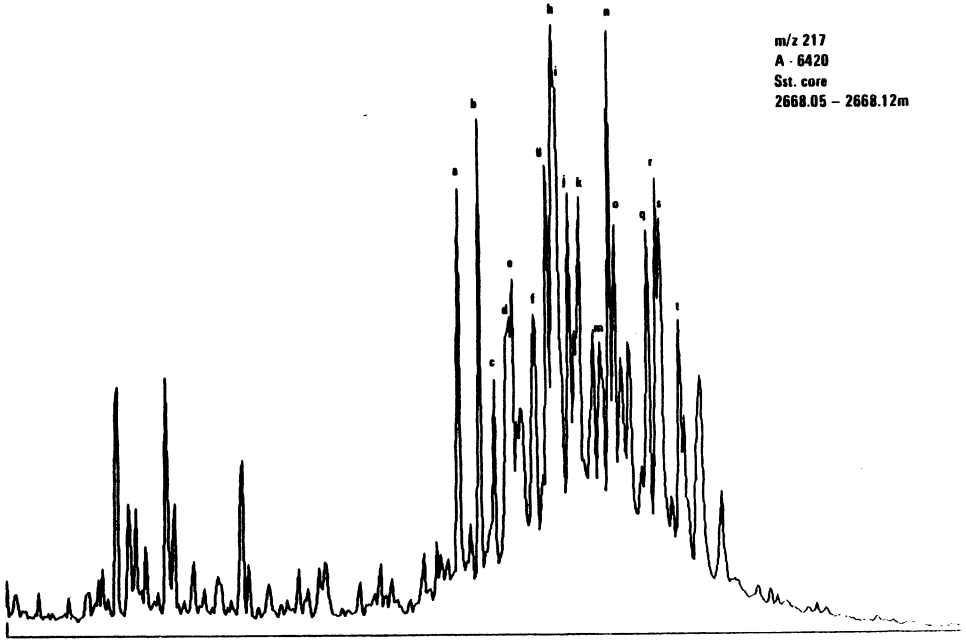
m/z 217
A - 6420
Sst. core
2668.05 – 2668.12m

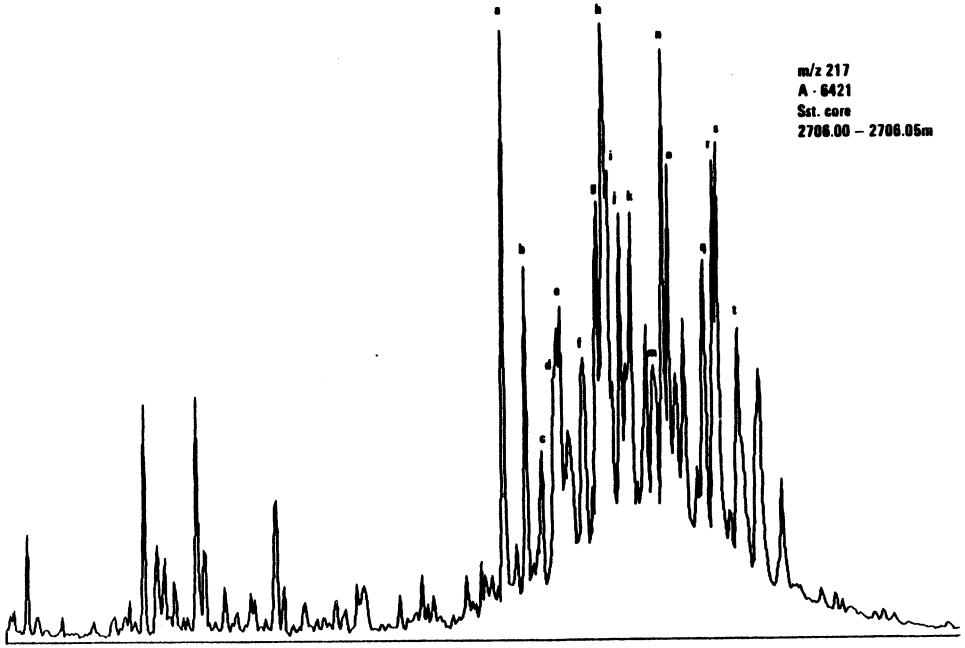
m/z 217
A - 6421
Sst. core
2706.00 – 2706.05m

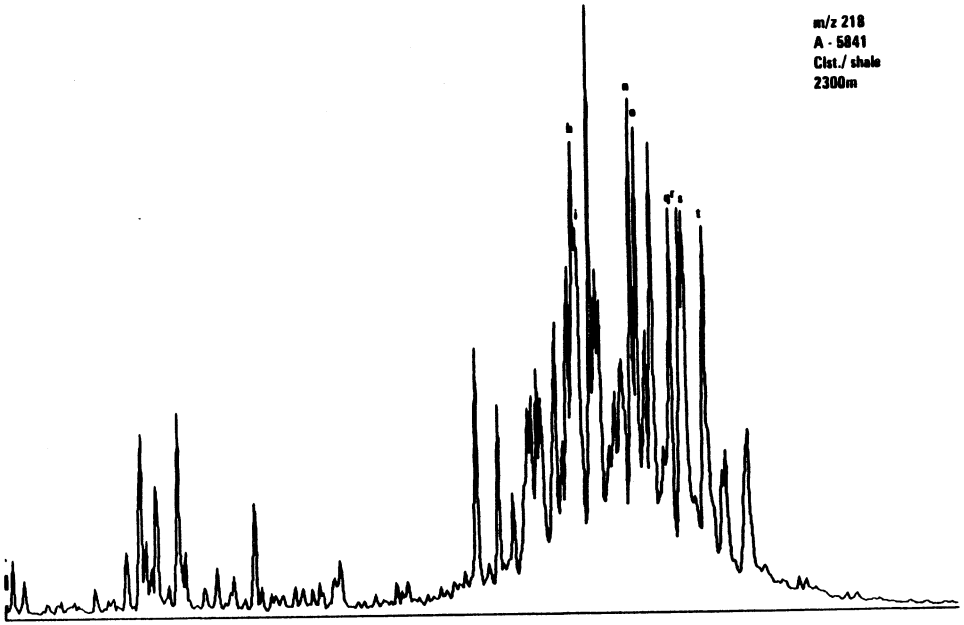
m/z 218
A - 5841
Clst./ shale
2300m

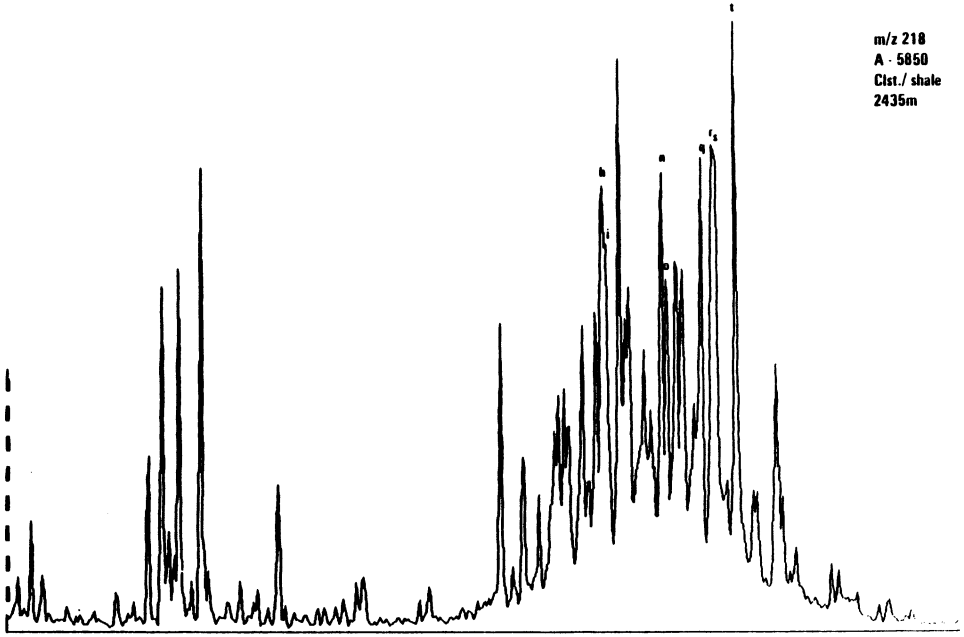
m/z 218
A - 5850
Clst./ shale
2435m

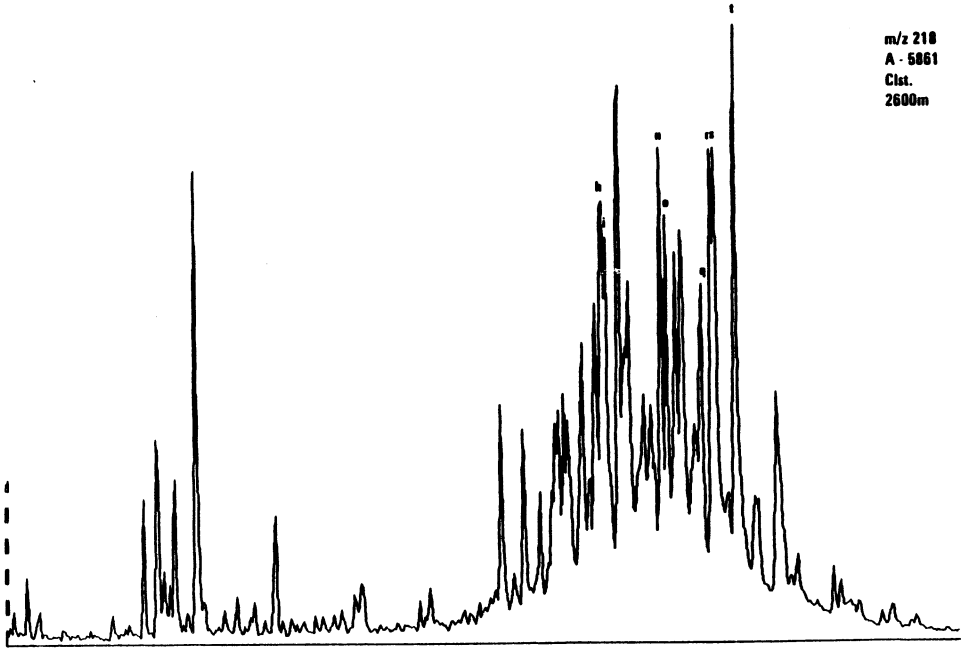
m/z 218
A - 5861
Clst.
2600m

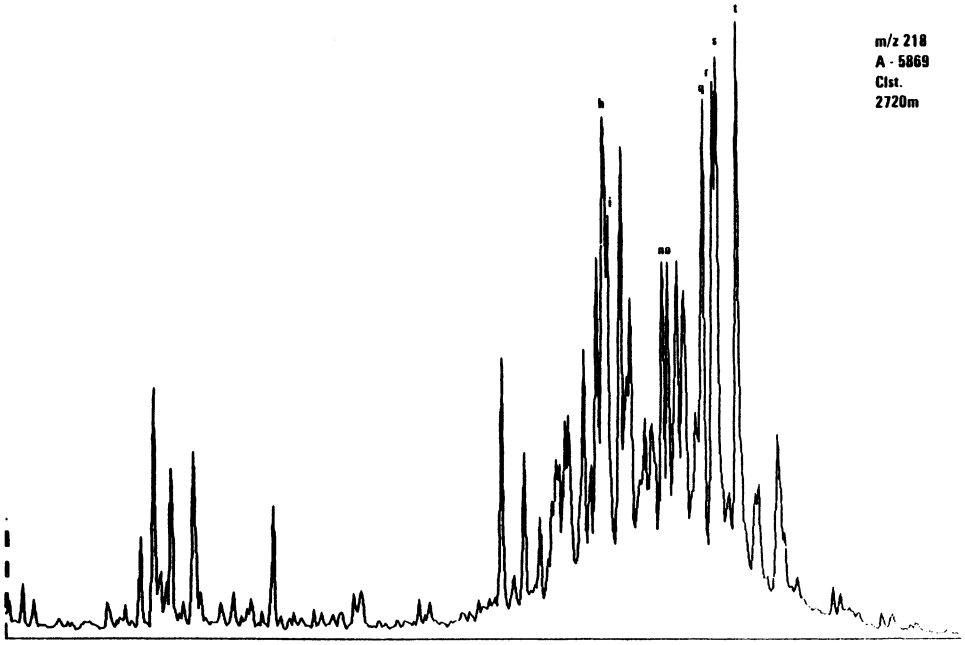
m/z 218
A - 5869
Clst.
2720m

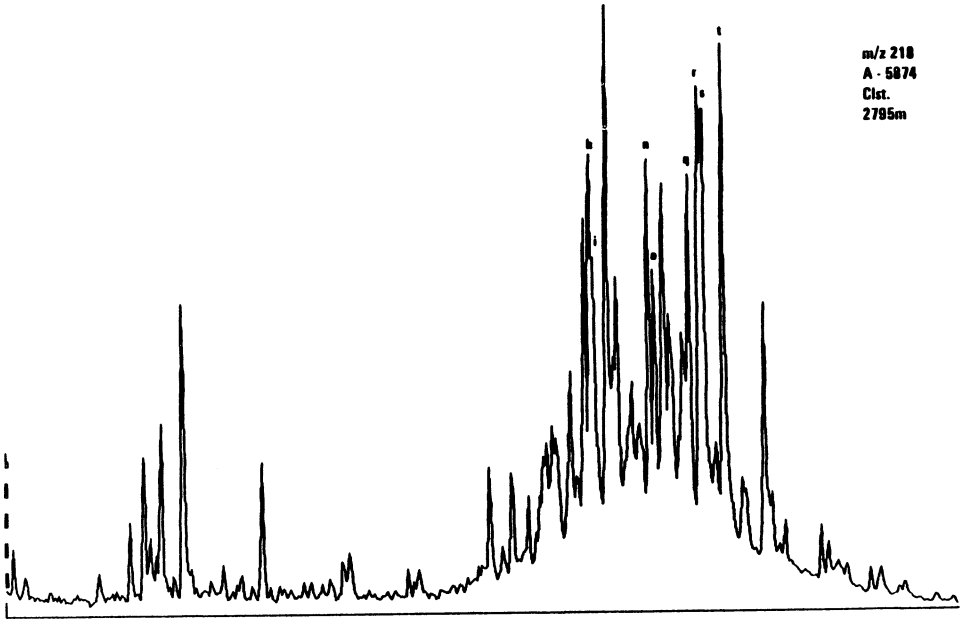
m/z 218
A - 5874
Clst.
2795m

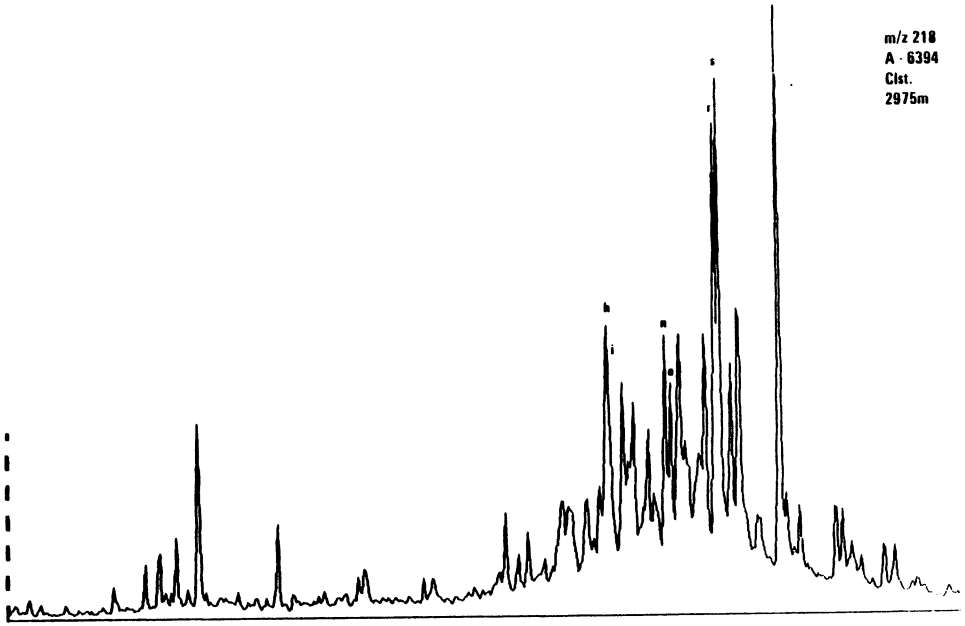
m/z 218
A - 6394
Clst.
2975m

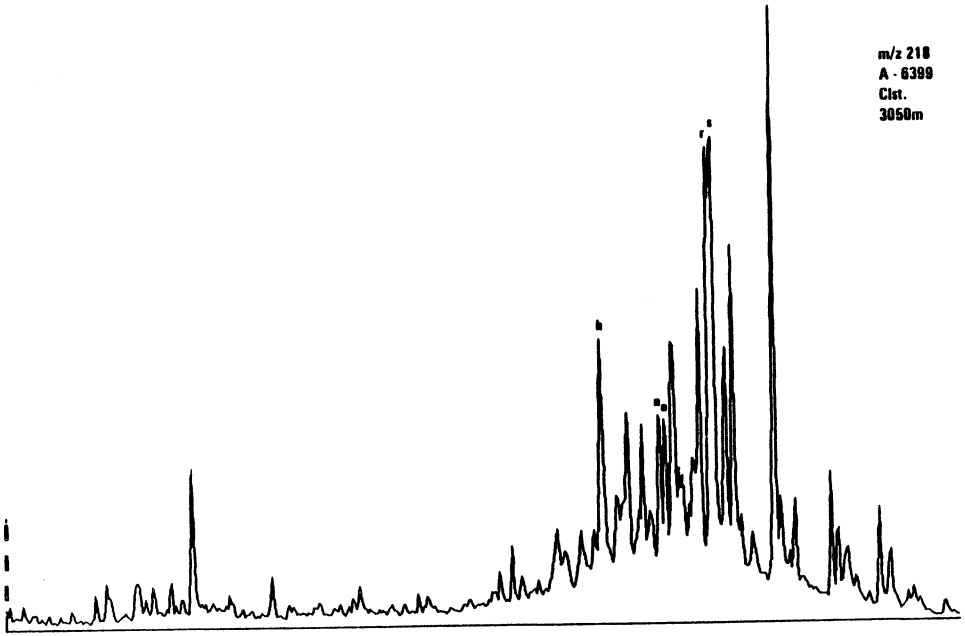
m/z 218
A - 6399
Clst.
3050m

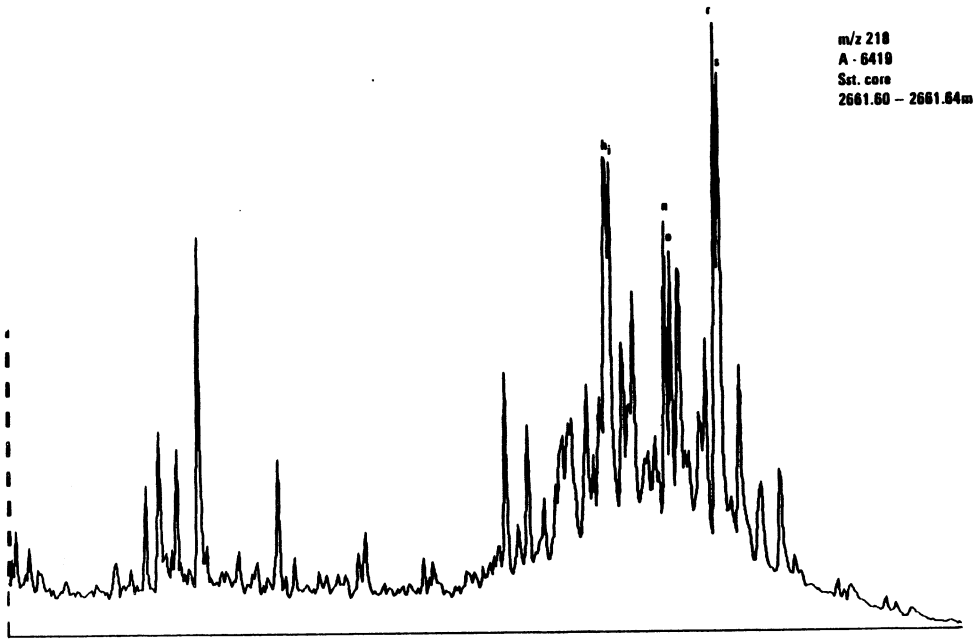
m/z 218
A - 6419
Sst. core
2661.60 – 2661.64m

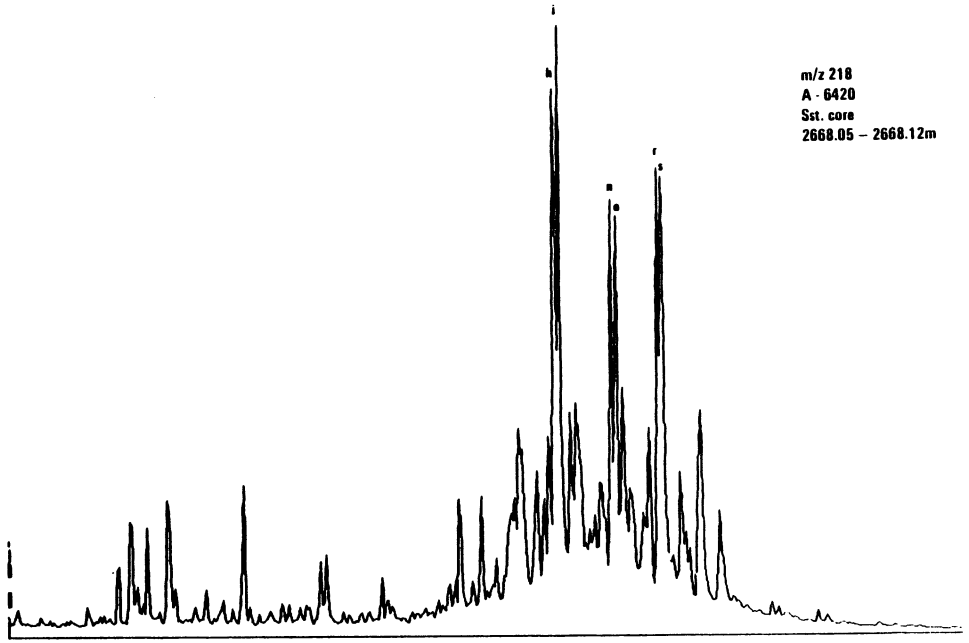
m/z 218
A - 6420
Sst. core
2668.05 – 2668.12m

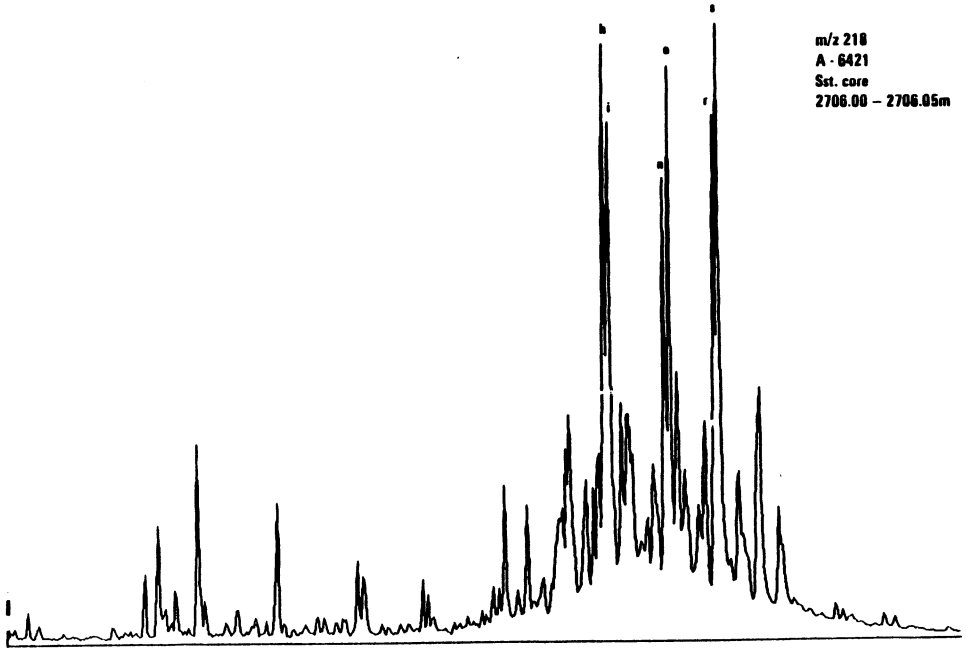
m/z 218
A - 6421
Sst. core
2706.00 – 2706.05m

FIGURE 4.

Mass chromatograms representing aromatic hydrocarbons.

m/z 92+106	Monoaromatic hydrocarbons
m/z 142	C_1-naphthalenes
m/z 156	C_2-naphthalenes
m/z 170	C_3-naphthalenes
m/z 178	phenanthrene
m/z 192	C_1-phenanthrenes
m/z 206	C_2-phenanthrenes
m/z 231	triaromatic steranes
m/z 253	monoaromatic steranes

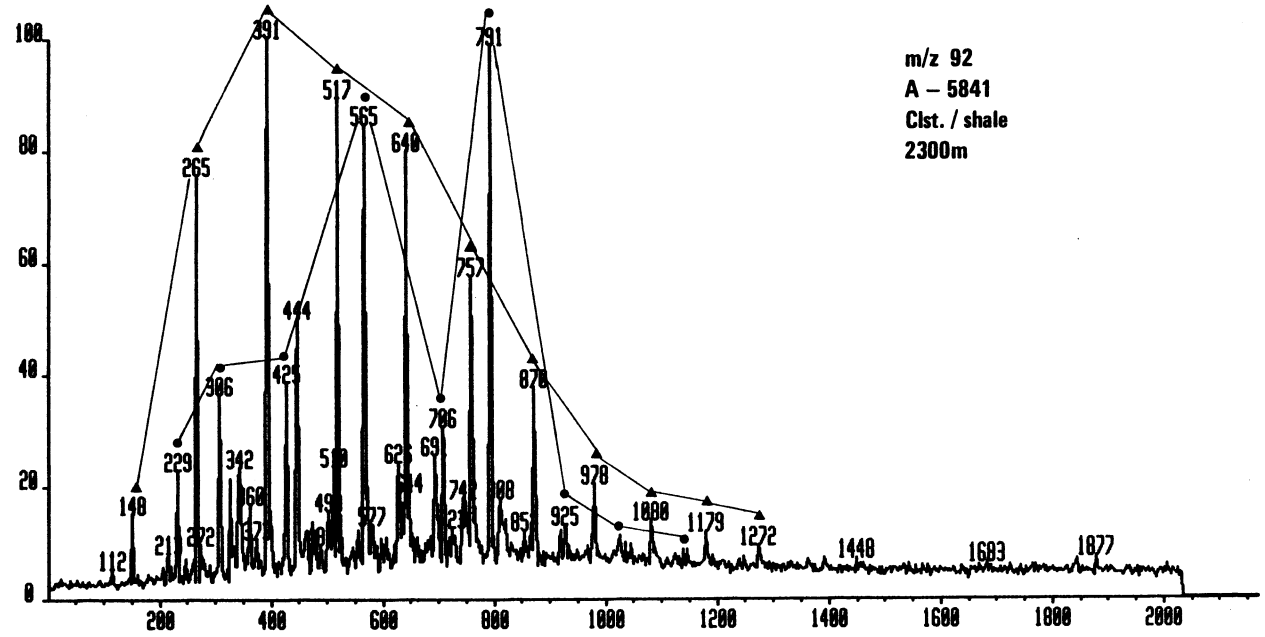
m/z 92
A – 5841
Clst. / shale
2300m

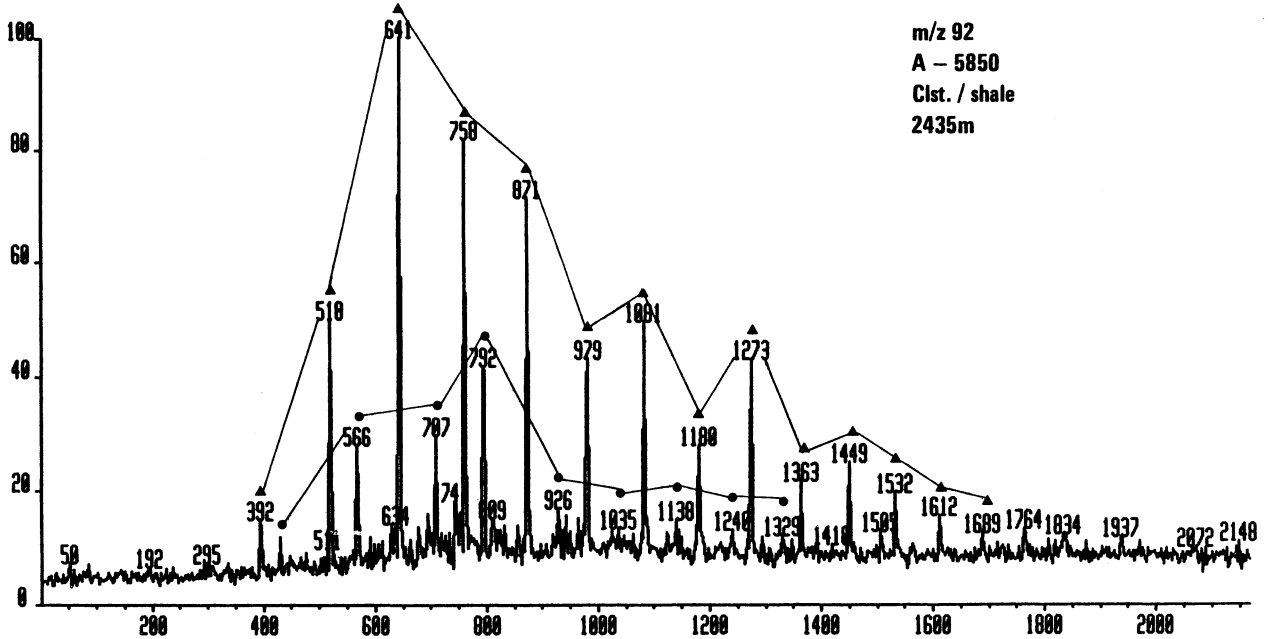
m/z 92
A – 5850
Clst. / shale
2435m

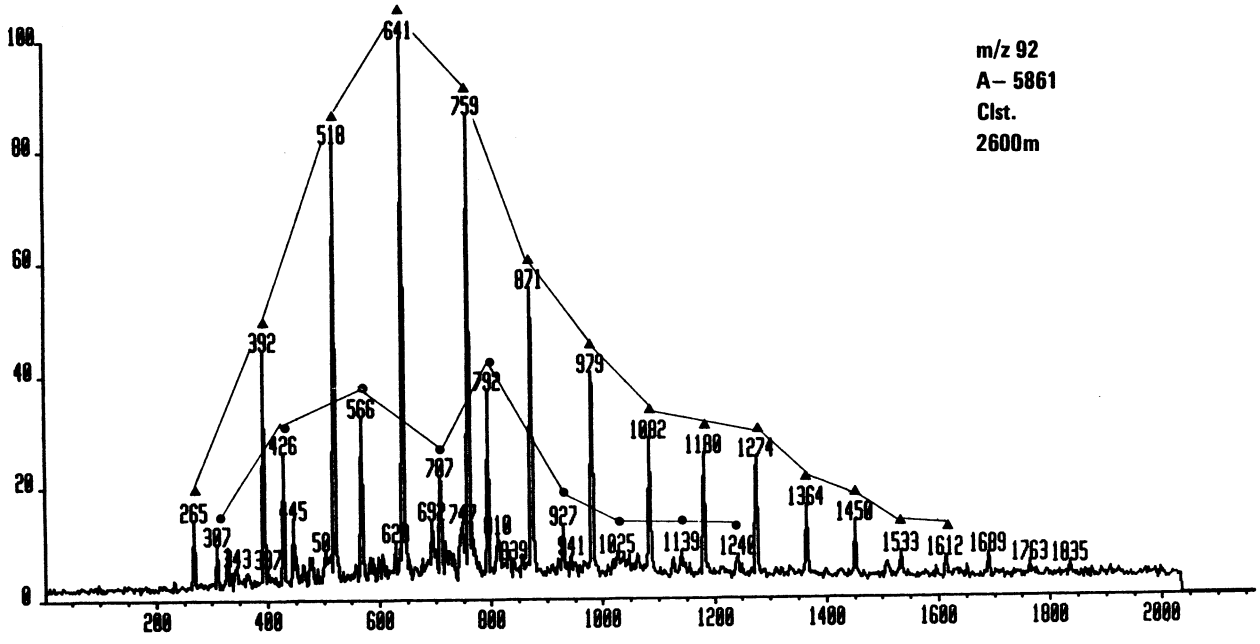
m/z 92
A– 5861
Clst.
2600m

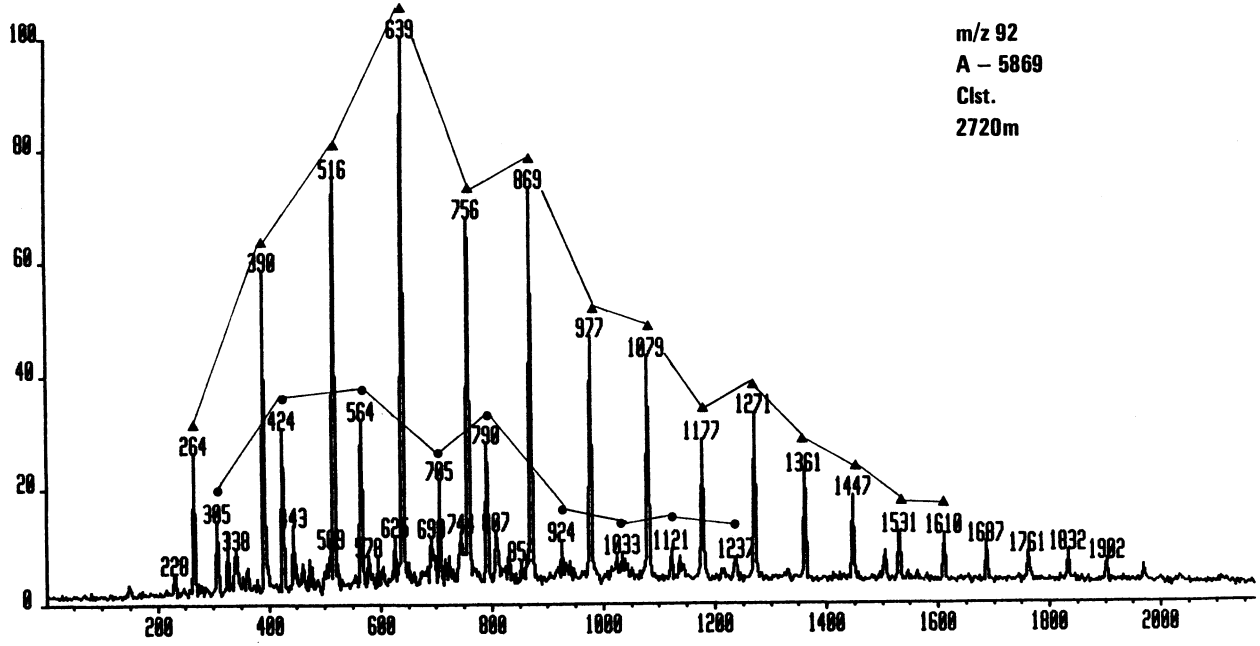
m/z 92
A – 5869
Clst.
2720m

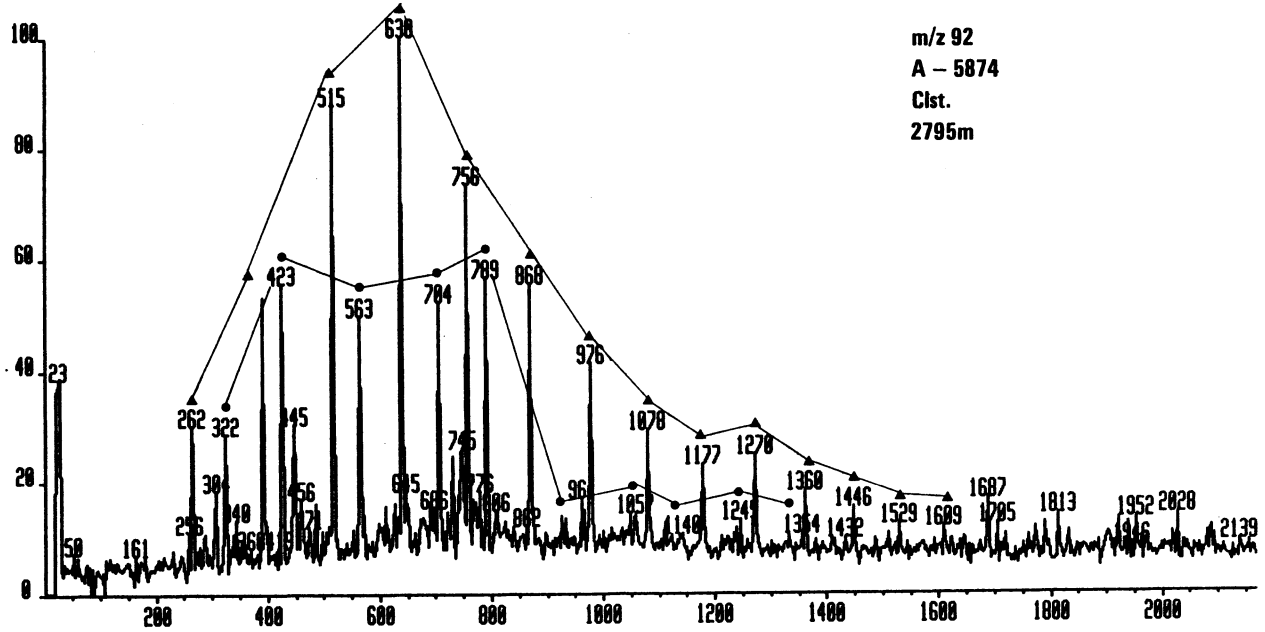
m/z 92
A – 5874
Clst.
2795m

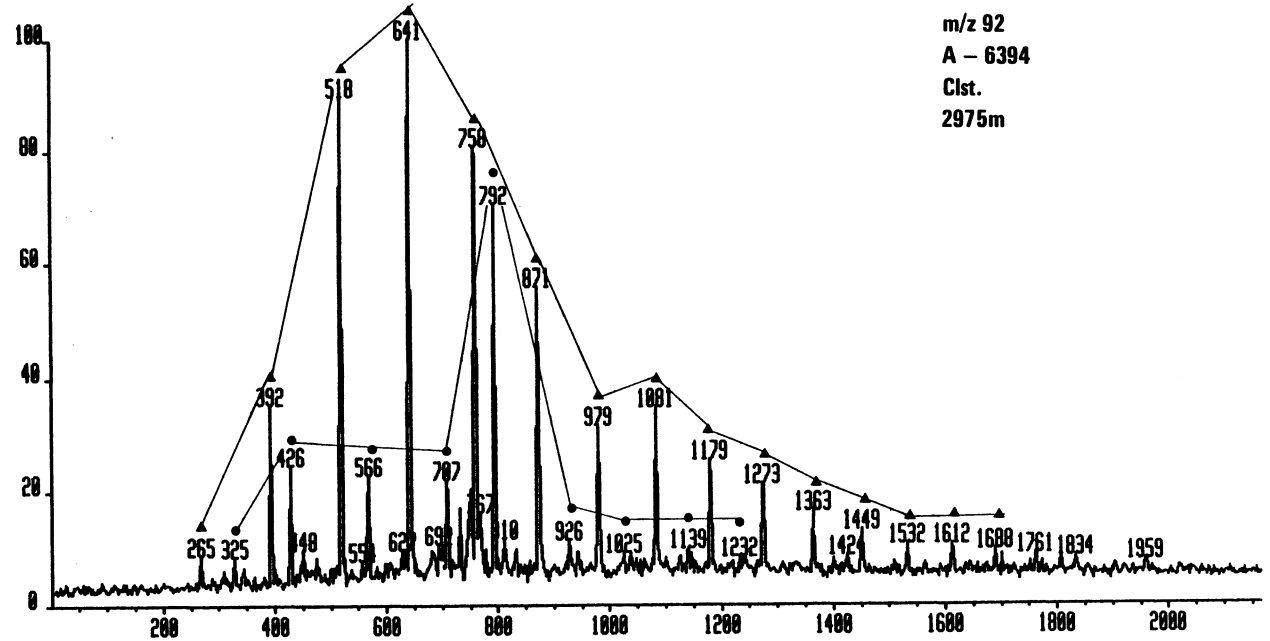
m/z 92
A – 6394
Clst.
2975m

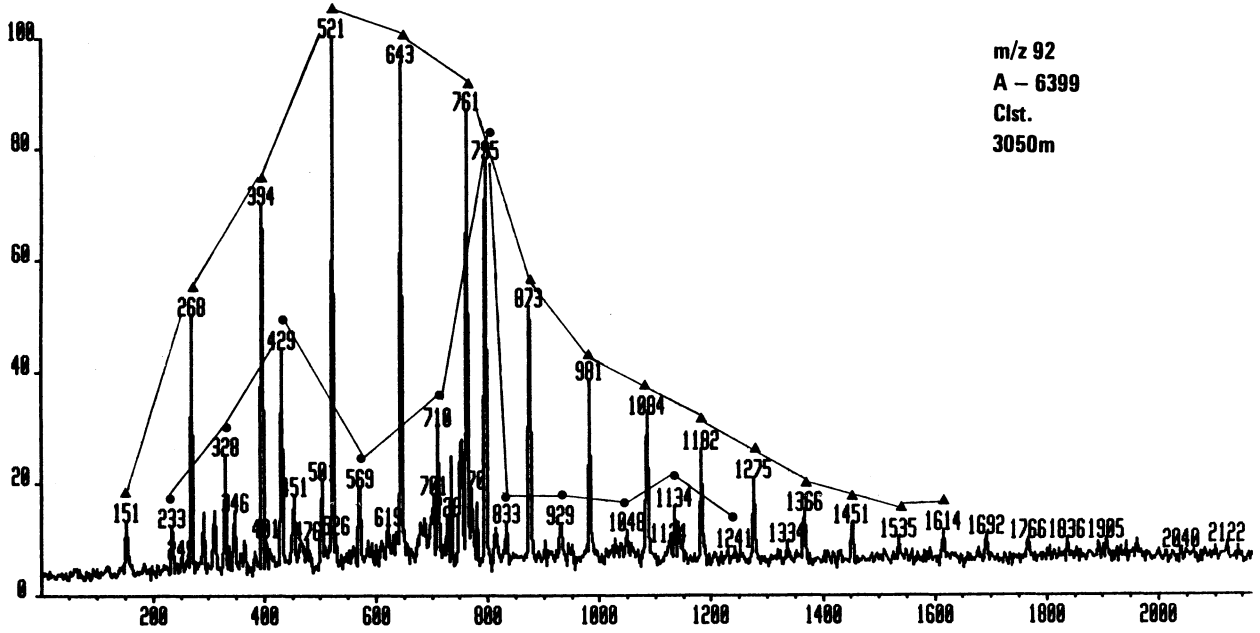
m/z 92
A – 6399
Clst.
3050m

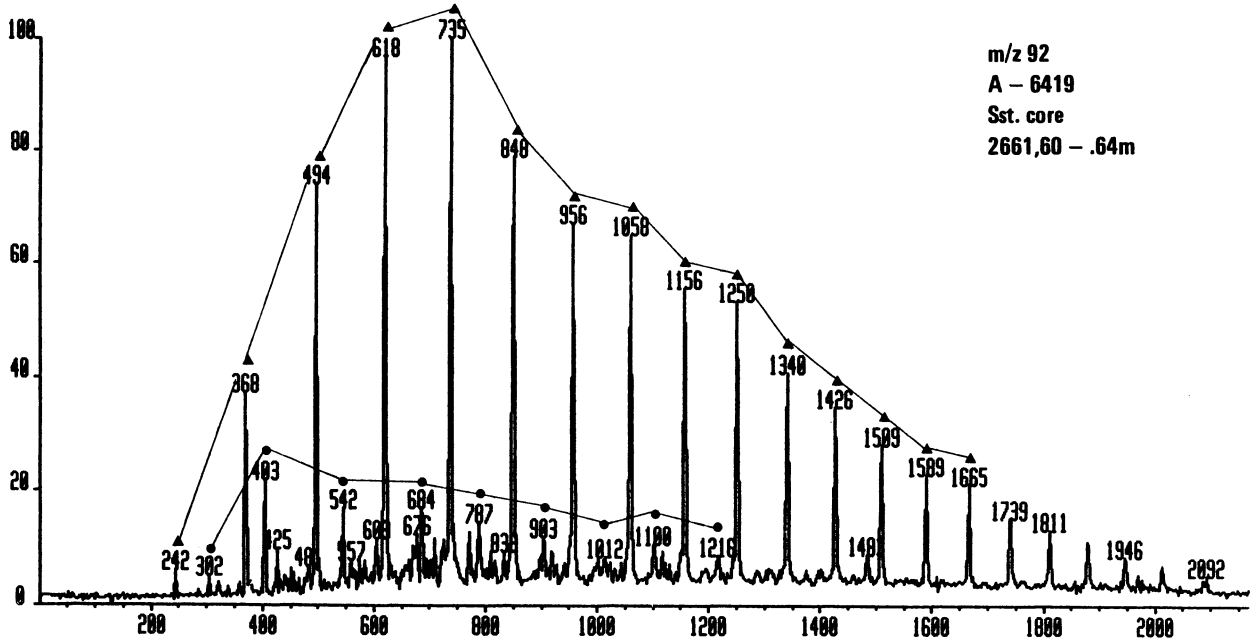
m/z 92
A – 6419
Sst. core
2661,60 – .64m

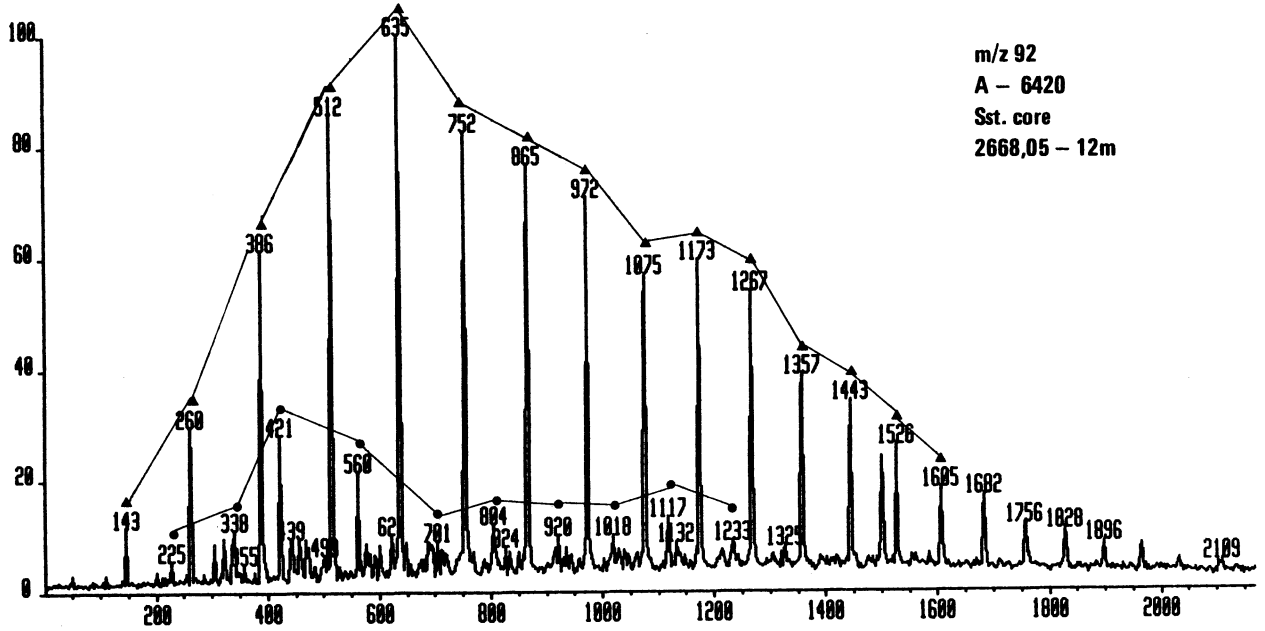
m/z 92
A – 6420
Sst. core
2668,05 – 12m

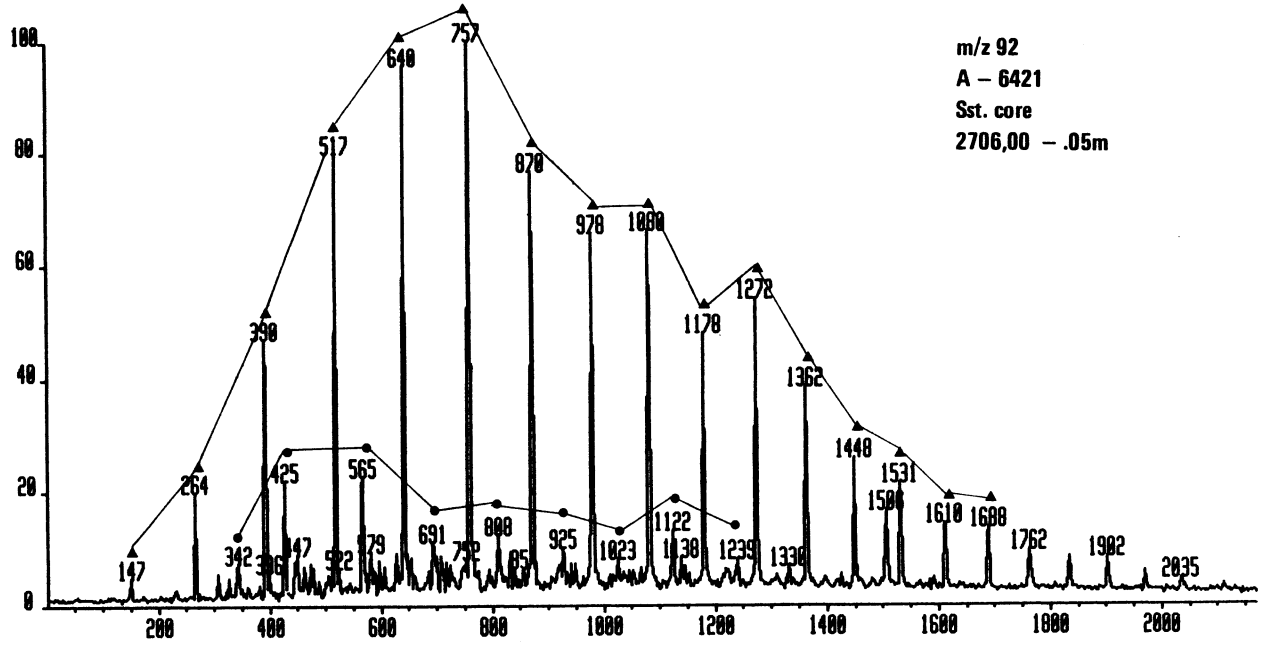
m/z 92
A – 6421
Sst. core
2706,00 – .05m

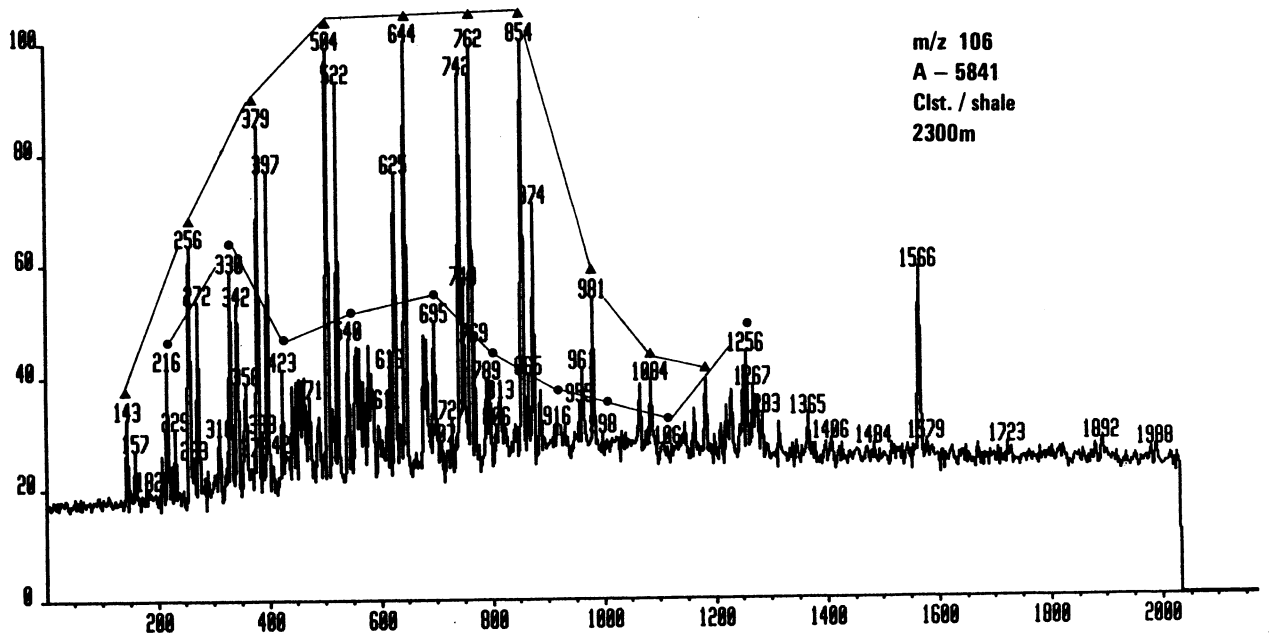
m/z 106
A – 5841
Clst. / shale
2300m

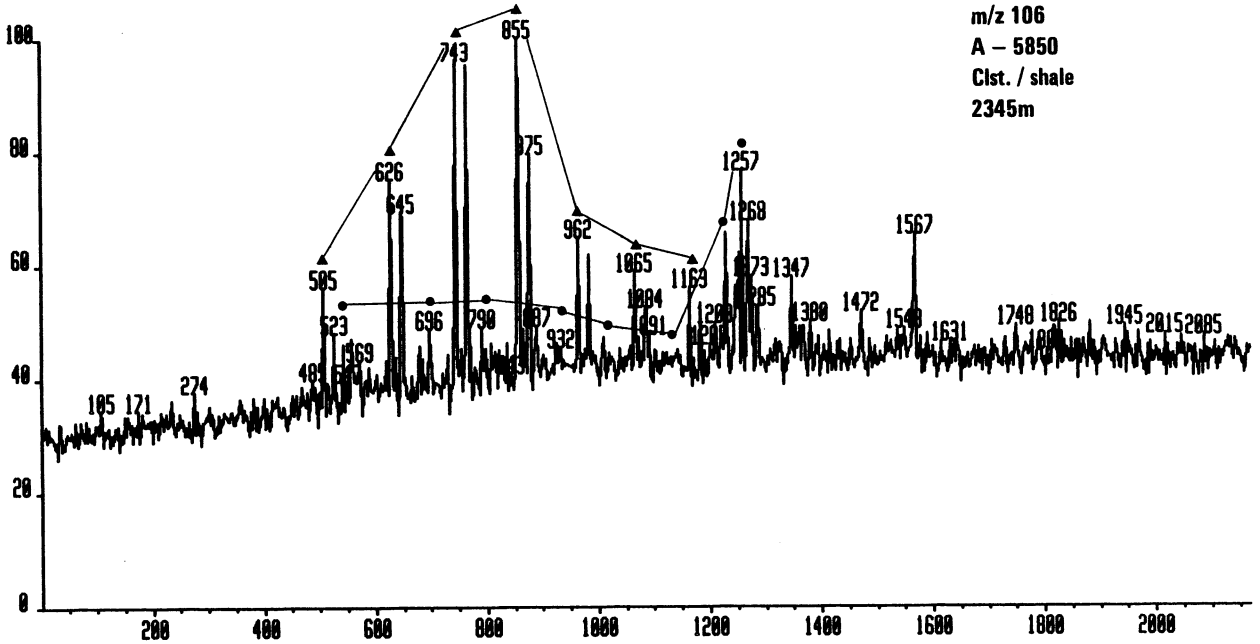
m/z 106
A – 5850
Clst. / shale
2345m

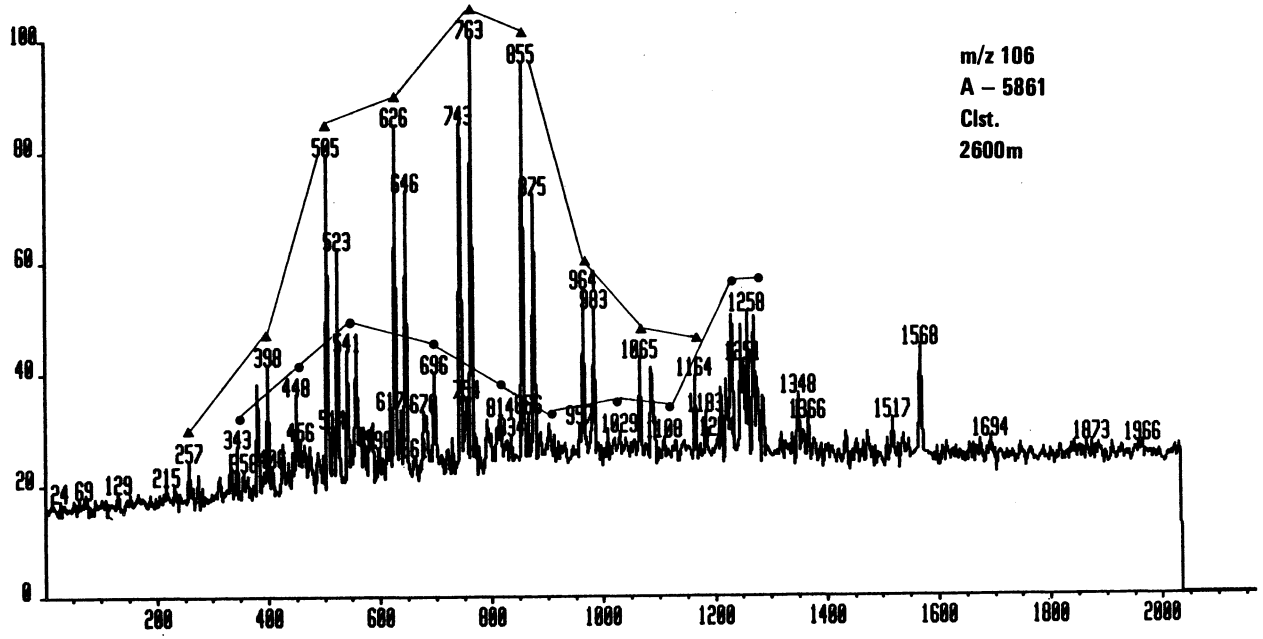
m/z 106
A – 5861
Clst.
2600m

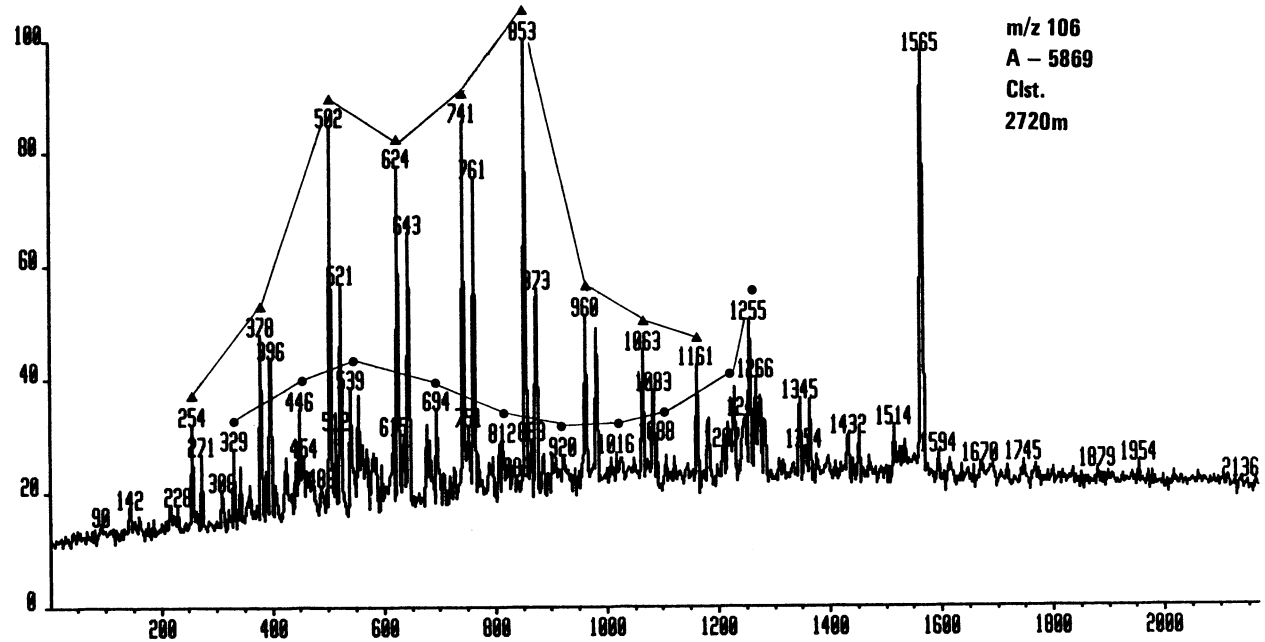
m/z 106
A – 5869
Clst.
2720m

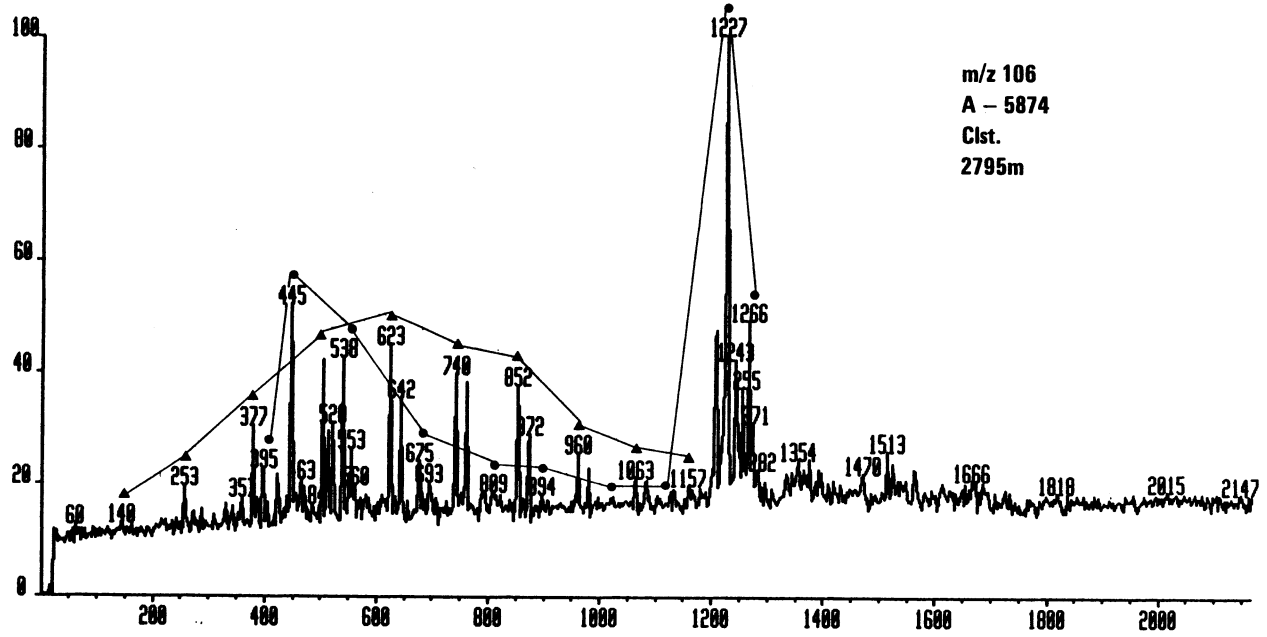
m/z 106
A – 5874
Clst.
2795m

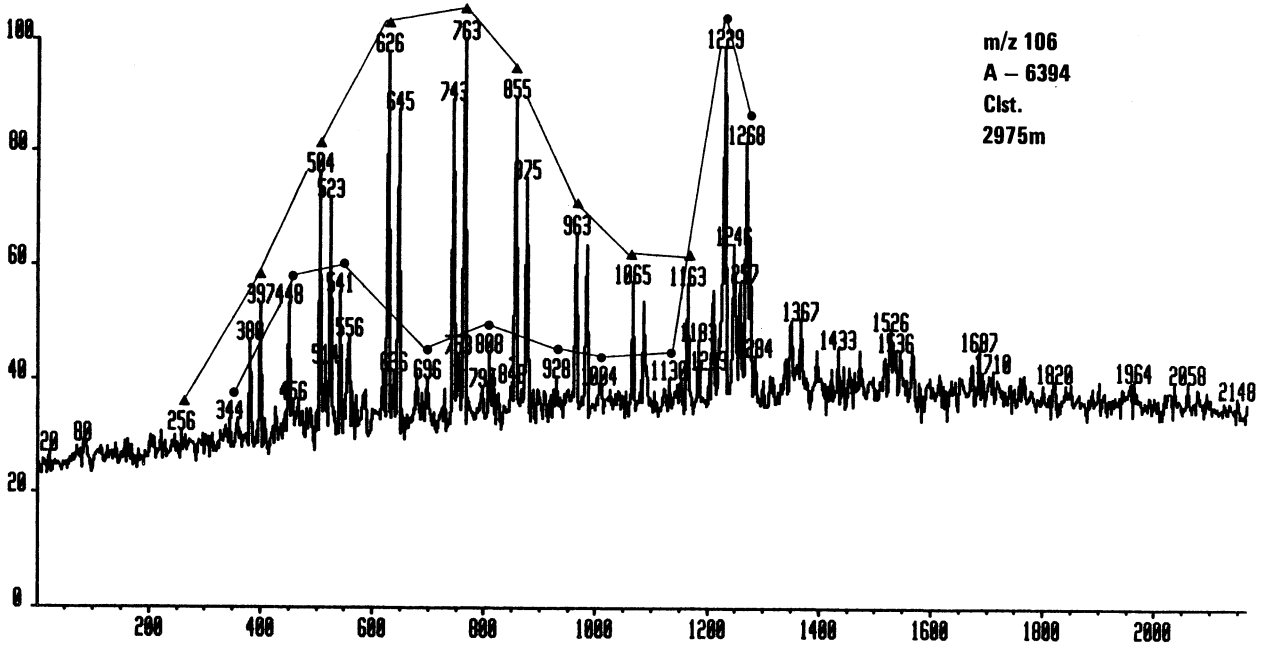
m/z 106
A – 6394
Clst.
2975m

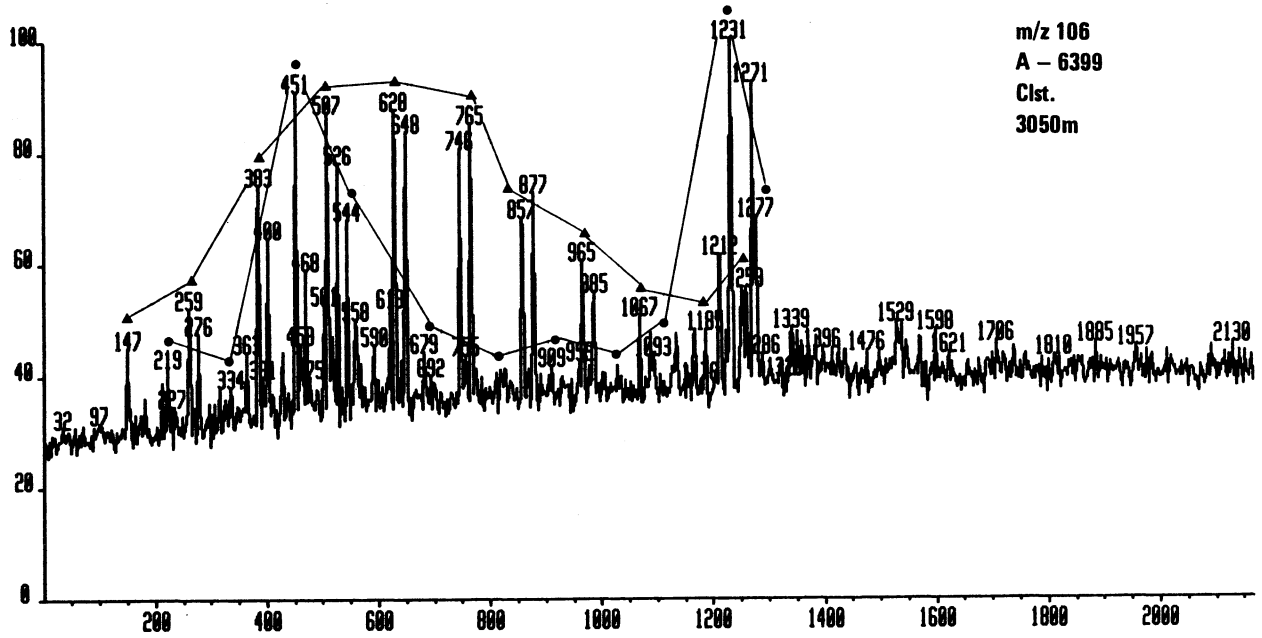
m/z 106
A – 6399
Clst.
3050m

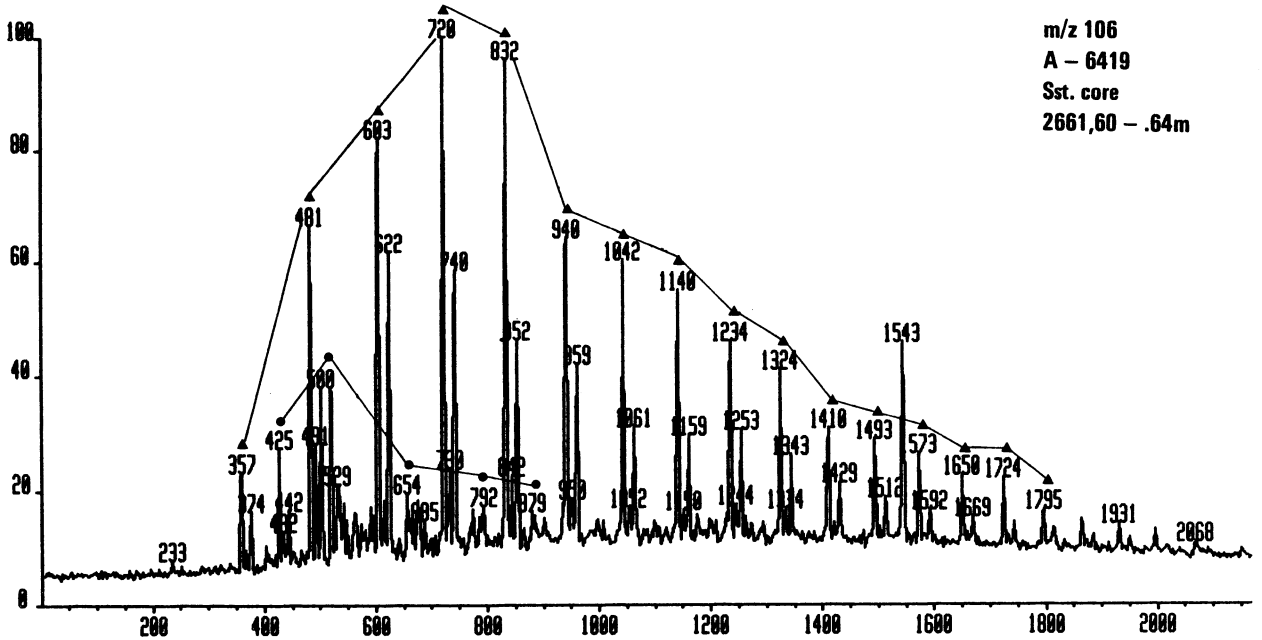
m/z 106
A – 6419
Sst. core
2661,60 – .64m

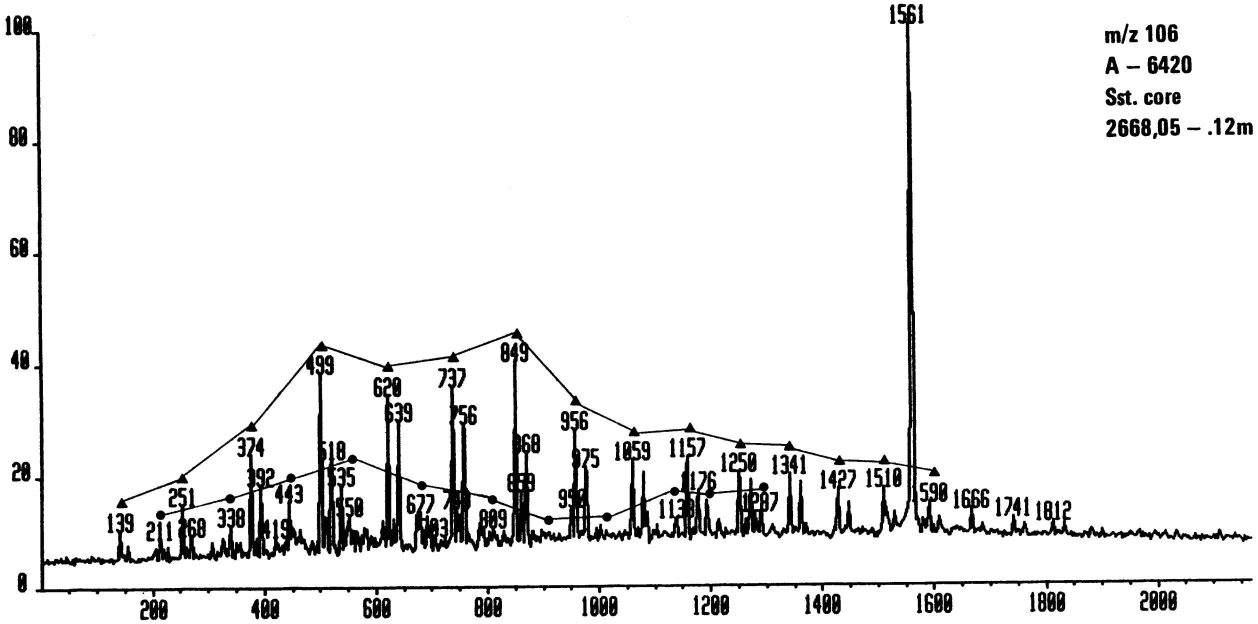
m/z 106
A – 6420
Sst. core
2668,05 – .12m

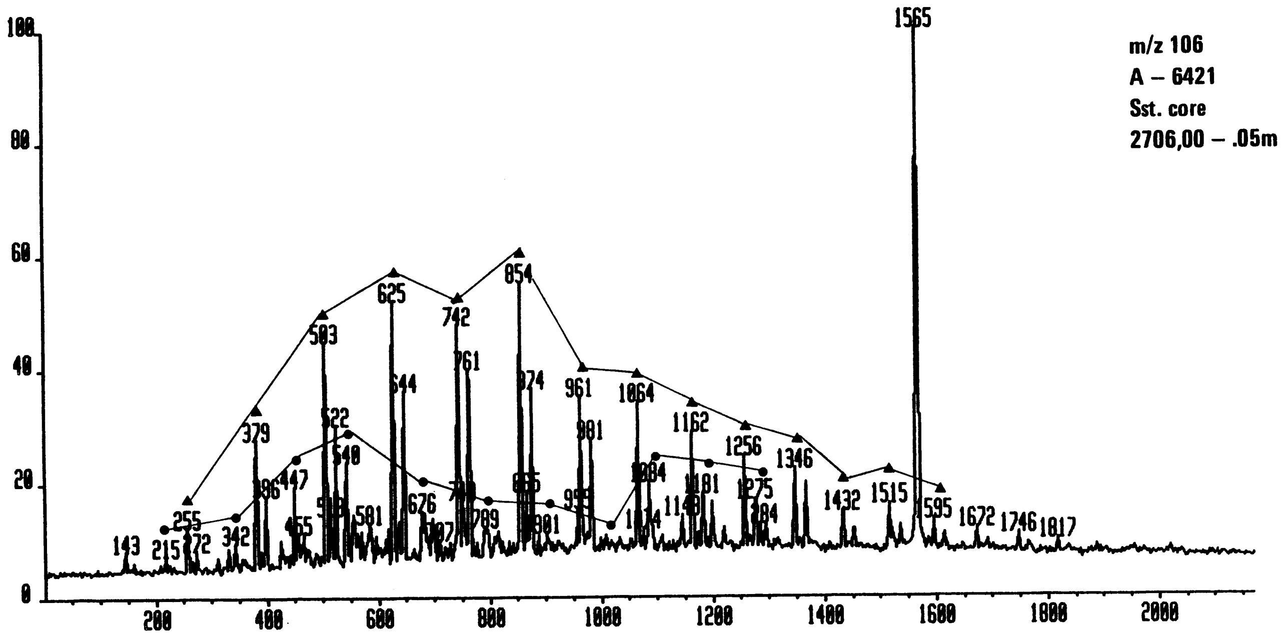
m/z 106
A – 6421
Sst. core
2706,00 – .05m

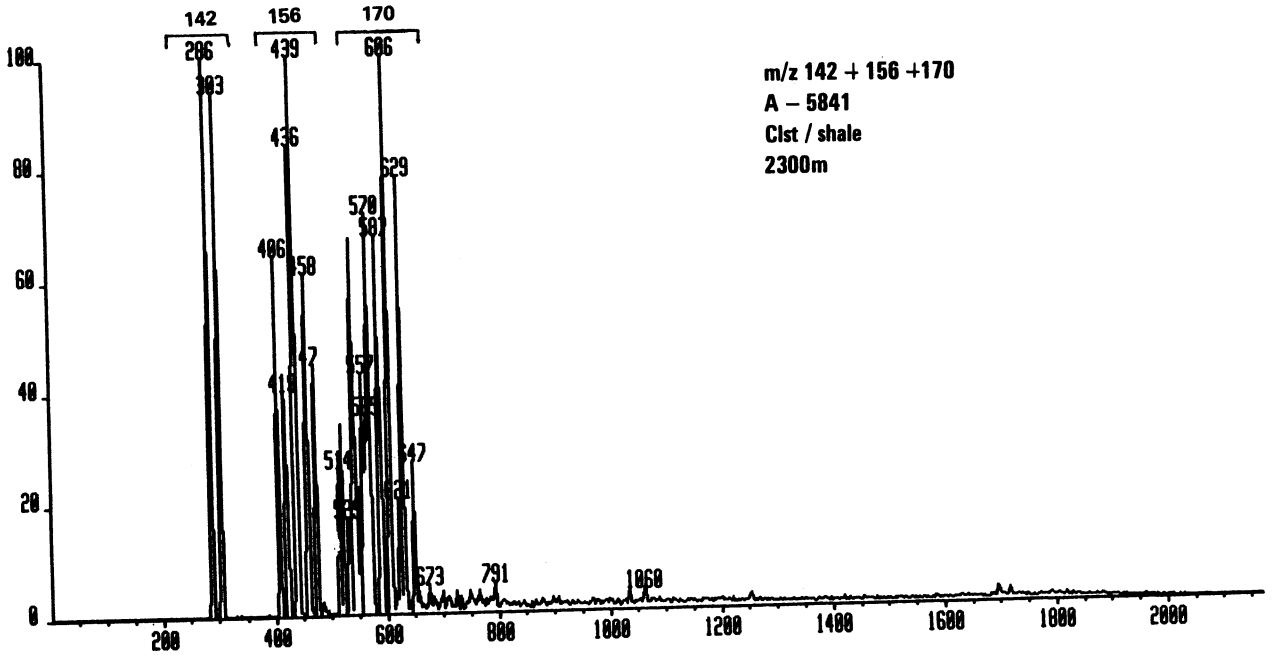
142
156
170
m/z 142 + 156 +170
A – 5841
Clst / shale
2300m

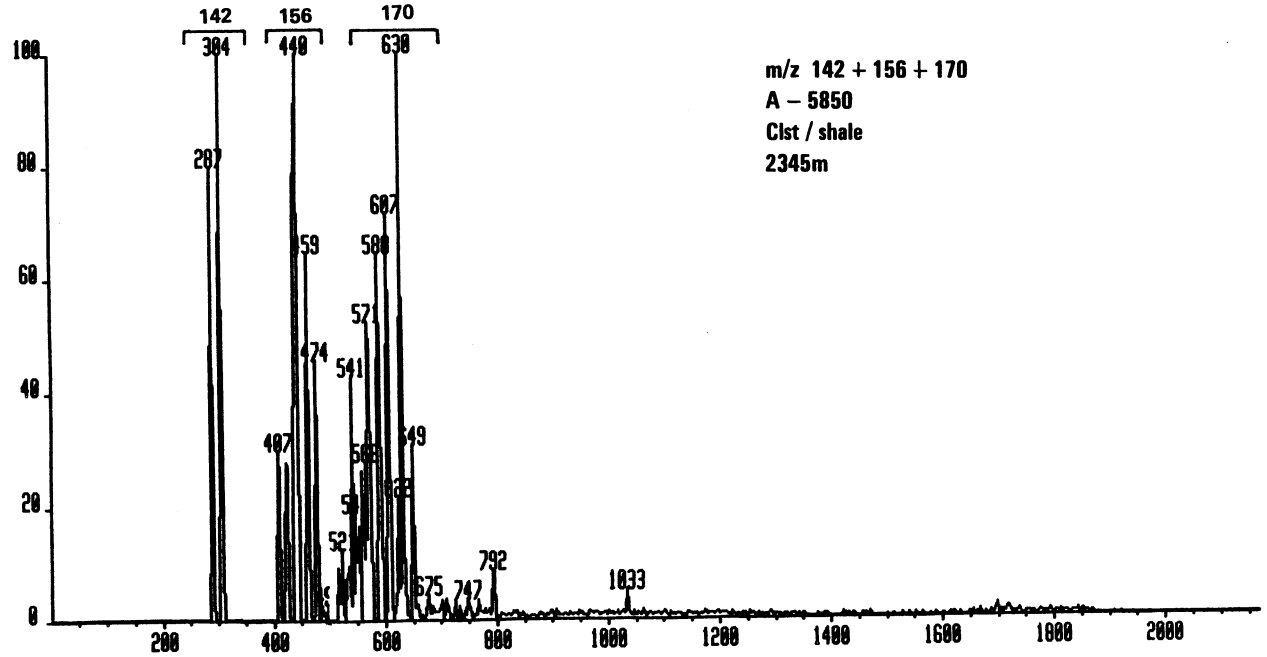
142
156
170
m/z 142 + 156 + 170
A – 5850
Clst / shale
2345m

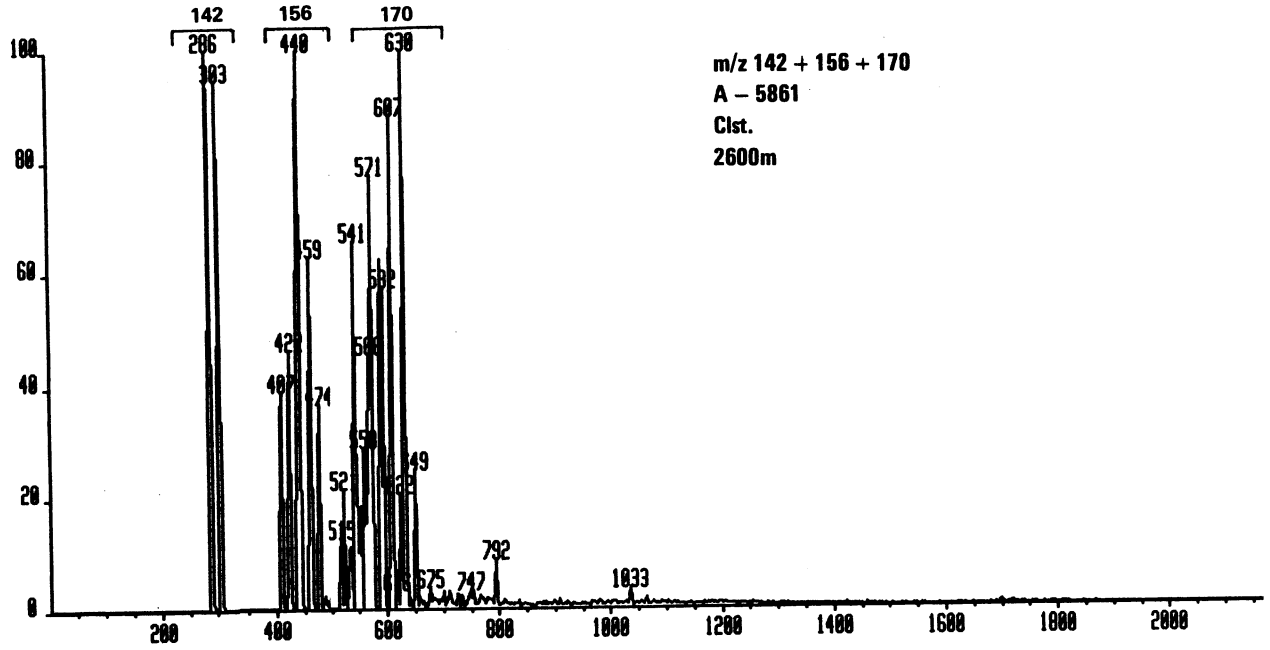

m/z 142 + 156 + 170
A – 5861
Clst.
2600m

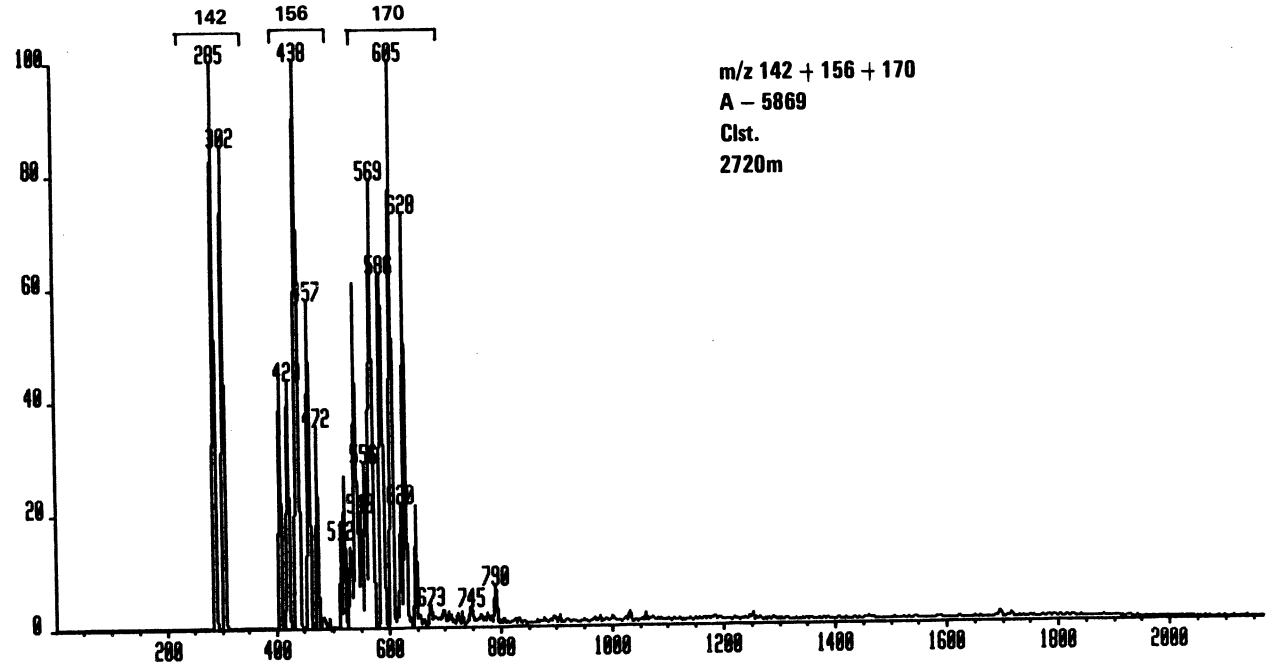

m/z 142 + 156 + 170
A – 5869
Clst.
2720m

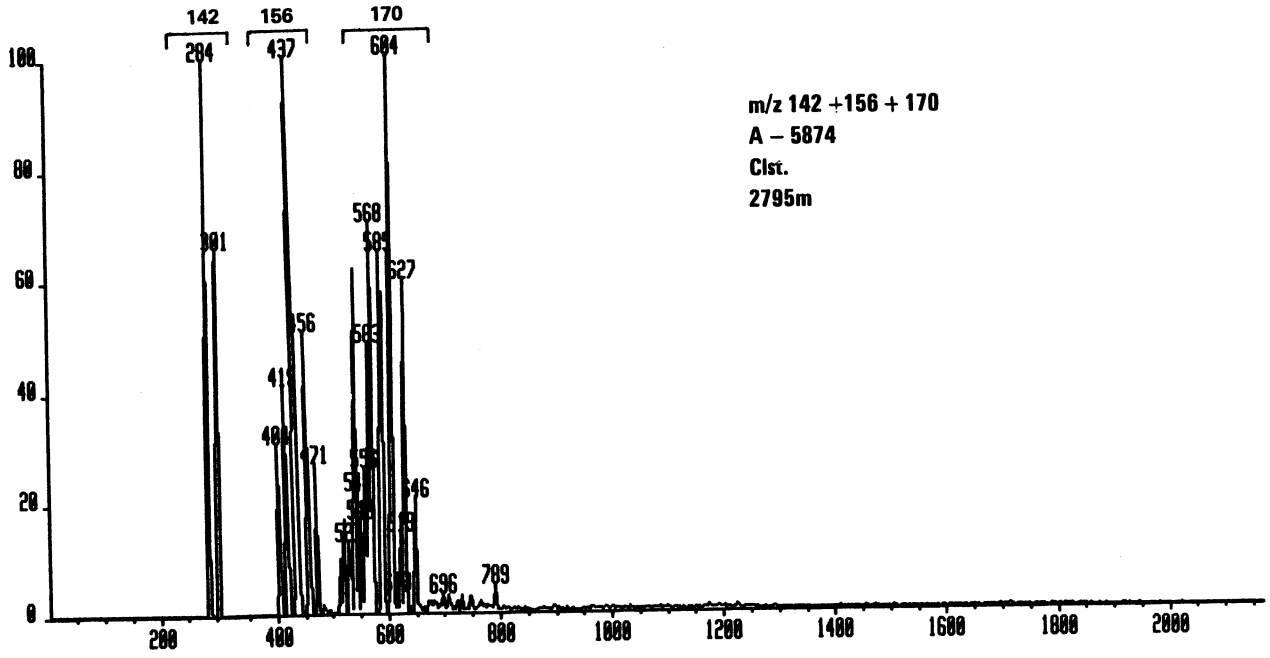

m/z 142 +156 + 170
A – 5874
Clst.
2795m

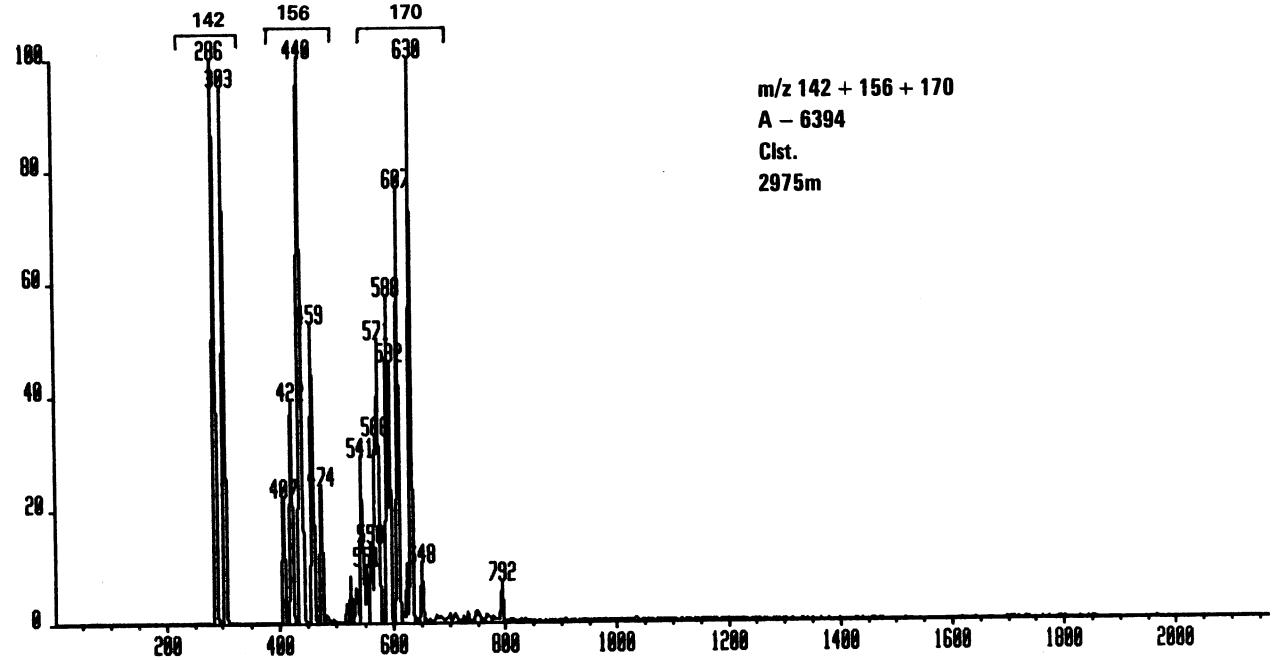

m/z 142 + 156 + 170
A – 6394
Clst.
2975m

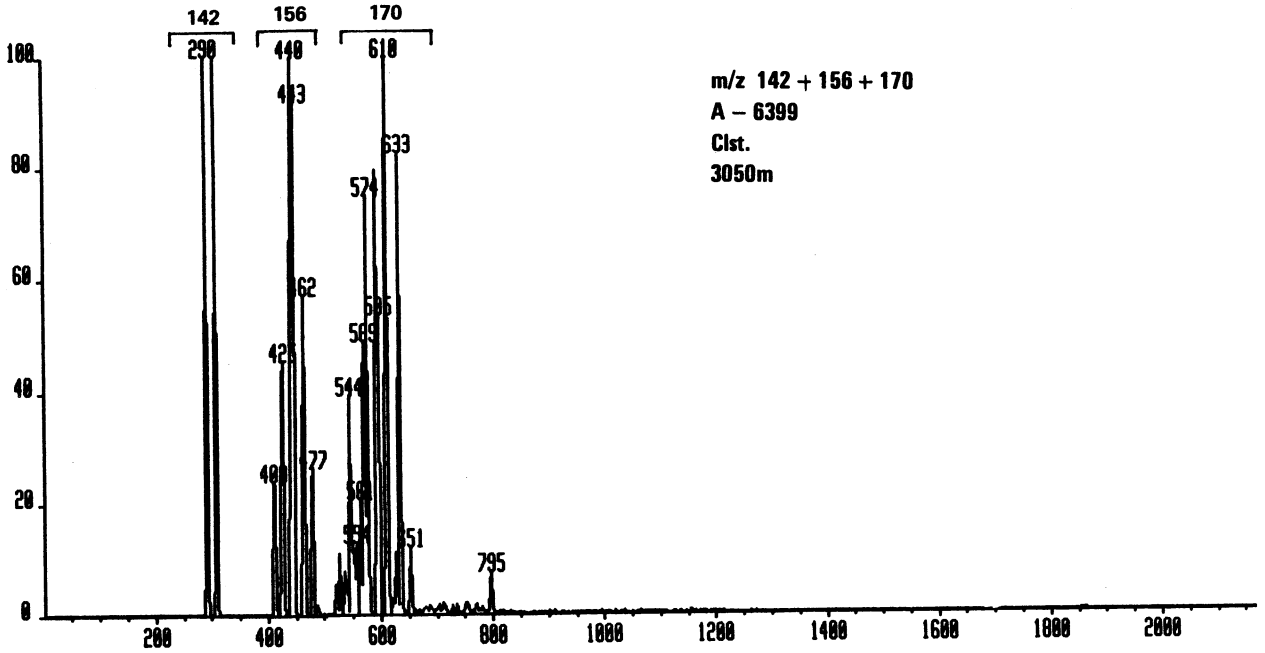
142
156
170
m/z 142 + 156 + 170
A – 6399
Clst.
3050m

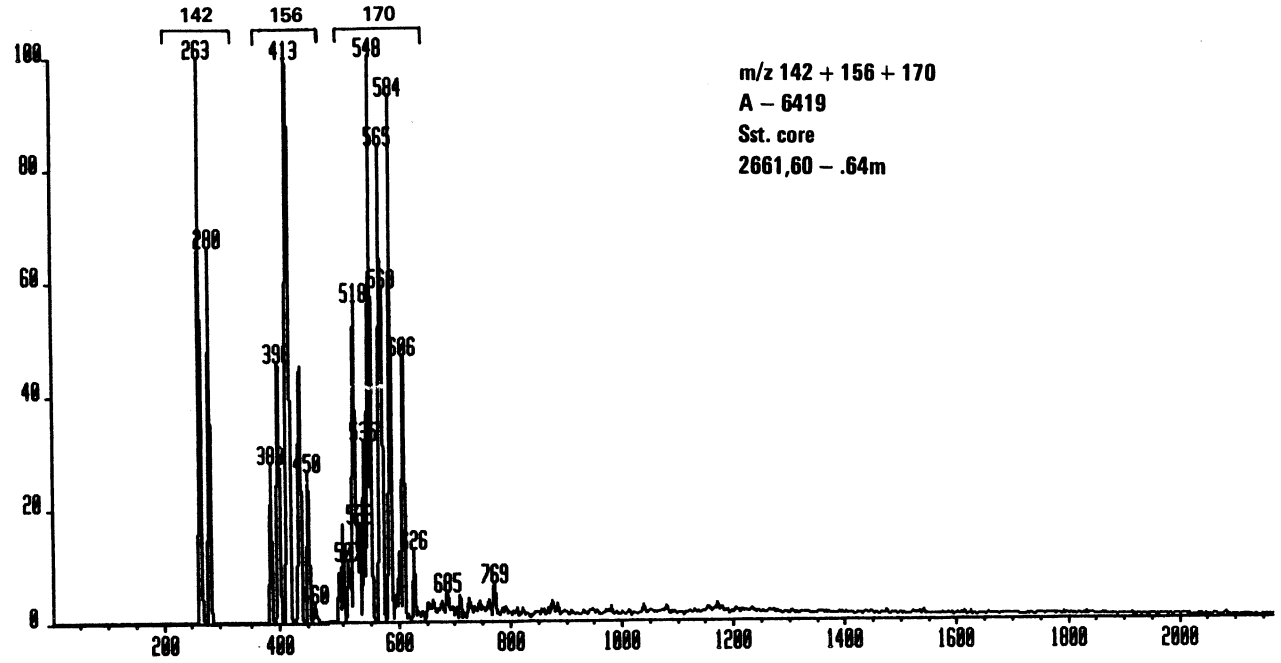
142
156
170
m/z 142 + 156 + 170
A – 6419
Sst. core
2661,60 – .64m

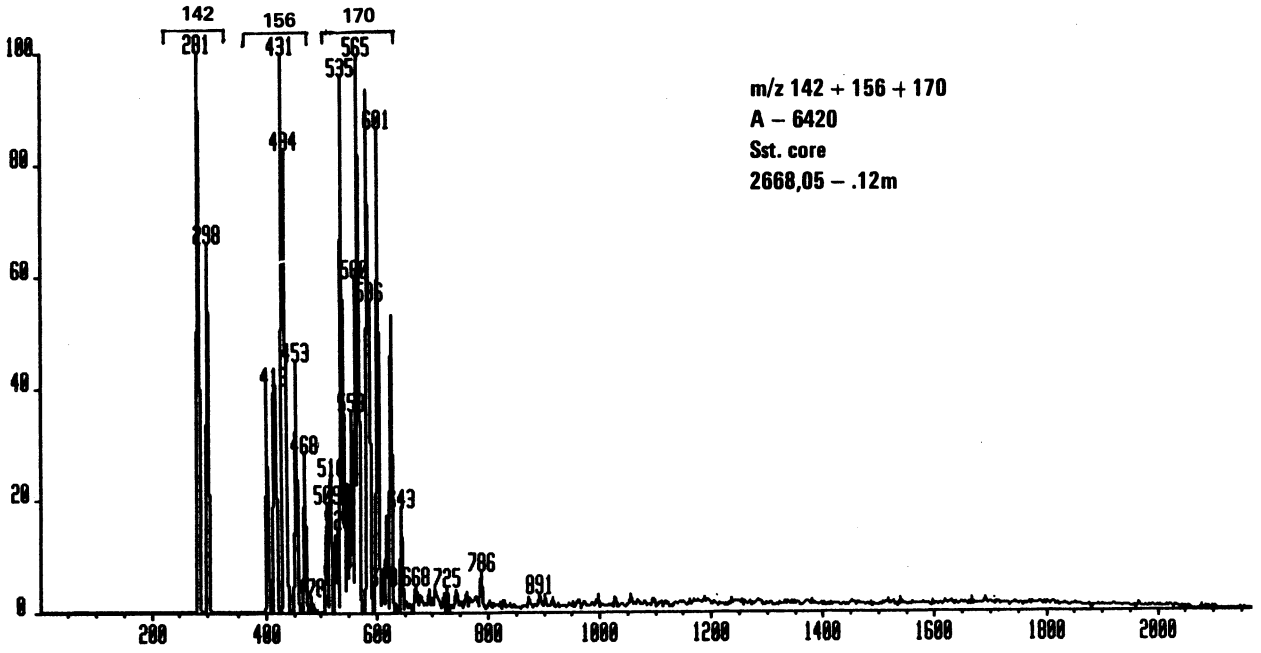

m/z 142 + 156 + 170
A – 6420
Sst. core
2668,05 – .12m

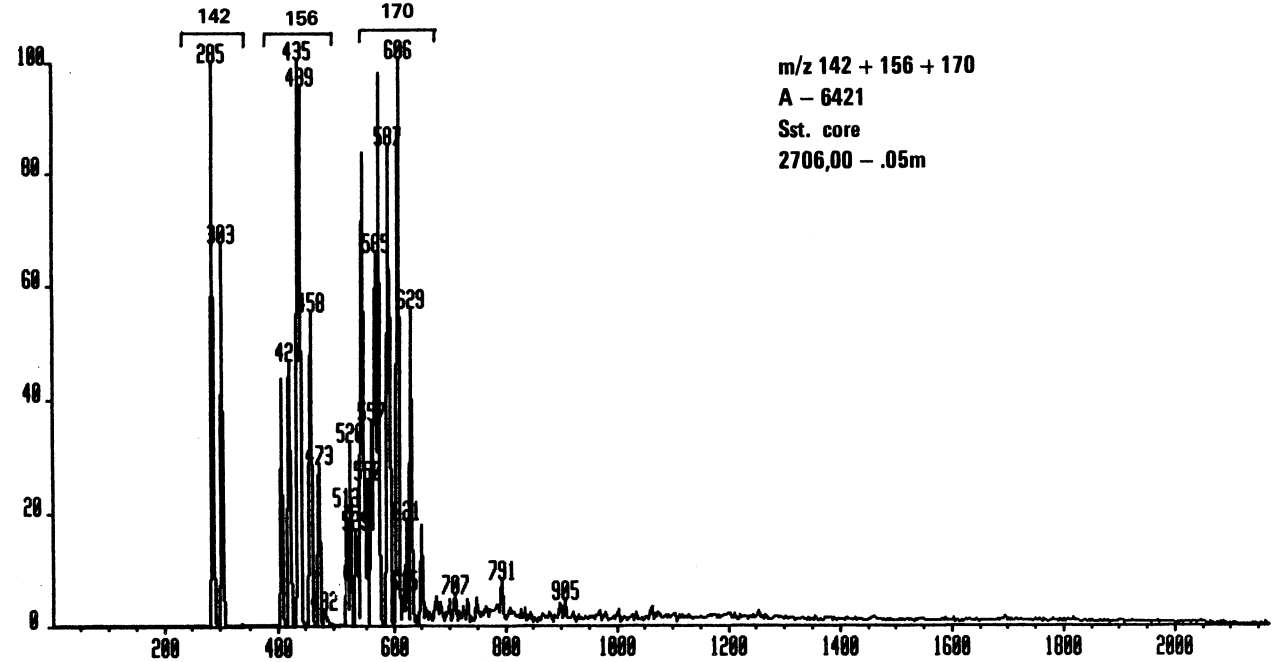

m/z 142 + 156 + 170
A – 6421
Sst. core
2706,00 – .05m

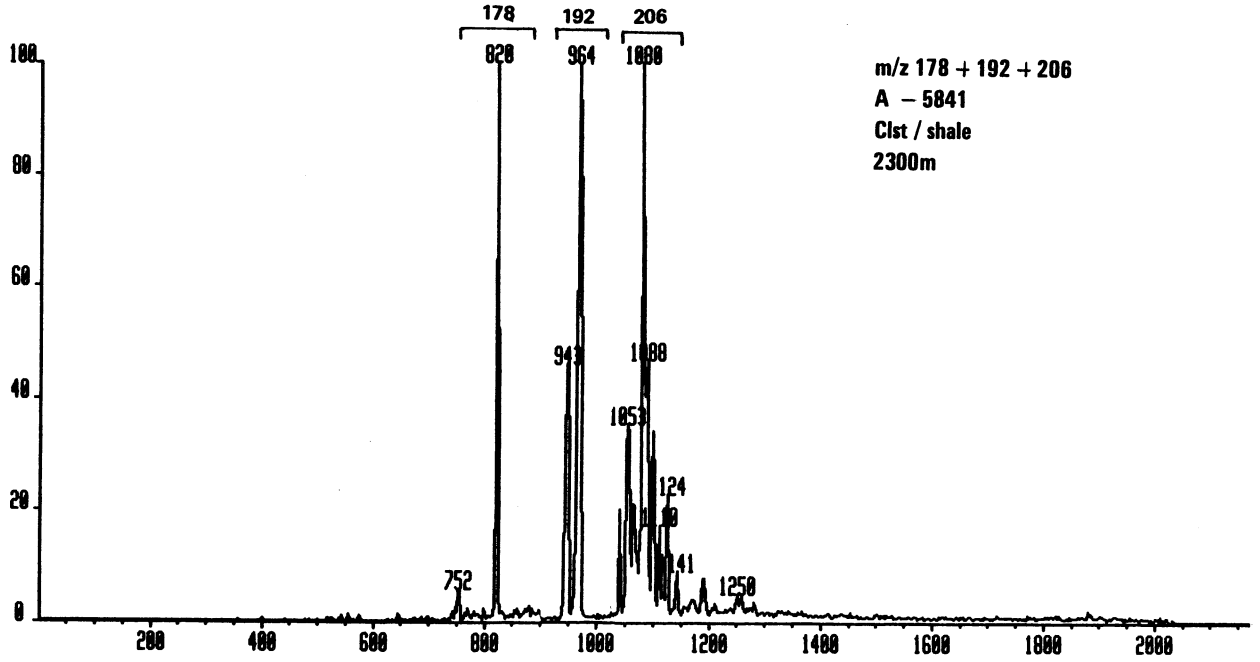
178
192
206
820
964
1000
m/z 178 + 192 + 206
A – 5841
Clst / shale
2300m
752
1250
100
80
60
40
20
0
200
400
600
800
1000
1200
1400
1600
1800
2000

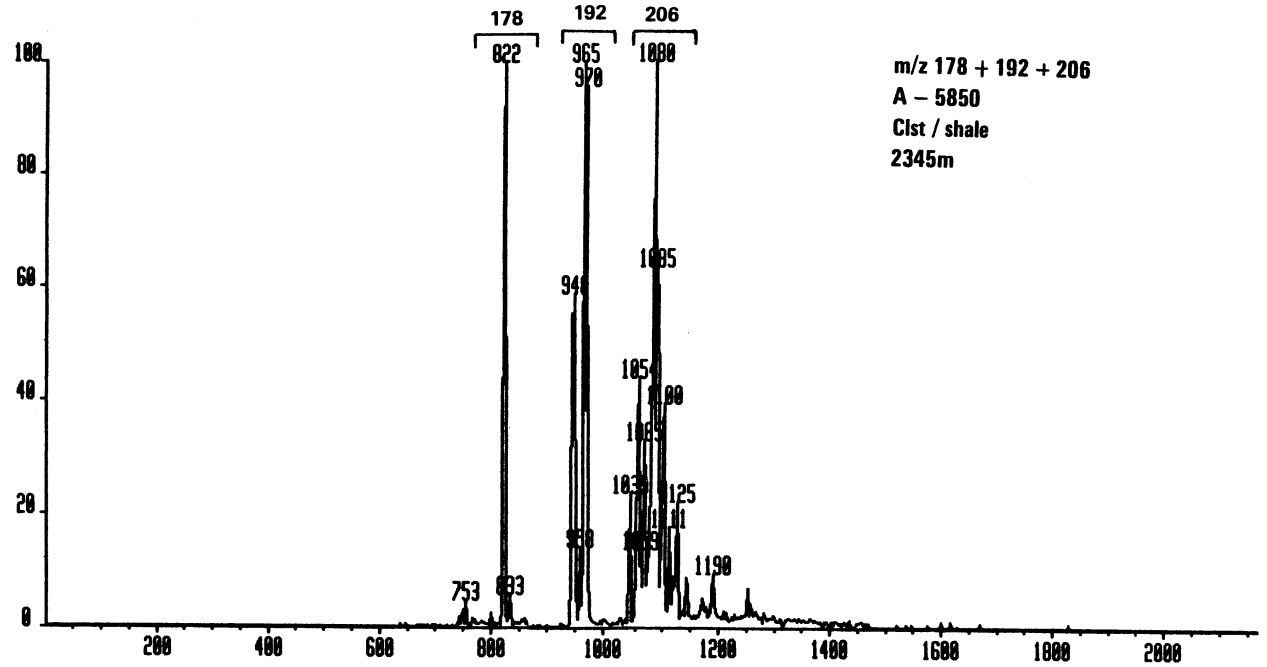
178
192
206
822
965
970
1000
m/z 178 + 192 + 206
A – 5850
Clst / shale
2345m
753
1190
100
80
60
40
20
0
200
400
600
800
1000
1200
1400
1600
1800
2000

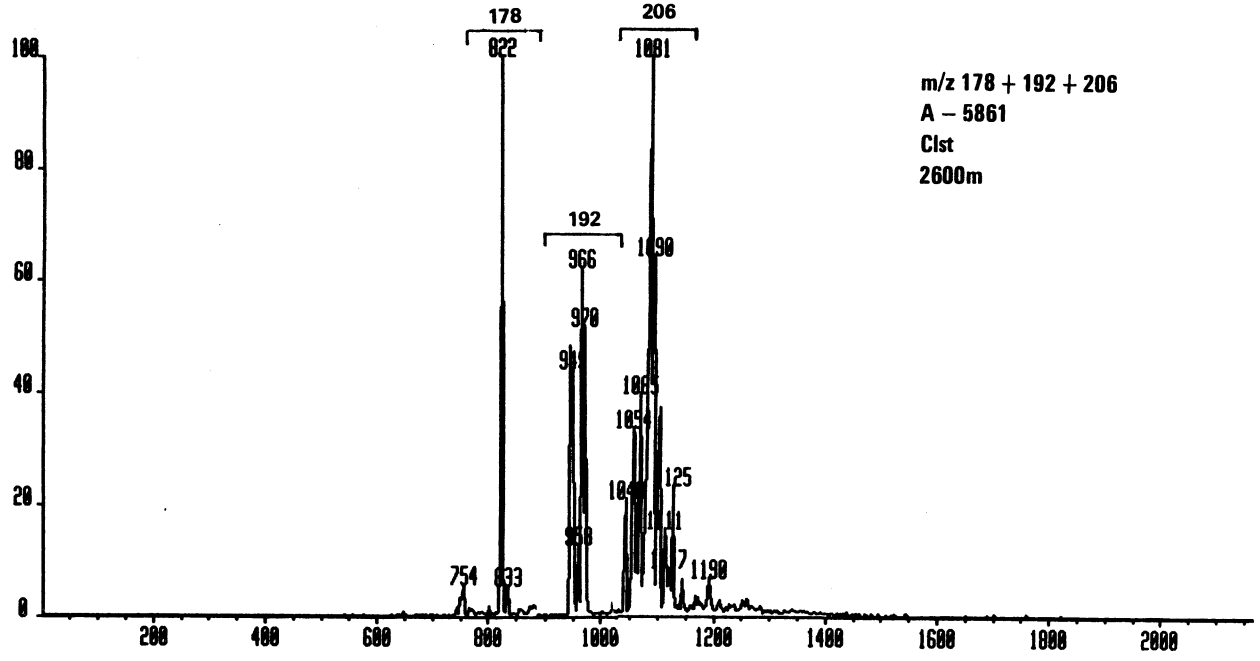
178
822
206
1081
192
966
970
1090
754
833
1190
125
m/z 178 + 192 + 206
A – 5861
Clst
2600m

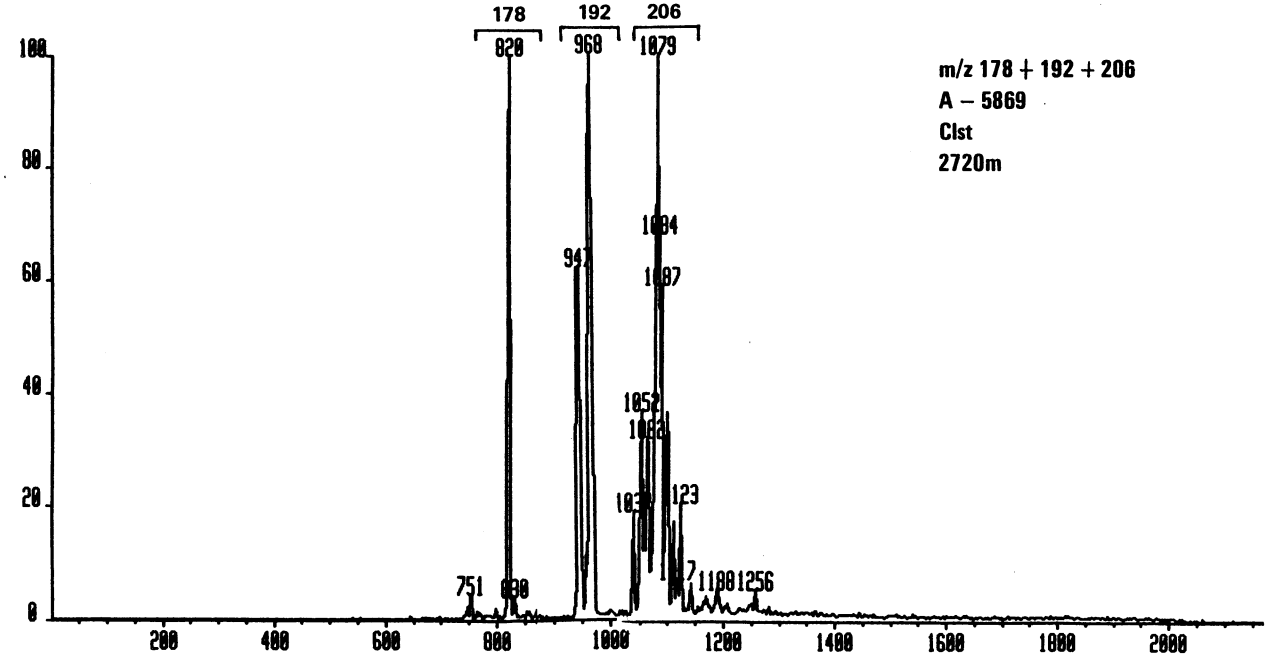
178
820
192
968
206
1079
942
1084
1087
1052
123
751
1188
1256
m/z 178 + 192 + 206
A – 5869
Clst
2720m

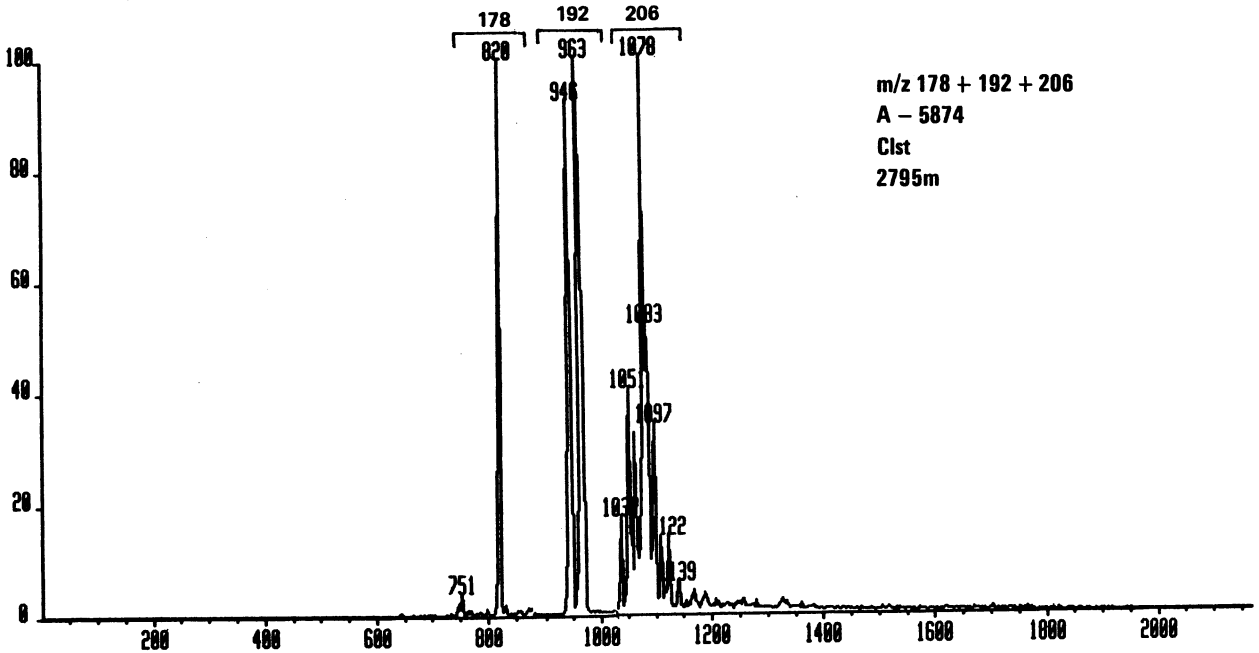
178
192
206
820
963
946
1078
1083
1085
1097
1122
751
m/z 178 + 192 + 206
A – 5874
Clst
2795m

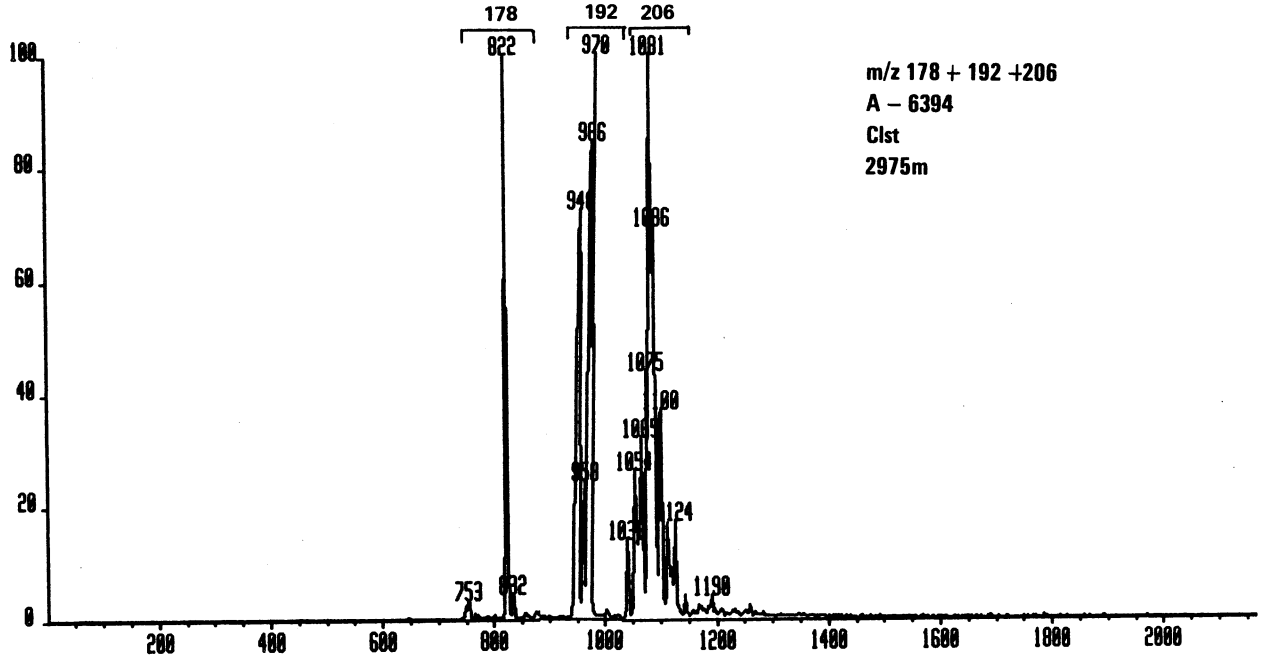
178
192
206
822
970
1081
966
946
1086
1075
1124
753
1190
m/z 178 + 192 +206
A – 6394
Clst
2975m

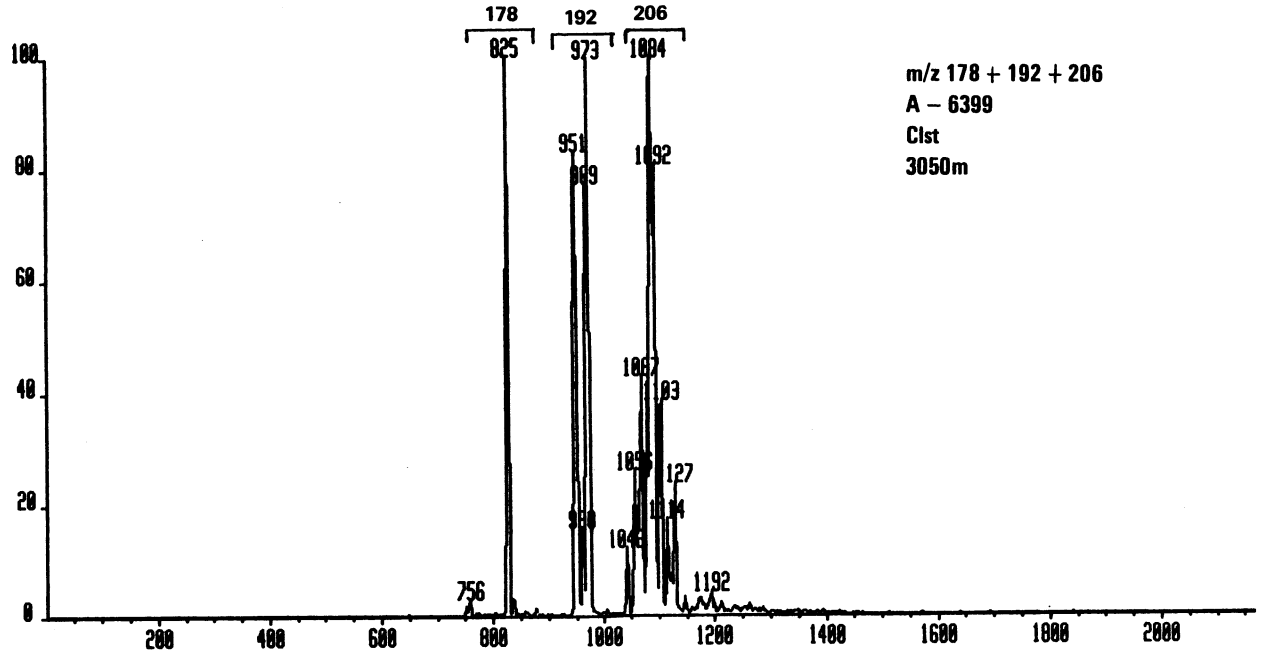
178
192
206
825
973
1084
951
969
1092
1083
1127
1192
756
m/z 178 + 192 + 206
A – 6399
Clst
3050m

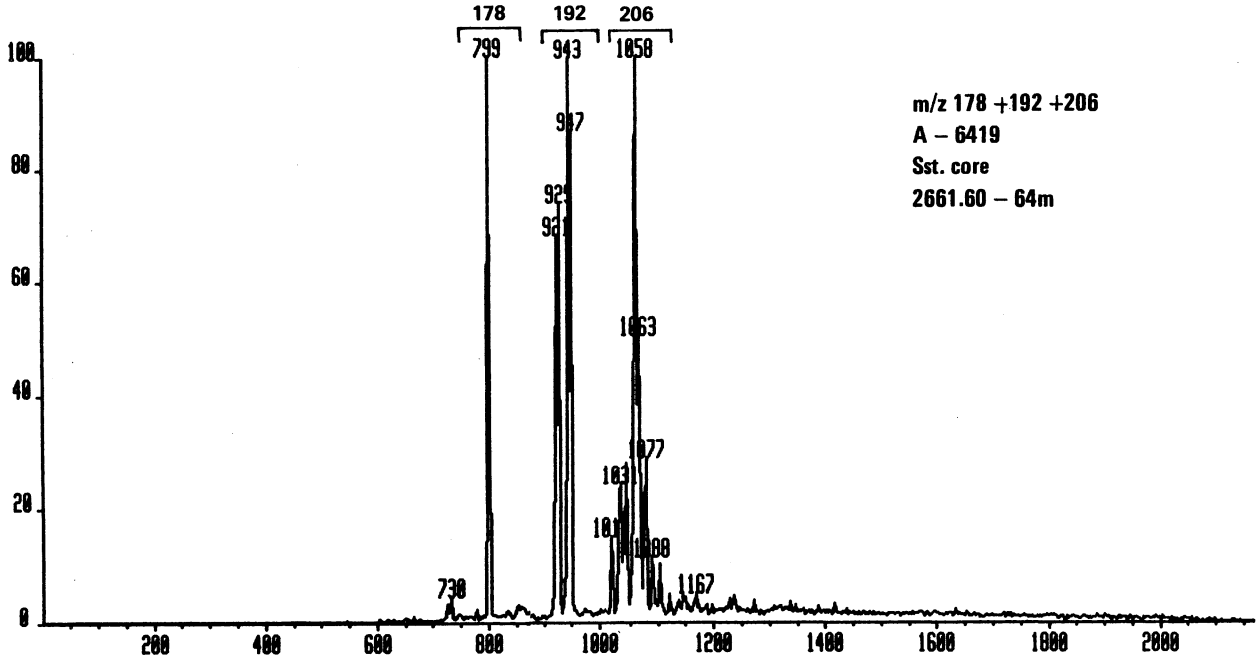
178
192
206
799
943
1058
987
929
931
1063
1077
1167
738
m/z 178 +192 +206
A – 6419
Sst. core
2661.60 – 64m

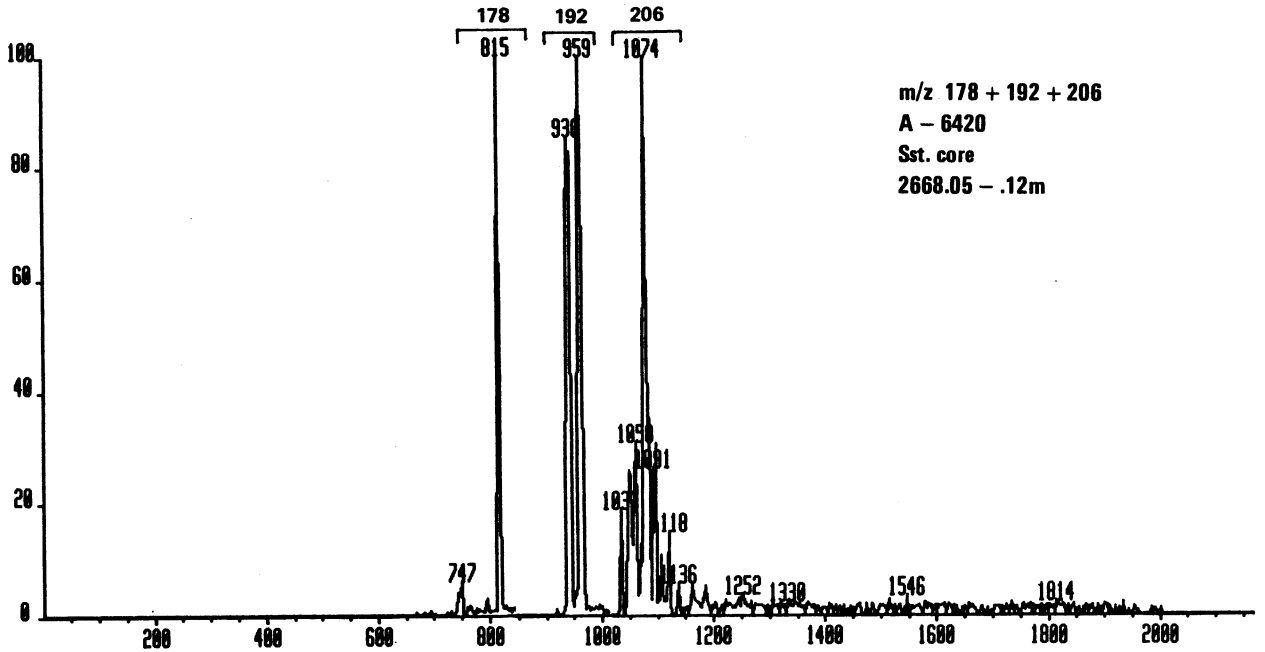
178
192
206
815
959
1074
m/z 178 + 192 + 206
A – 6420
Sst. core
2668.05 – .12m
747
1252
1330
1546
1814
100
80
60
40
20
0
200
400
600
800
1000
1200
1400
1600
1800
2000

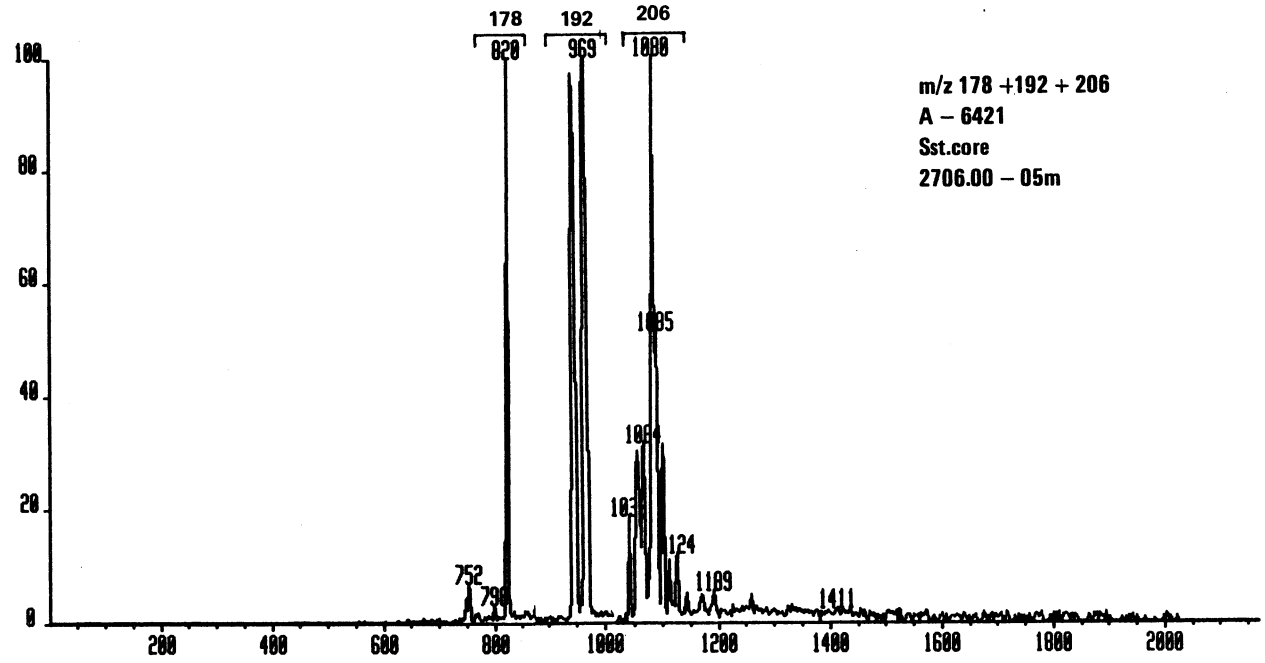
178
192
206
820
969
1080
m/z 178 +192 + 206
A – 6421
Sst.core
2706.00 – 05m
752
790
1189
1411
100
80
60
40
20
0
200
400
600
800
1000
1200
1400
1600
1800
2000

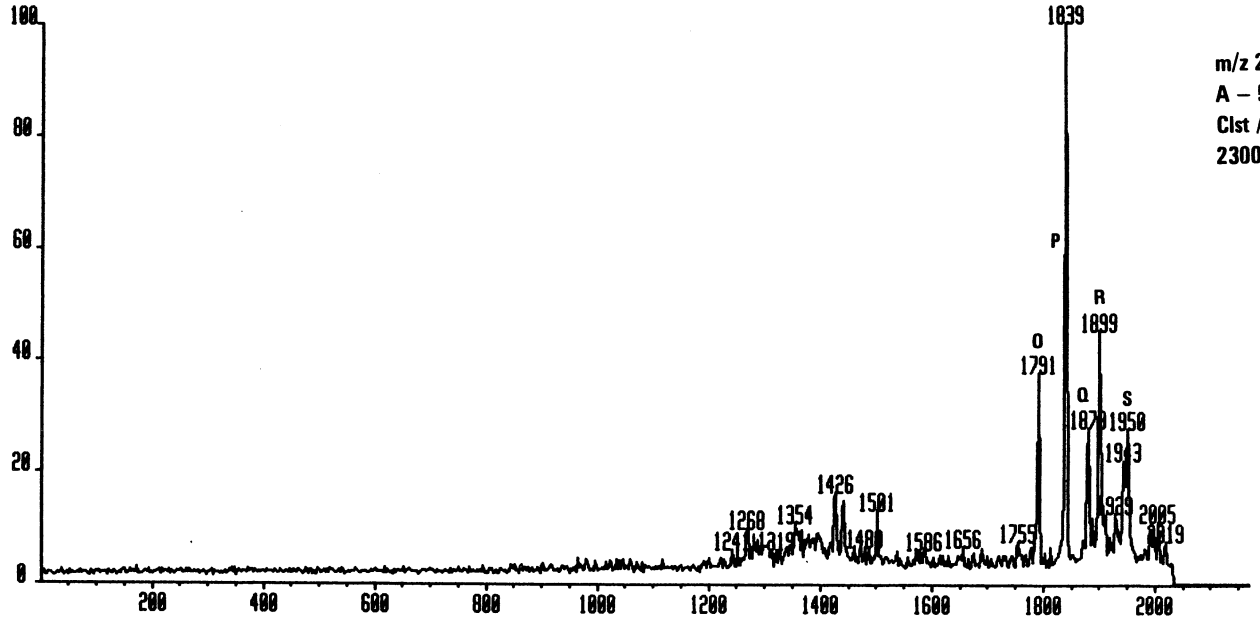
m/z 231
A – 5841
Clst / shale
2300m
1839
P
R
1899
O
1791
Q
S
1950
1426
1501
1268
1354
1586
1656
1759
2005

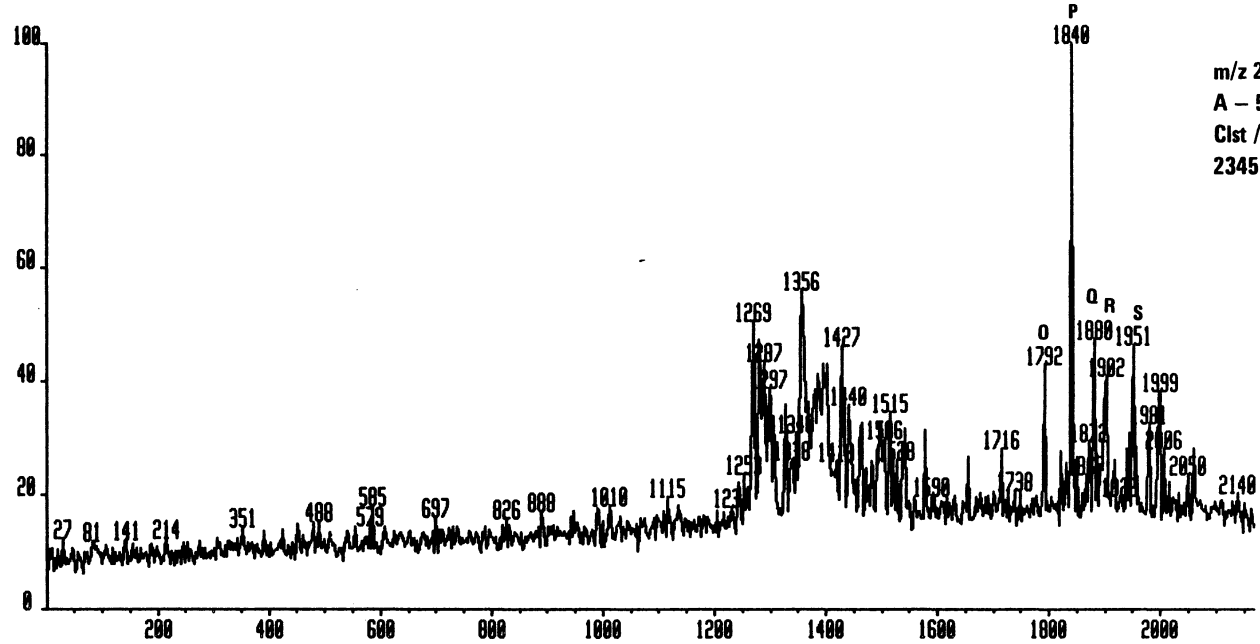
m/z 231
A – 5850
Clst / shale
2345m
P
1840
1356
1269
1427
Q
R
S
O
1792
1880
1951
1982
1999
1716
1515
585
697
826
880
1010
1115
2140

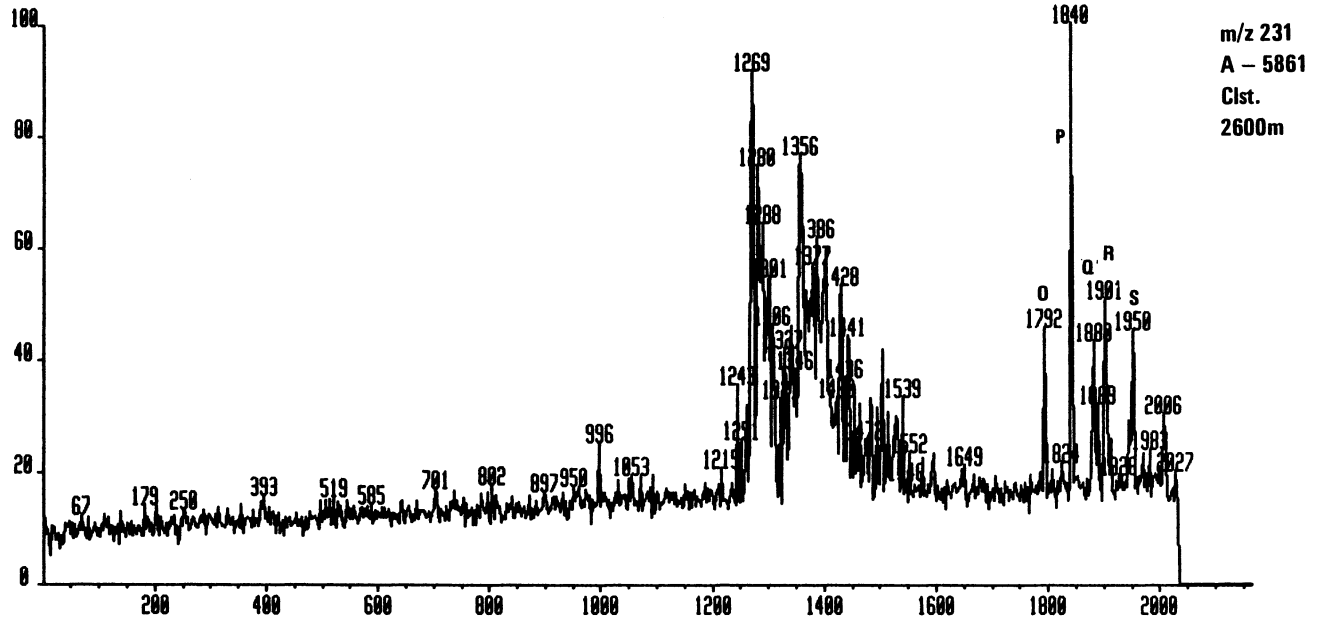
m/z 231
A – 5861
Clst.
2600m
1840
P
1269
1356
O
1792
Q
R
1901
S
1950
996
1539
2006
1649
67
179
250
393
519
585
701
802
897
950
1053
200
400
600
800
1000
1200
1400
1600
1800
2000

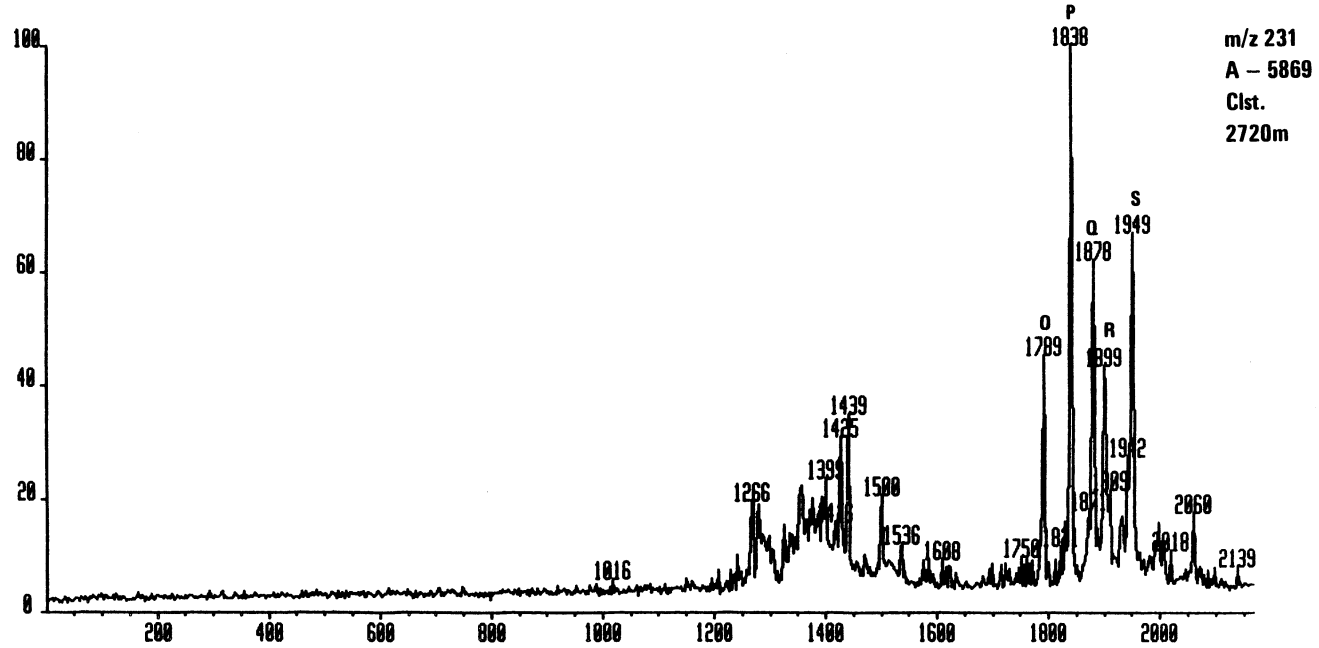
m/z 231
A – 5869
Clst.
2720m
P
1838
S
1949
Q
1878
O
1789
R
1439
1425
1399
1500
1266
1962
2060
1536
1016
2139
200
400
600
800
1000
1200
1400
1600
1800
2000

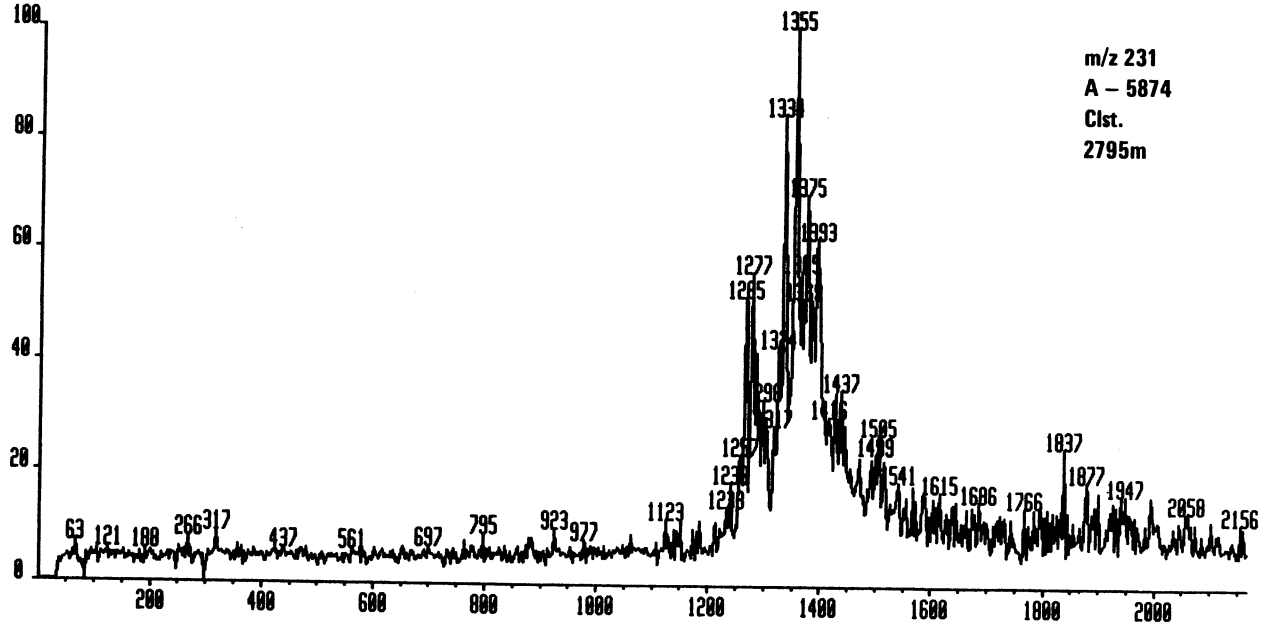
m/z 231
A – 5874
Clst.
2795m

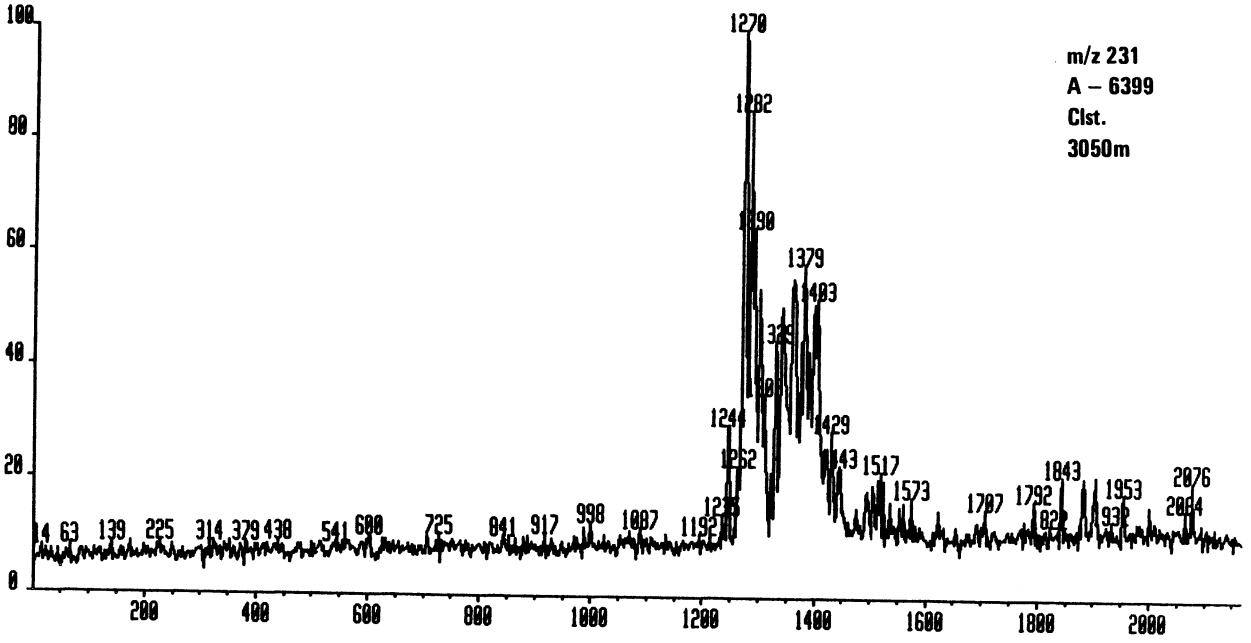
m/z 231
A – 6399
Clst.
3050m

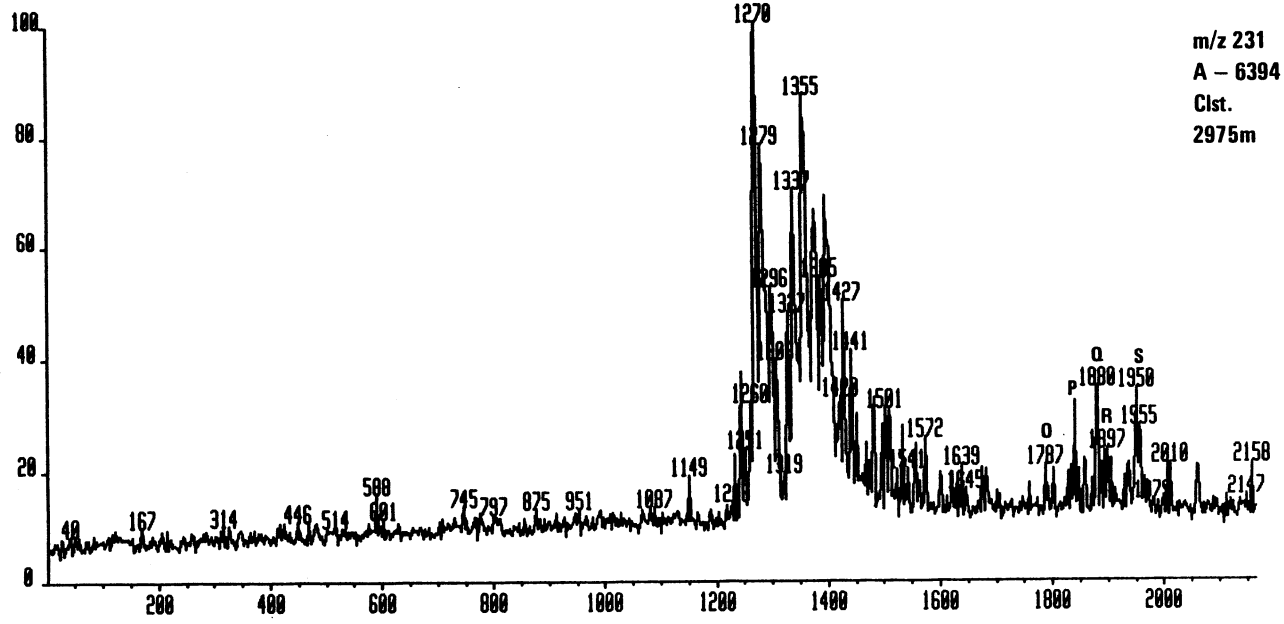
m/z 231
A – 6394
Clst.
2975m

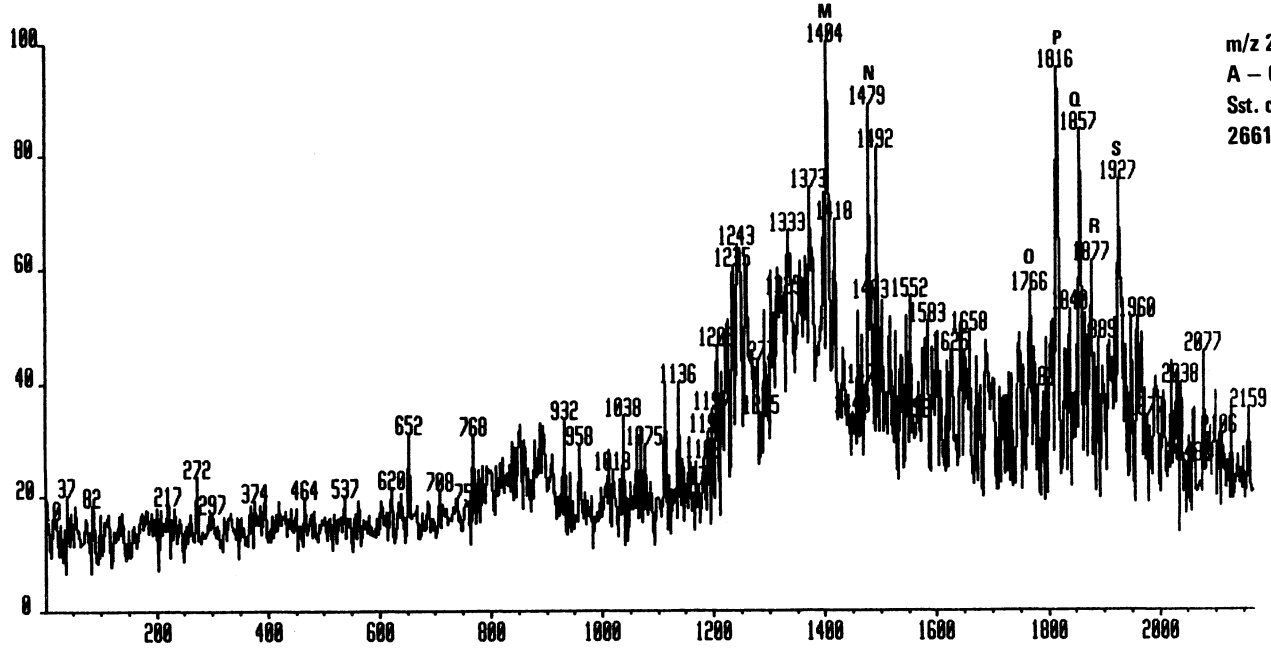
m/z 231
A – 6419
Sst. core
2661,60 – .64m

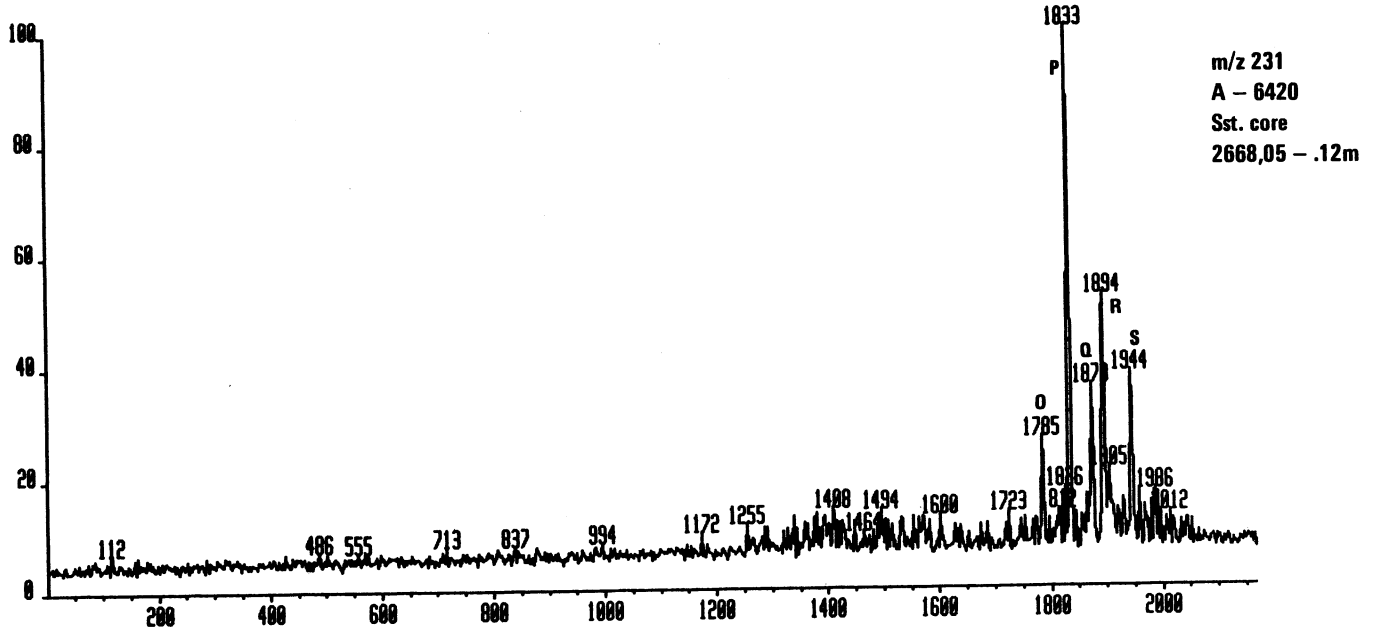
m/z 231
A – 6420
Sst. core
2668,05 – .12m
1833
P
1894
R
S
1944
Q
1878
O
1785
1886
1986
1812
1723
1688
1494
1488
1255
1172
994
837
713
555
486
112
100
80
60
40
20
0
200
400
600
800
1000
1200
1400
1600
1800
2000

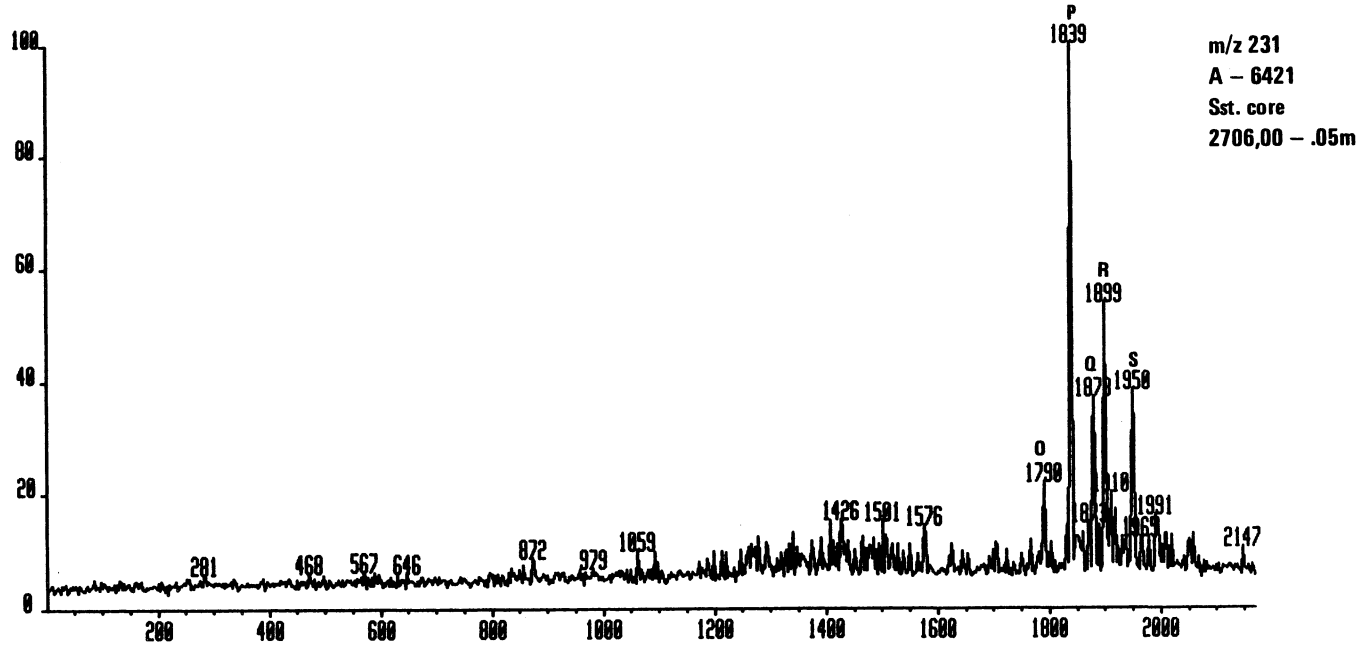
m/z 231
A – 6421
Sst. core
2706,00 – .05m
P
1839
R
1899
Q
1878
S
1950
O
1790
1991
2147
1576
1591
1426
1059
979
872
646
562
468
281
100
80
60
40
20
0
200
400
600
800
1000
1200
1400
1600
1800
2000

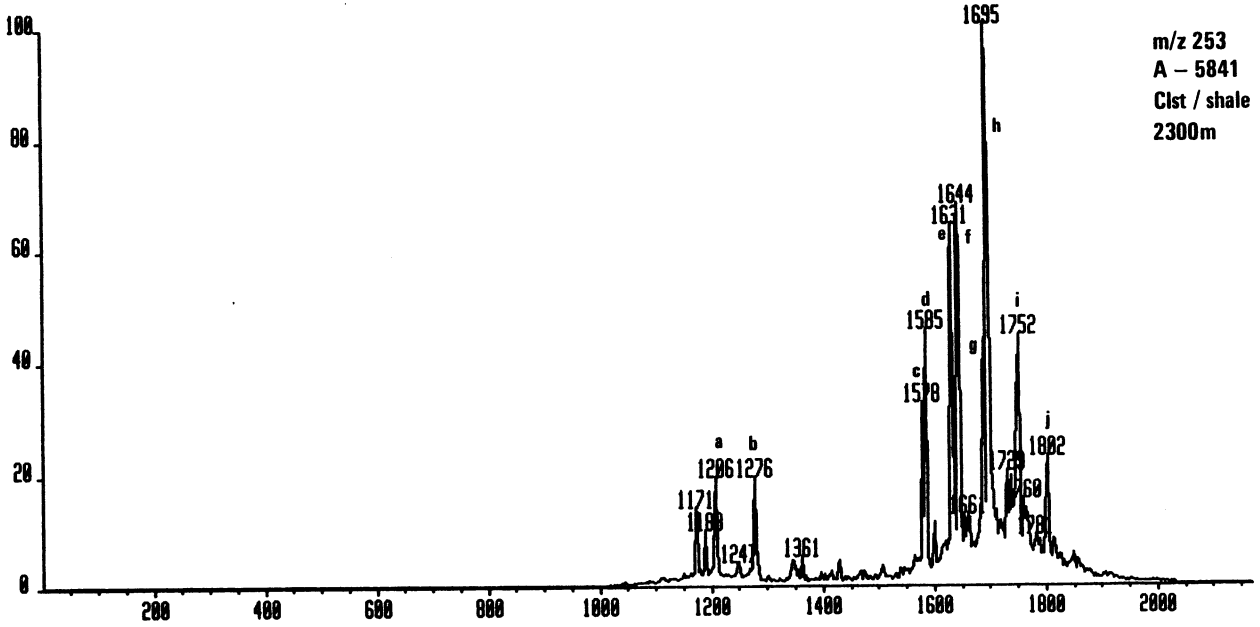
m/z 253
A – 5841
Clst / shale
2300m
1695
h
1644
1631
e
f
d
1585
i
1752
g
c
1578
a
b
1206
1276
j
1882
1171
1247
1361
100
80
60
40
20
0
200
400
600
800
1000
1200
1400
1600
1800
2000

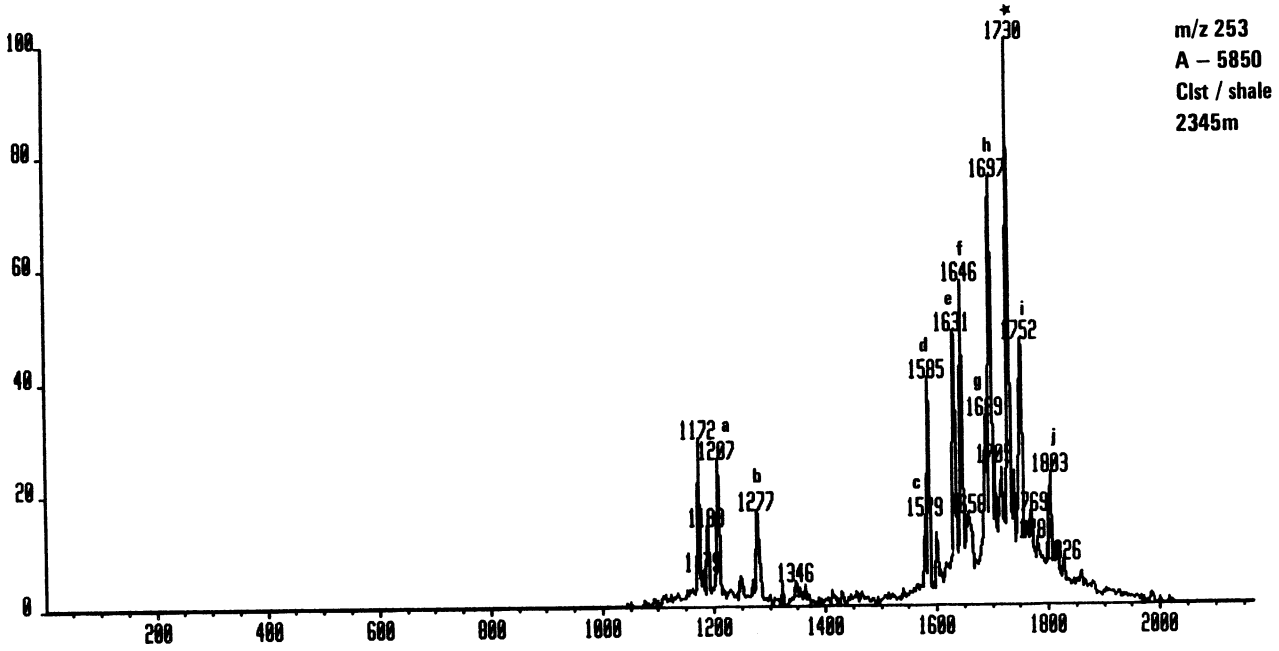
m/z 253
A – 5850
Clst / shale
2345m
*
1730
h
1697
f
1646
e
1631
i
1752
d
1585
g
1689
j
1883
1172
a
1207
b
1277
c
1579
1346
100
80
60
40
20
0
200
400
600
800
1000
1200
1400
1600
1800
2000

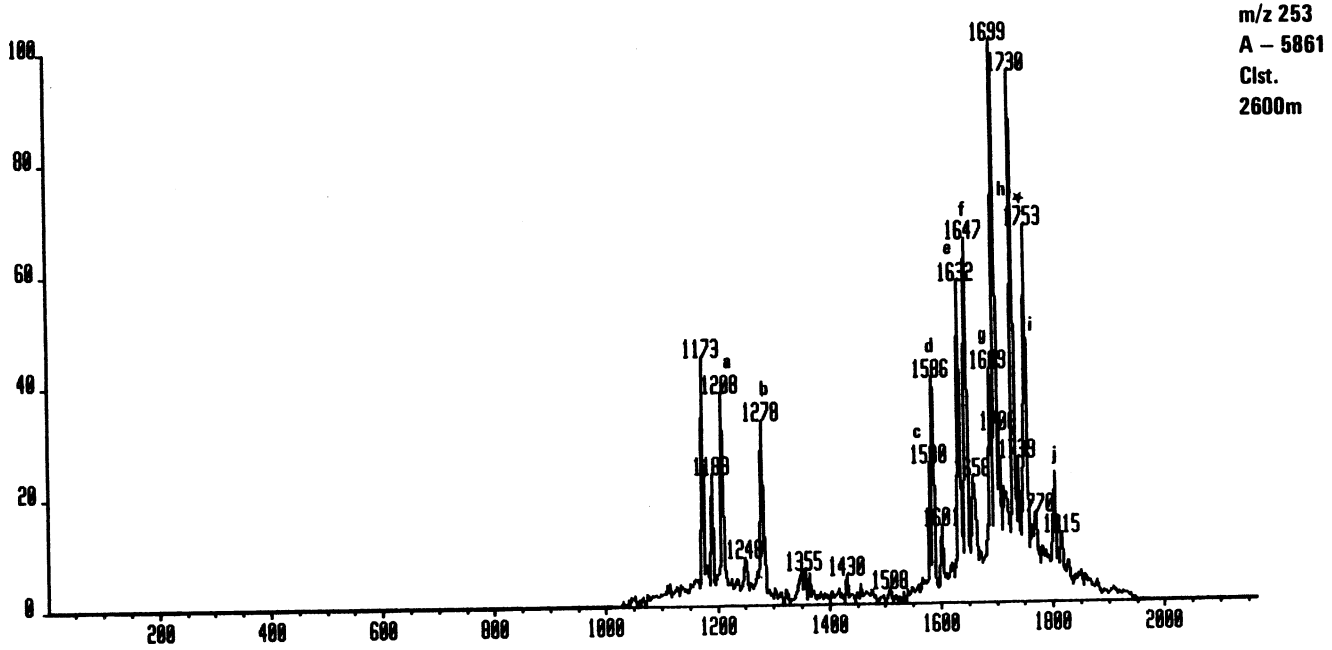
m/z 253
A – 5861
Clst.
2600m
1699
1730
1753
1647
1632
1586
1500
1173
1200
1278
1355
1430
1508
1249
100
80
60
40
20
0
200
400
600
800
1000
1200
1400
1600
1800
2000

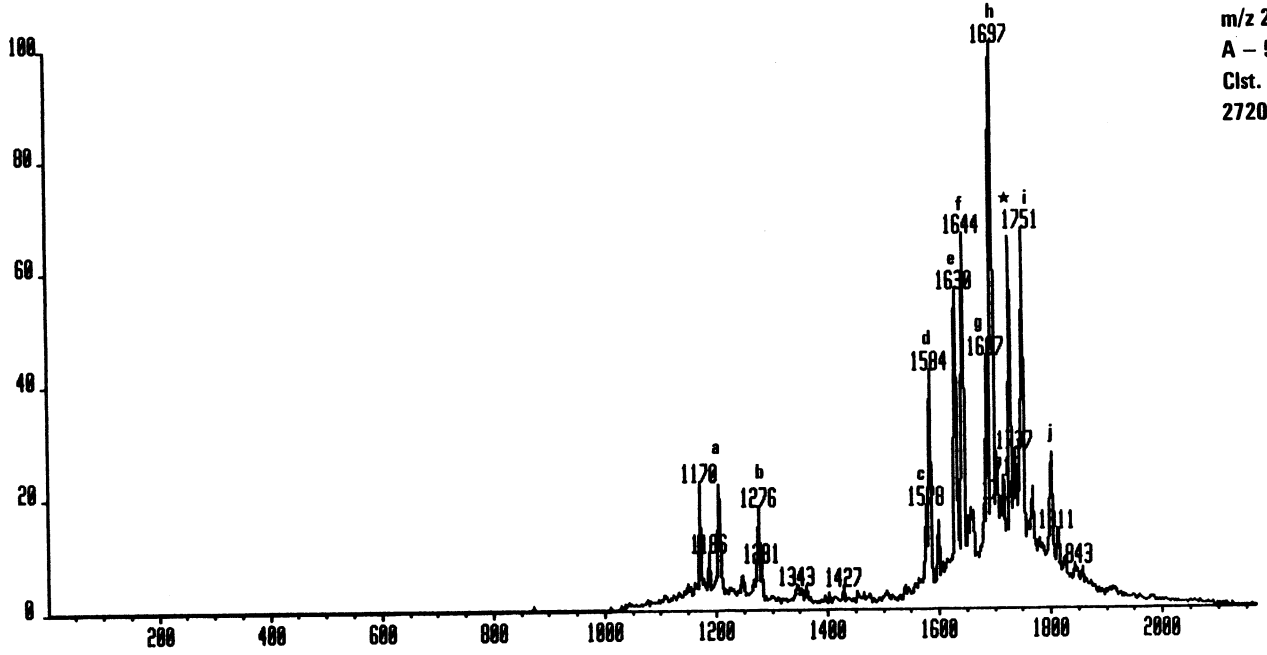
m/z 253
A – 5869
Clst.
2720m
1697
1644
1751
1630
1584
1170
1276
1343
1427
1511
1843
100
80
60
40
20
0
200
400
600
800
1000
1200
1400
1600
1800
2000

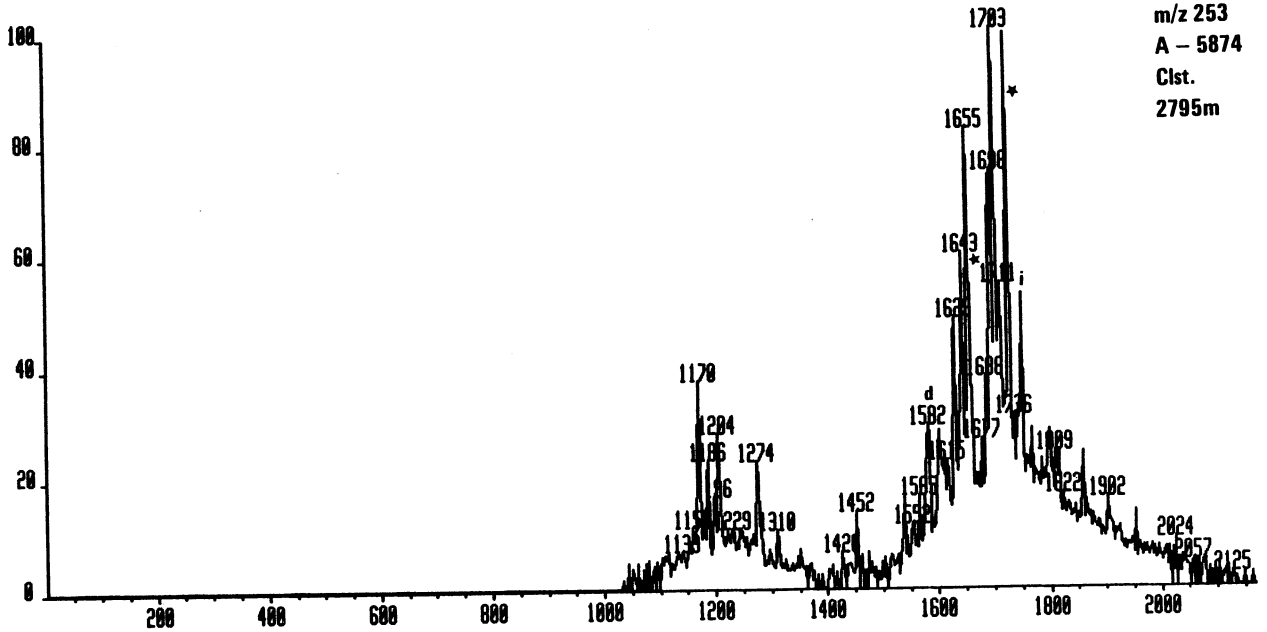
m/z 253
A – 5874
Clst.
2795m
1703
1655
1170
1284
1274
1452
1582
1310
1902
2024
2125
100
80
60
40
20
0
200
400
600
800
1000
1200
1400
1600
1800
2000

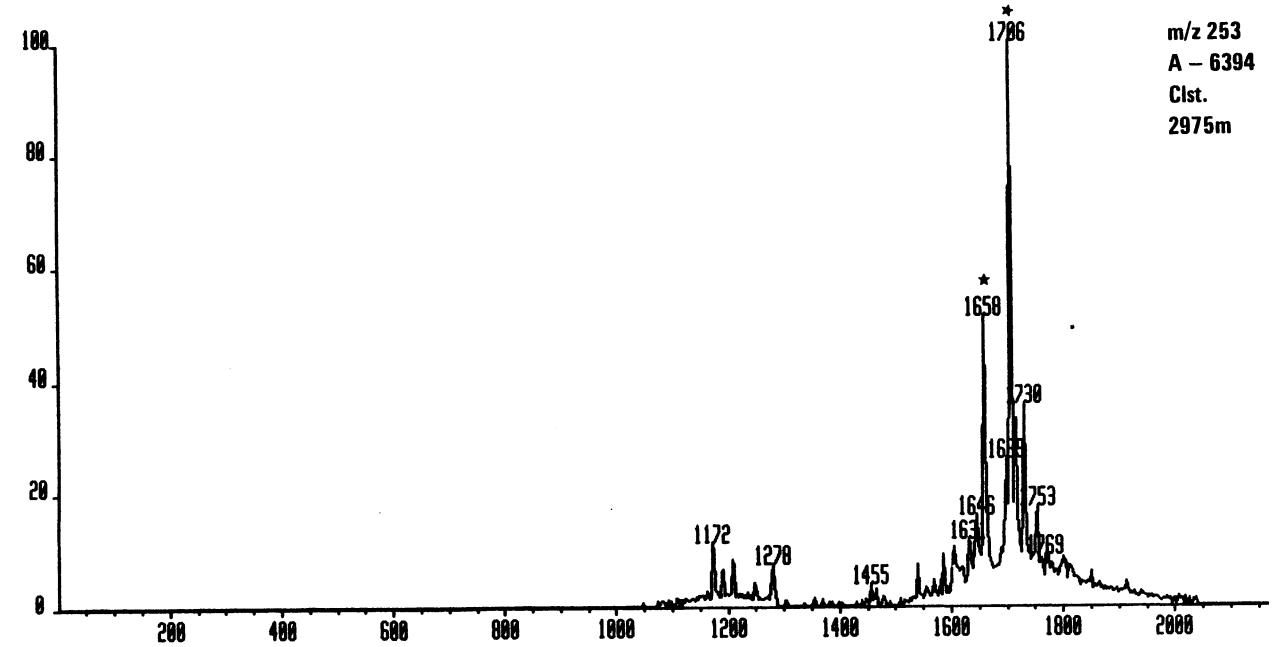
m/z 253
A – 6394
Clst.
2975m
1706
1658
1730
1753
1646
1172
1278
1455
100
80
60
40
20
0
200
400
600
800
1000
1200
1400
1600
1800
2000

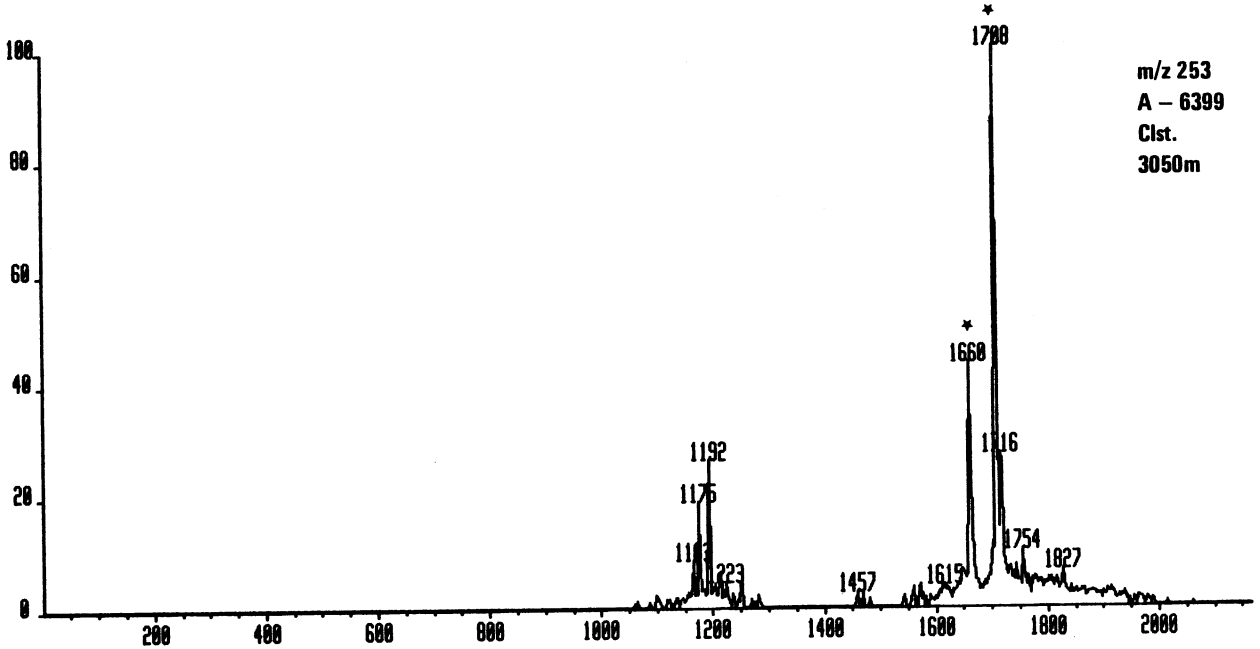
m/z 253
A – 6399
Clst.
3050m
1700
1660
1192
1176
1754
1827
1457
1615
223
200
400
600
800
1000
1200
1400
1600
1800
2000

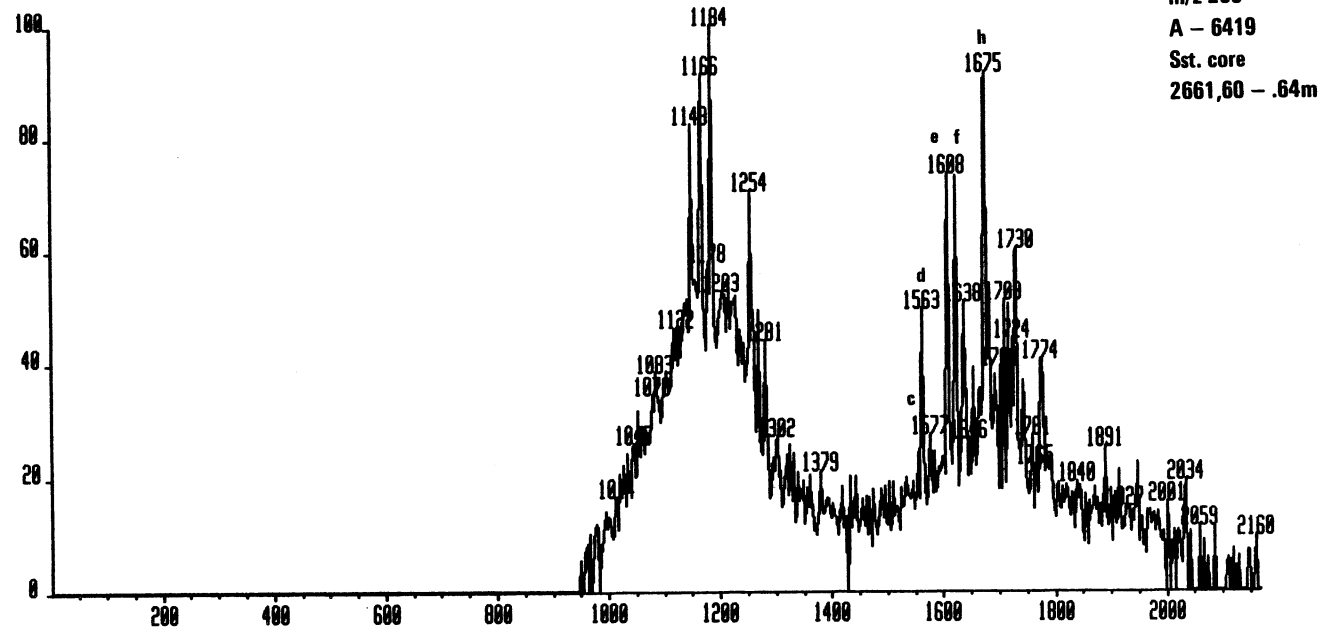
m/z 253
A – 6419
Sst. core
2661,60 – .64m
1184
1166
1148
1254
1675
h
e
f
1608
1730
d
1563
1774
c
1379
1891
1840
2034
2160
200
400
600
800
1000
1200
1400
1600
1800
2000

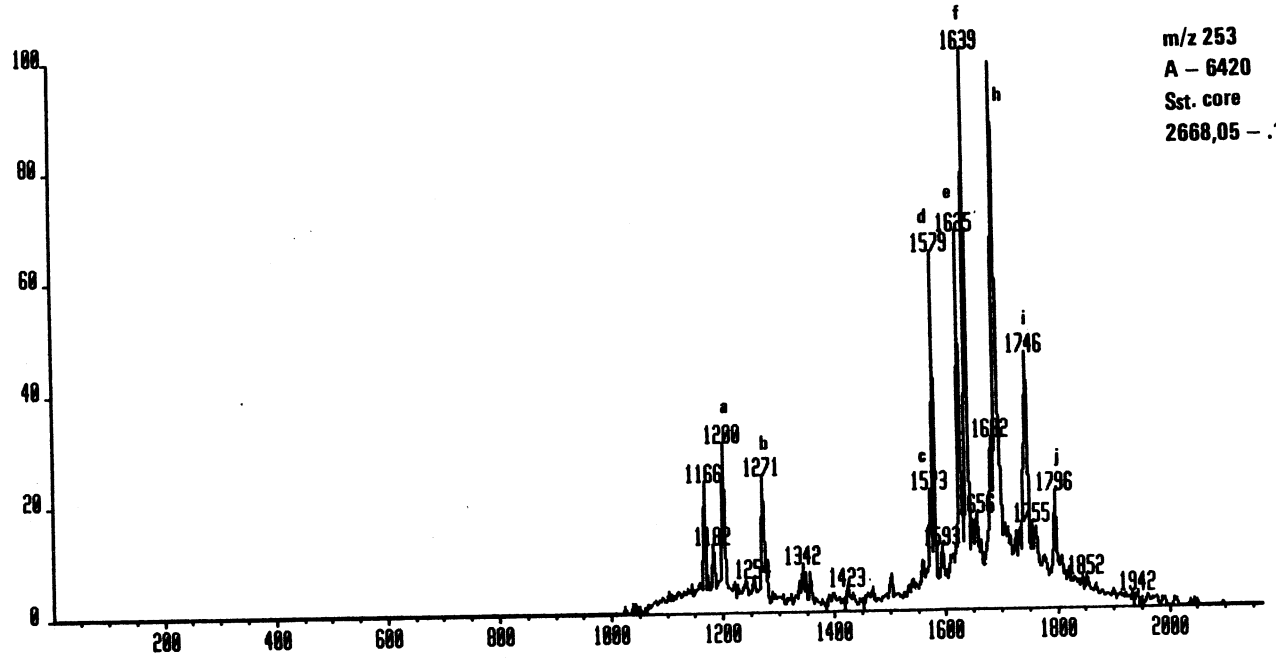
m/z 253
A – 6420
Sst. core
2668,05 – .12m
f
1639
h
e
d
1579
i
1746
a
1200
b
1271
1166
c
j
1796
1342
1423
1852
1942
100
80
60
40
20
0
200
400
600
800
1000
1200
1400
1600
1800
2000

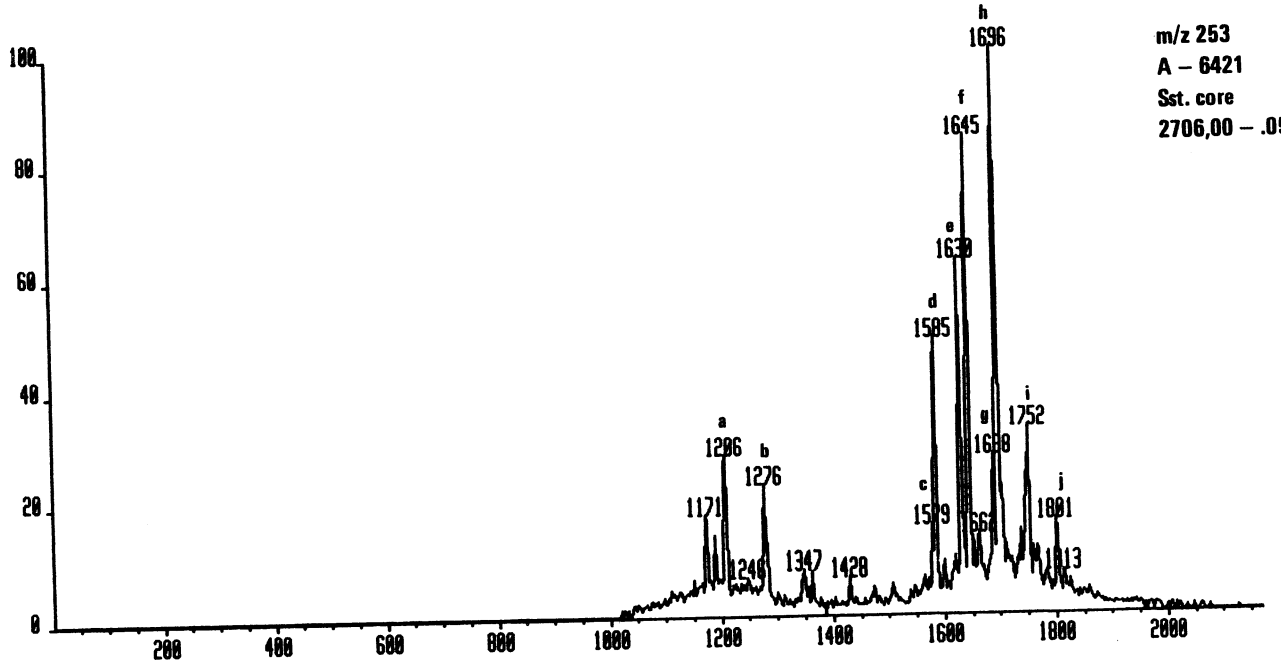
m/z 253
A – 6421
Sst. core
2706,00 – .05m
h
1696
f
1645
e
d
1585
i
1752
a
1206
b
1276
g
c
j
1881
1171
1347
1428
1813
100
80
60
40
20
0
200
400
600
800
1000
1200
1400
1600
1800
2000

FIGURE 5.

Triangular plot showing molecular weight distribution of C_{27}, C_{28} and C_{29} regular steranes

6610/7-1

100% C27

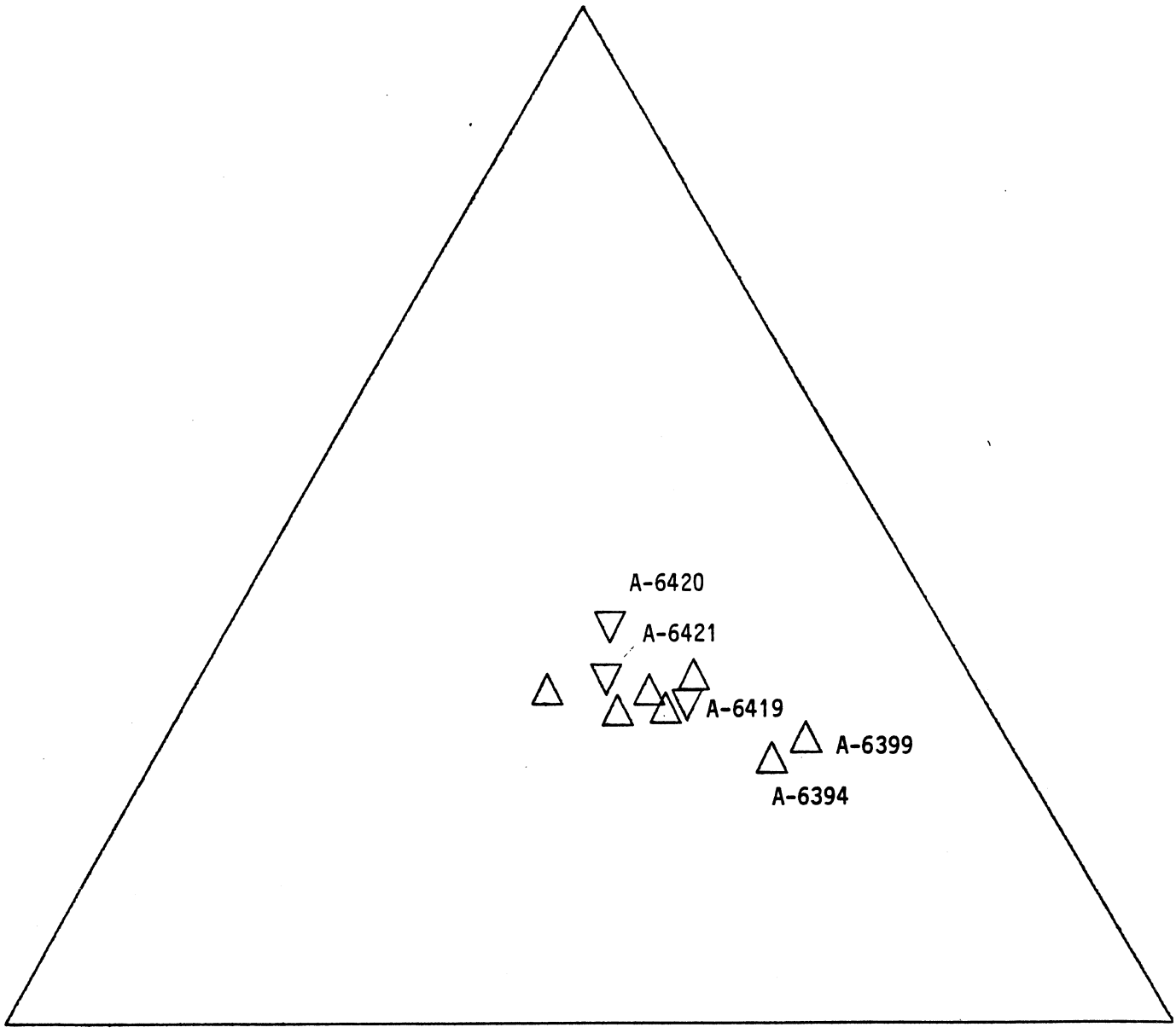

100% C28

100% C29